NASA CONTRACTOR
REPORT

NASA CR-993

GPO PRICE $ _____

CFSTI PRICE(S) $ _____

Hard copy (HC) _____ 3.00 _____

Microfiche (MF) _____ .65 _____

ff 653 July 65

'S IN

L OU

AXIA

g, and

N • W
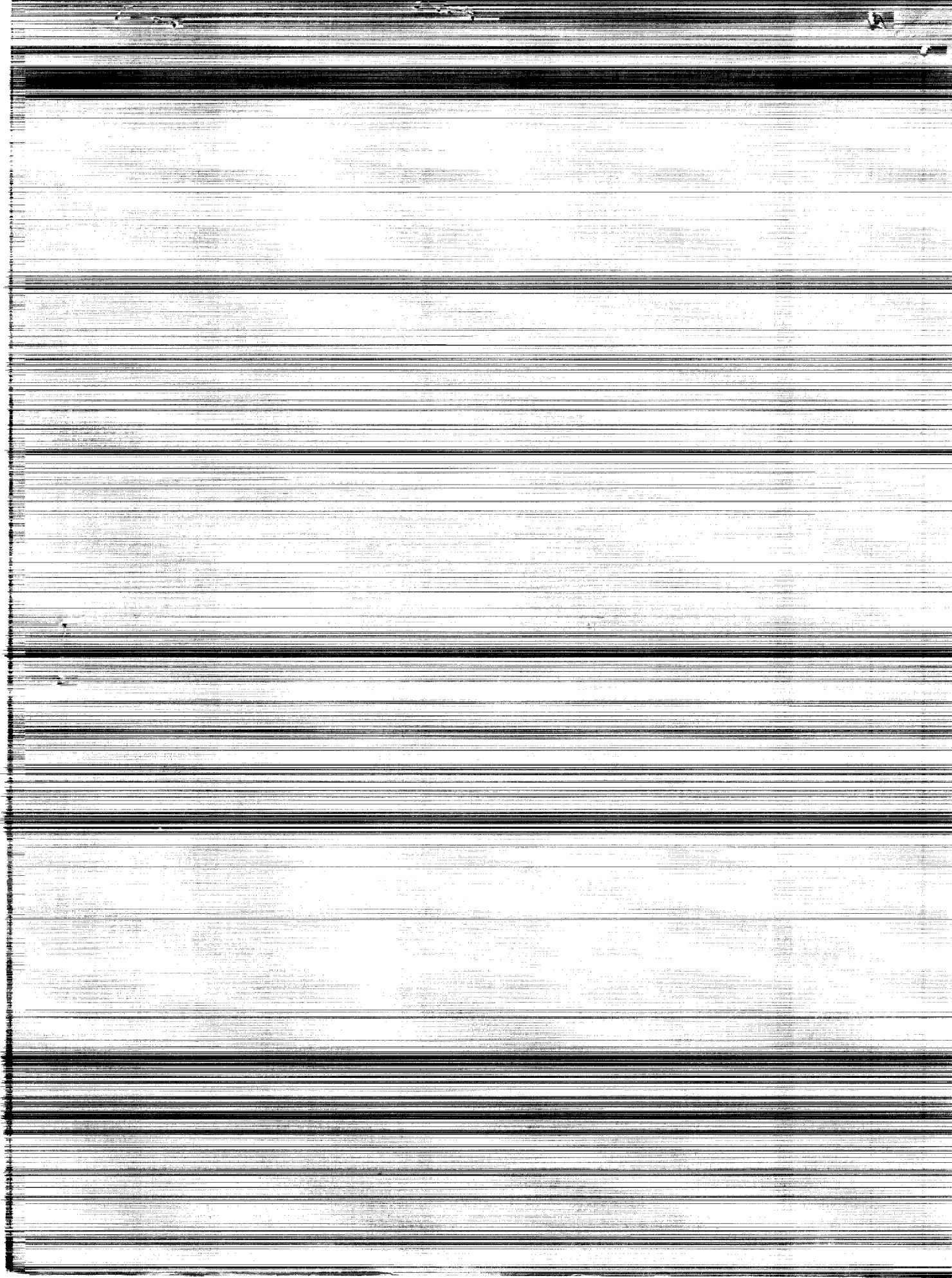
CONTAINMENT EXPERIMENTS IN VORTEX TUBES

WITH RADIAL OUTFLOW AND LARGE

SUPERIMPOSED AXIAL FLOWS

By John S. Kendall, Arthur E. Mensing,
and Bruce V. Johnson

FOREWORD

An exploratory experimental and theoretical investigation of gaseous nuclear rocket technology is being conducted by the United Aircraft Corporation Research Laboratories under Contract NASw-847 with the joint AEC-NASA Space Nuclear Propulsion Office. The Technical Supervisor of the Contract for NASA is Captain W. A. Yingling (USAF). Results of the fluid mechanics portion of the investigation conducted during the period between September 15, 1965 and May 30, 1967 are described in the following four reports (including the present report) which comprise the required fifth Interim Summary Technical Report under the Contract:

1. Travers, A.: Experimental Investigation of Flow Patterns in Radial-Outflow Vortexes Using a Rotating-Peripheral-Wall Water Vortex Tube. UAC Research Laboratories Report F-910091-10, May 1967 (NASA CR-991, 1968).

2. Johnson, B. V.: Exploratory Flow and Containment Experiments in a Directed-Wall-Jet Vortex Tube with Radial Outflow and Moderate Superimposed Axial Flows. UAC Research Laboratories Report F-910091-11, May 1967 (NASA CR-992, 1968).

3. Kendall, J. S., A. E. Mensing, and B. V. Johnson: Containment Experiments in Vortex Tubes with Radial Outflow and Large Superimposed Axial Flows. UAC Research Laboratories Report F-910091-12, May 1967 (present report, NASA CR-993, 1968).

4. Clark, J. W., B. V. Johnson, J. S. Kendall, A. E. Mensing, and A. Travers: Summary of Gaseous Nuclear Rocket Fluid Mechanics Research Conducted Under Contract NASw-847. UAC Research Laboratories Report F-910091-13, May 1967. (Submitted to AIAA for publication.)

Containment Experiments in Vortex Tubes With

Radial Outflow and Large Superimposed Axial Flows

TABLE OF CONTENTS

TABLE OF CONTENTS (Cont'd.)

Containment Experiments in Vortex Tubes With

Radial Outflow and Large Superimposed Axial Flows

SUMMARY

An experimental investigation was conducted to determine the heavy-gas containment characteristics of radial-outflow vortexes for potential application to a vortex-stabilized, open-cycle gaseous nuclear rocket engine. Tests were conducted in a constant-temperature vortex with Reynolds numbers based on the superimposed axial flow up to those expected in a full-scale engine. Air was employed to simulate the seeded hydrogen propellant and a heavy fluorocarbon was used in most tests to simulate the gaseous nuclear fuel. The effects on heavy-gas containment of changes in the vortex tube length-to-diameter ratio, the light-gas injection geometry and area, the ratio of average heavy-gas density to light-gas density, and the density of the heavy gas at injection were studied.

The heavy-gas containment parameters obtained were one to two order of magnitude less than are presently estimated to be required for an economically practical open-cycle engine. The containment parameters varied significantly only with vortex tube length-to-diameter ratio and the ratio of average heavy-gas density to light-gas density. The results of some tests using helium injected near the centerline of the vortex indicated that the presence of a light gas in the central region of the vortex has a significant favorable effect on containment characteristics; these results have potential application to the nuclear light bulb engine.

1

1. Experimentally determined containment parameters (the ratio of the average heavy-gas dwell time to the average light-gas dwell time in the vortex tube) for vortexes with radial outflow and large superimposed axial flows are between one and two orders of magnitude lower than are now estimated to be required for an economically practical, vortex-stabilized open-cycle gaseous nuclear rocket engine.

2. The containment parameters in tests with a vortex tube length-to-diameter ratio equal to 1.0 increased from approximately 3.5 to 10 as the ratio of the light-gas weight flow rate to the heavy-gas weight flow rate was increased from 7 to 50. The corresponding ratio of average heavy-gas density to light-gas density decreased from 0.5 to 0.2. The containment parameter was independent of axial-flow Reynolds number, tangential injection Reynolds number, axial component of the light-gas injection velocity, and light-gas injection area and geometry.

3. The containment parameters decreased as the vortex tube length-to-diameter ratio was increased. For example, with a ratio of light-gas weight flow rate to heavy-gas weight flow rate of 50, the containment parameter decreased from approximately 10 to 5 and the corresponding ratio of average heavy-gas density to light-gas density decreased from 0.2 to 0.1 when the vortex tube length-to-diameter ratio was increased from 1.0 to 3.0.

4. The presence of helium in the central region of vortexes with radial outflow and superimposed axial flow resulted in a stabilizing density gradient near the peripheral wall of the vortex tube. This result indicates that the presence of the radial density gradient caused by the temperature gradient in the coolant buffer region of a nuclear light bulb engine should significantly reduce the fuel concentration in this region by reducing or eliminating turbulent diffusion.

INTRODUCTION

An experimental and theoretical investigation of gaseous nuclear rocket technology is being conducted by the United Aircraft Research Laboratories under Contract NASw-847 administered by the joint AEC-NASA Space Nuclear Propulsion Office. The research performed under this contract is applicable to two vortex-stabilized gaseous nuclear rocket concepts: the open-cycle engine concept and the nuclear light bulb concept.

In the open-cycle concept (one engine design is shown schematically in Fig. 1), hydrogen propellant is injected from the peripheral wall of the rocket chamber to drive the vortex. The propellant sprials axially in an annular region near the peripheral wall into an exhaust annulus at one end of the chamber and through the exhaust nozzles. Gaseous nuclear fuel is contained in the central region of the vortex flow. Heat is transferred by thermal radiation from the gaseous nuclear fuel to the seeded hydrogen propellant passing over the fuel region. Details of the engine concept -- including the fluid mechanics, heat transfer, nucleonics and structure -- are described in Ref. 1.

In the nuclear light bulb concept, propellant is heated by thermal radiation passing through an internally cooled transparent wall located between the fuel and the propellant. Coolant gas is injected tangent to the inner surface of the transparent peripheral wall to establish the vortex flow which is utilized to contain gaseous nuclear fuel and to isolate it from the transparent wall.

Two primary factors which determine the flow patterns in confined vortexes are (1) whether or not there is a superimposed axial flow near the peripheral wall, and (2) whether or not the net flow of fluid is radially inward or outward with respect to the centerline of the vortex. In a vortex with superimposed axial flow, fluid is injected at the peripheral wall to drive the vortex and is withdrawn through an annulus located near the outer edge of one end wall. The radial-inflow vortex is formed by removing a small amount of fluid through ports at the centers of the end walls. The radial-outflow vortex also is driven by injecting fluid at the peripheral wall, but in this case additional fluid is injected through the ports at the centers of the end walls.

Flow visualization tests of radial-inflow vortexes (Refs. 2 and 3) have indicated that the flow in the central region of the vortex is relatively laminar and, hence, may lead to satisfactory containment of gaseous nuclear fuel. However, two-component gas tests with radial-inflow vortexes (Refs. 4, 5, and 6) have shown that the density of the heavy gas in the simulated fuel-containment region of the vortex (i.e., the relatively laminar central region) cannot be substantially greater than that of the surrounding light gas without creating instabilities and turbulence.

3

In an open-cycle engine the density of the fuel must be considerably greater than that of the surrounding propellant; the fuel-to-propellant density ratios attainable with a radial-inflow vortex are not large enough for such an engine. However, since the nuclear light bulb engine could utilize a heavier gas, such as neon, between the fuel and the transparent wall, radial-inflow vortex appear suitable for the nuclear light bulb engine.

Initial flow visualization tests of radial-outflow vortexes (Ref. 2) indicated that the flow was turbulent in the central region of the vortex. Two-component gas tests (Refs. 5 and 6) indicated that the density of the heavy gas in the simulated fuel-containment region could be increased to a value substantially greater than the density of the surrounding light gas. However, no measurements had been made of the amount of heavy gas contained and the heavy-gas loss rates for flow conditions with large amounts of superimposed axial flow. Thus, further research was required to determine whether radial-outflow vortexes with superimposed axial flow would be suitable for application to an open-cycle engine.

Three different experimental investigations were conducted concurrently to investigate the characteristics of radial-outflow vortexes for potential application to an open-cycle engine. This report presents the results of heavy-gas containment tests conducted at Reynolds numbers up to those that are presently estimated to be required in a full-scale engine. The results of a parallel investigation of radial-outflow vortexes (conducted at lower Reynolds numbers) are reported in Ref. 8. That report describes flow visualization tests, flow-field velocity measurements and heavy-gas containment tests. The results of flow visualization tests directed toward obtaining fundamental information on the stability and flow patterns in radial-outflow vortexes are reported in Ref. 7. A summary of the principal results of the fluid mechanics research conducted under Contract NASw-847 and a comparison of the observed flow characteristics with those that are now estimated to be required for both open-cycle and nuclear light bulb engines are presented in Ref. 9.

Background and Objectives of This Investigation

Previous two-component gas tests (e.g., Refs. 4, 5, and 6) were conducted at Reynolds numbers one to two orders of magnitude less than would be required for a typical vortex-stabilized, open-cycle engine. The vortex tubes used in previous tests employed a length-to-diameter ratio of 3.0 and a low value of the ratio of the average axial velocity in the vortex to the light-gas injection velocity (less than 0.2). For comparison, velocity ratios and length-to-diameter ratios approaching 1.0 are anticipated in an open-cycle engine (Ref. 10). In addition, no previous tests were conducted with geometries that provided light-gas injection with both tangential and axial velocity components.

4

Accordingly, the principal objectives of the investigation reported herein were to determine the effects on heavy-gas containment in radial-outflow vortexes with superimposed axial flow of (1) increasing the Reynolds numbers to values that are estimated to be required for the open-cycle engine, (2) varying the light-gas injection configuration and area, and (3) changing the vortex tube length-to-diameter ratio. In addition, several related investigations of basic vortexes (no superimposed axial flow) were also performed; results of these investigations are discussed in APPENDIXES I and II.

TEST EQUIPMENT

High Reynolds Number Test Facility

The high Reynolds number test facility consists of four systems: the light-gas (simulated-propellant) supply system, the heavy-gas (simulated-fuel) supply system, the test section and exhaust system, and the control console and data acquisition system. Figure 2 is a schematic diagram of the first three systems which comprise the test facility.

Light-Gas Supply System

The light-gas supply system provides a metered quantity of simulated propellant to the test section at the pressure, temperature, and weight flow rate required for a particular flow condition. A photograph of the heater and associated piping for the light-gas supply system is shown in Fig. 3. Light gas enters this system from the Research Laboratories 400 psi air supply or from the atmosphere. Light-gas flow rates up to 5 lb/sec were available using the 400 psi air supply. A combination steam and electric heater was used to heat the light gas to the desired temperature of 300 F. The weight flow rate of light gas into the test section was measured using ASME long-radius flow nozzles.

Heavy-Gas Supply System

The heavy-gas (simulated-fuel) supply system provides a metered quantity of simulated fuel to the test section at the pressure, temperature, and weight flow rate required for a particular flow condition. For most tests reported herein, the heavy gas consisted of a mixture of gaseous iodine and the vapor of an inert fluoro-carbon, FC-77 (a 3M Company trademark). The molecular weight of FC-77 is approximately 400. FC-77 vapor was produced from liquid FC-77 in a specially constructed boiler. Gaseous iodine was produced in a similar manner. A photograph of the boiler and associated piping for the heavy-gas supply system is presented in Fig. 4. Valves in the heavy-gas supply system allow a portion of the FC-77 to flow through the iodine boilder to control the fraction of the total heavy gas which is iodine. Control of the amount of iodine in the heavy-gas mixture is essential to the accuracy of the data-acquisition system which measures the amount of iodine vapor by the fraction of light absorbed. The FC-77 weight flow rate was measured using a turbine flow meter; the iodine weight flow rate was determined using a light absorption technique. Flow rates of FC-77 up to about 0.75 lb/sec could be used.

For a few tests, the simulated fuel consisted of a mixture of iodine vapor and one of several other gases: helium, nitrogen, or sulphur hexafluoride. These gases were heated in a heat exchanger (not shown in Fig. 2) located in the heavy-gas supply system. When gases other than FC-77 were used, their weight flow rates were measured using rotameters.

Test Section and Exhaust System

A photograph of the test section with a vortex tube installed is shown in Fig. 5. (Details of the vortex tubes employed in this investigation will be described in a following section.) The test section in which the vortex tubes were mounted consists of a 20-in.-ID by 30-in.-long cylindrical shell with end flanges. One of the end flanges is mounted on rollers, thus providing access to the vortex tube within the test section. The vortex tube is cantilevered from this flange-roller combination. The inlet ducts connect to the end flanges and lead to the injection plenum, which consists of an annular space between the vortex tube and test section outer cylindrical shell. For the basic vortex tube configuration, the exhaust ducts also connect to the end flanges.

The exhaust system consists of valves and associated piping necessary to connect the test facility to the Research Laboratories' vacuum system. A throttling valve installed in the exhaust system provided pressure regulation for the test section.

Control Console and Data Acquisition System

The control console (shown in Fig. 6) is used for remote operation of the high-Reynolds-number test facility. Also shown in Fig. 6 are components of the data acquisition system which record information from which the heavy-gas weight flow rate, the radial distribution of heavy-gas density, and amount of heavy gas stored within the vortex tube can be determined.

The amount of heavy gas stored and the radial distribution of heavy-gas density within the vortex tube were obtained using a collimated light beam which passed axially through the test section. The light absorbed by iodine vapor was proportional to the average heavy-gas density at a given radius. The beam was traversed along the vertical diameter of the vortex tube. Fig. 7 is a schematic diagram of the optical system used to obtain these measurements. Further details and discussion of the data acquisition system are presented in APPENDIX III.

A vortex configuration with a superimposed region of high axial velocity near the peripheral wall was employed for most tests reported herein. Figure 8 is a shetch of an axial-flow vortex tube mounted in the test section. A total of four vortex tubes, designated by their light-gas injection configurations, were used: three were multiple-fixed-port vortex tubes and one was directed-wall-jet vortex tube. These are described below: The vortex tubes used for the related tests of basic vortexes are described in APPENDIXES I and II.

Multiple-Fixed-Port Vortex Tubes

A sketch of the light-gas injection geometry of the multiple-fixed-port tubes and a photograph of one tube are presented in Fig. 9. All three vortex tubes are 10-in.-ID by 30-in.-long steel cylinders. The total injection areas are $A_j = 13.1$, 20.5, and 40.2 sq in. These vortex tubes each have 4284 holes drilled inward at an angle of 19 deg with respect to the local tangent (see Fig. 9 and TABLE I). There are 36 holes located at each of 119 axial locations along the vortex tube length. The hole diameters for the three vortex tubes having different injection areas are 0.062 in., 0.078 in., and 0.108 in., respectively. The holes are drilled in the tangential direction so that the light gas does not have an axial component of velocity at injection. As noted in TABLE I, the tube having 0.108-in.-dia holes was used with an end-wall insert (see following section) which provided a length-to-diameter ratio of 1.0; the injection area for this configuration was 13.3 sq in.

Directed-Wall-Jet Vortes Tube

A single directed-wall-jet vortex tube, similar to that described in Ref. 8, was constructed for this investigation. This vortex tube is also an 10-in.-ID by 30-in.-long steel cylinder and employs the directed-wall-jet injection geometry shown in Fig. 10a. The vortex tube has 900 individually directable injection ports spaced uniformly on the peripheral wall. There were 30 rows of inserts (Fig. 10b) located at each of 30 axial locations along the vortex tube length. Injection areas up to 45 sq in. were attainable using inserts having different slot heights. The inserts were oriented to provide an axial component to the light-gas injection velocity. For the tests conducted in this investigation the injection angle, β_j, varied from 0 deg to 63.5 deg along the length of the vortex tube. This distribution was chosen on the basis of results reported in Ref. 8. Figure 11 is a photograph of the partially assembled directed-wall-jet vortex tube in the high Reynolds number test facility. The volume outside of the vortex tube was divided into 15 separate plenums by plenum dividers and inflatable seals located between the vortex tube and the test section outer cylindrical shell (see Fig. 11). The pressure and

weight flow rate through each plenum were individually controlled. As noted in TABLE I, one series of tests was conducted with only 300 inserts in the L/D = 3.0 tube. In addition, a special end wall (see following section) was employed in some tests to reduce the L/D to 2.0 or 1.0. For these configurations, the number of inserts within the vortex tube was reduced to 600 and 300, respectively.

End Walls

Flow was exhausted from the vortex tubes at the axial-flow end wall (see Fig. 8). The essential components of the axial-flow end wall were a glass disc located in the exit plane of the vortex tube and a plenum downstream of the disc. The space between the edge of the disc and the vortex tube peripheral wall formed an exhaust annulus which, for most tests, extended from a radius of 4.0 in. to 5.0 in. A plenum divider (see Fig. 8) was installed in the axial-flow end-wall plenum. This divider provided an optical path for the axial-light beam through the plenum which prevented absorption of the light beam due to the presence of iodine vapor in the plenum. The plenum was connected to the axial-flow exhaust system (see Fig. 11).

Two types of nonaxial-flow end walls were employed. One was a plain 10-in.-dia steel disc which attached to an end flange of the test section; the other was a plain 10-in.-dia steel disc which could be positioned at any axial location within the vortex tube to change the vortex-tube length-to-diameter ratio. These end walls had glass windows along their vertical diameter to allow the light beam to pass axially through the vortex tube (see Fig. 7). Both end walls had 1.0-in.-dia holes at their centers for heavy-gas injection. For all tests discussed in the main text of this report, heavy gas was injected through the hole at the center of the nonaxial-flow end wall.

9

TEST AND DATA-REDUCTION PROCEDURES

Test Procedures

The flow condition for a typical heavy-gas containment test was specified by a fixed vortex tube geometry operating with fixed Reynolds numbers, heavy-gas injection configuration and flow rate. Vortex tube geometry was specified by the light-gas injection geometry (either multiple fixed port or directed wall jet) and the total light-gas injection area. For these employing directed-wall-jet vortex tubes, the axial distribution of light-gas injection angle was specified for each flow condition. The flow rate of the light gas was specified in terms of an axial-flow Reynolds number and a tangential injection Reynolds number. The former is defined as

$$Re_{z,w} = \frac{\rho_{P_1} \bar{V}_{z,w} r_1}{\mu_{P_1}} \qquad (1)$$

where ρ_{P_1} and μ_{P_1} are the density and viscosity of the light gas at injection and r_1 is the radius of the vortex tube. The velocity $\bar{V}_{z,w}$ is equal to the average velocity which would exist at the vortex tube exit if all the light-gas flow were removed through an annular area extending from $r = 0.75 \ r_1$ to $r = r_1$. This definition of axial-flow Reynolds number was developed in Refs. 1 and 11; it is useful in applying the results of containment tests to engine studies such as those reported in Refs. 1 and 10. For the tests reported herein, the average axial velocity $\bar{V}_{z,w}$ is

$$\bar{V}_{z,w} = \frac{W_P}{(7/16) \pi r_1^2 \rho_{P_1}} \qquad (2)$$

where W_P is the weight flow rate of light gas. Therefore, the axial-flow Reynolds number, $Re_{z,w}$, can be written as

$$Re_{z,w} = \frac{W_P}{(7/16) \pi r_1 \mu_{P_1}} \qquad (3)$$

10

The tangential injection Reynolds number, $Re_{t,j}$, is a measure of the angular momentum of the light gas at injection into the vortex tube and is defined as

$$Re_{t,j} = \frac{\rho_{P_1} V_{\phi,j} \, r_1}{\mu_{P_1}} = \frac{W_P \, r_1 \cos \beta_j}{A_j \, \mu_{P_1}} \qquad (4)$$

where $V_{\phi,j}$ is the tangential component of the average light-gas injection velocity. For tests employing multiple-fixed-port vortex tubes, $V_{\phi,j}$ was equal to the average light-gas injection velocity since the injected light gas had no axial velocity component. For tests employing directed-wall-jet vortex tubes, the light-gas weight flow per unit length and the tangential component of average light-gas injection velocity, $V_{\phi,j}$, were constant along the length of the vortex tube.

For most tests described herein, the temperature of the light gas at injection was approximately 300 F and the light-gas stagnation pressure was between 0.9 and 1.0 atm. Since air was used as the light gas in all tests, the Reynolds numbers were varied by changing the light-gas weight flow rate (see Eqs. (3) and (4)).

Tests to determine the amount of heavy gas that could be contained in a light-gas vortex were conducted in the following manner. For a given vortex tube geometry, both the light- and heavy-gas flow rates were established (the heavy-gas flow rate was monitored using an iodine absorptometer -- similar to that described in Ref. 4 -- located on the heavy-gas injection duct). The light beam of the axial absorptometer (described in detail in APPENDIX III) was traversed along a vertical diameter of the vortex tube. This provided information on both the radial distribution and the total amount of heavy gas stored within the vortex tube. The light beam traverse was repeated at least twice to verify that the total amount of heavy gas within the vortex tube was constant (i.e., that a steady-state condition had been reached). The time required for a single traverse of the axial light beam was approximately 3 seconds (many times the average residence time for the heavy gas within the vortex tube).

Data Reduction Procedures

One measure of the containment characteristics of a confined vortex flow is the heavy-gas density ratio, $\bar{\rho}_{F_1} / \rho_{P_1}$ (i.e., the ratio of the volume-averaged heavy-gas density to the light-gas density at the injection conditions). The density $\bar{\rho}_{F_1}$ is given by

11

$$\overline{\rho}_{F_1} = \frac{\mathcal{W}_F}{V}$$

$$(5)$$

where $\mathcal{W}_F$ is the amount of heavy gas stored and V is the total volume of the vortex tube; $V = \pi r_1^2 L$. The amount of heavy gas stored was determined by averaging the data obtained from radial traverses both above and below the vortex tube centerline. For most tests reported herein, this average value of heavy gas stored deffered from the value determined from individual upper and lower traverses by less than 10 percent. A detailed description of the technique employed to determine the amount of heavy gas stored, the operation of the axial absorptometer, and the data acquisition system is given in APPENDIX III.

The heavy-gas time constant, t_F , is a measure of the heavy-gas loss rate characteristics of a confined vortex flow. It is defined as

$$t_F = \mathcal{W}_F / W_F$$

$$(6)$$

where W_F is the weight flow rate of heavy gas. The heavy-gas time constant is the average residence time for all the heavy-gas in the vortex tube. Heavy-gas time constants were converted to dimensionless time constants by dividing by ($\rho_{P_1} r_1^2 / \mu_{P_1}$), a scaling parameter proportional to a characteristic time for similar flows (this parameter is derived and discussed in Ref. 12). Hence,

$$\tau_{F_1} = \frac{t_F}{\left(\rho_{P_1} r_1^2 / \mu_{P_1}\right)}$$

$$(7)$$

Results of the containment tests reported herein are discussed in terms of the so-called "containment parameter" $\tau_{F_1} / \tau_{F_1 MIN}$, where $\tau_{F_1 MIN}$ is the dimensionless time constant which would result if the heavy and light gases were uniformly mixed before injection into the vortex tube:

$$\tau_{F_1 MIN} = \frac{t_{F MIN}}{\rho_{P_1} r_1^2 / \mu_{P_1}}$$

$$(8)$$

In Eq. (8), $t_{F MIN}$ is given by

$$t_{F MIN} = \frac{V}{Q_{P_1}\left[1 + \left(\frac{Q_F}{Q_P}\right)_{INJ}\right]}$$

$$(9)$$

12

If $(Q_F/Q_P)_{INJ} \ll 1$, then

$$t_{F_{MIN}} = \frac{V}{Q_{P_1}} \qquad (10)$$

Equation (8) may be combined with Eqs. (3) and (10) to yield

$$\tau_{F_1 MIN} = \frac{(32/7)(L/D)}{Re_{z,w}} \qquad (11)$$

This indicates that $\tau_{F_1 MIN}$ is directly proportional to the length-to-diameter ratio of the vortex tube and inversely proportional to the axial-flow Reynolds number. By combining Eqs. (6) and (10), the expression for the containment parameter can also be written as

$$\tau_{F_1} / \tau_{F_1 MIN} = (t_F / t_{F_{MIN}}) = (\bar{\rho}_{F_1}/\rho_{P_1})(W_P/W_F) \qquad (12)$$

The ratio W_P/W_F is sometimes used as a parameter in discussing containment. A summary of other containment parameters and equations for converting from dimensionless to dimensional parameters is given in APPENDIX IV.

DISCUSSION OF RESULTS

The heavy-gas containment experiments described in this report are divided into three categories: (1) tests using multiple-fixed-port vortex tubes; (2) tests using directed-wall-jet vortex tubes; and (3) tests using different simulated fuels (heavy gases). Most of the heavy-gas containment data will be presented as the variation of the containment parameter, $\tau_{F_1}/\tau_{F_1 MIN}$, with the heavy-gas density ratio, $\bar{\rho}_{F_1}/\rho_{P_1}$. TABLE I presents a summary of the vortex tube geometries which were employed in the tests discussed in the main text of this report. Results of related tests conducted in vortex tubes having geometries different from those listed in TABLE I (basic vortex configurations) are discussed in APPENDIXES I and II.

Results of Tests with Multiple-Fixed-Port Vortex Tubes

The heavy-gas containment tests using the multiple-fixed-port vortex tubes were conducted to determine the effect on containment characteristics of (1) changes in light-gas injection area and axial-flow Reynolds number, and (2) changes in the length-to-diameter ratio of the vortex tube.

Effects of Light-gas Injection Area and Axial-flow Reynolds Number

Heavy-gas containment data obtained from tests using the $L/D = 3.0$ multiple-fixed-port vortex tubes having $A_j = 13.1$, 20.5 and 40.2 sq in. are presented in Figs. 12, 13 and 14, respectively. These data are summarized in Fig. 15 where a single curve is faired through all data points.

Examination of each set of data in Figs. 12 through 14 indicates that the containment parameter, $\tau_{F_1}/\tau_{F_1 MIN}$, for each vortex tube was independent of axial-flow Reynolds number, $Re_{z,w}$. Since $\tau_{F_1 MIN}$ is inversely proportional to $Re_{z,w}$ (see Eq. (11)), the dimensionless time constant τ_{F_1} (and, hence, the average heavy-gas residence time t_F) was also inversely proportional to $Re_{z,w}$ for each of these vortex tubes.

The faired curve from Fig. 15 fits the data in Figs. 13 and 14, but the data on Fig. 12 deviate a small amount. This small deviation is not believed to indicate any significant effect of A_j on heavy-gas containment. Thus, the results indicate that heavy-gas containment in the multiple-fixed-port vortex tubes was independent of light-gas injection area.

14

Since the containment parameter was independent of light-gas injection area and axial-flow Reynolds number, it was also independent of the tangential injection Reynolds number, $Re_{t,j}$, and the average axial-to-tangential velocity ratio, $\bar{V}_{z,w} / V_{\phi,j}$. This is because the parameters $Re_{t,j}$ and $\bar{V}_{z,w} / V_{\phi,j}$ can be expressed in terms of the light-gas injection area, the axial-flow Reynolds number, and the light-gas flow rate.

The summary in Fig. 15 indicates that the experimentally determined containment parameters for multiple-fixed-port vortex tubes ranged from a value of approximately 6 at a heavy-gas density ratio of 0.05 (corresponding to a light-to-heavy-gas flow rate ratio W_P/W_F of 120) to a value of approximately 1.5 at a heavy-gas density ratio of 1.0 (corresponding to a light-to-heavy-gas flow rate ratio $W_P/W_F = 1.5$). These values are approximately one to two orders of magnitude less than the values of the containment parameter and fuel-to-propellant density ratio required for economical operation of a full-scale open-cycle engine. The axial-flow Reynolds numbers in the tests were up to 481,000, which is close to the value required for a typical open-cycle engine (Ref. 10). A more detailed comparison of the results of the fluid mechanics tests with the requirements for full-scale engines is presented in Ref. 9.

Typical radial distributions of heavy-gas density for the three multiple-fixed-port vortex tubes are shown in Fig. 16. A radial distribution of heavy-gas density for a vortex configuration having radial outflow but without superimposed axial flow is also included in Fig. 16 (details of the tests of this configuration are presented in APPENDIX I). The results for the axial-flow vortex configuration indicate that light-gas injection area and axial-flow Reynolds number had no large effect on the shape of the density distributions. With superimposed axial flow, the variation of heavy-gas density with radius was small (see Fig. 16). Containment parameters for these particular configurations were very low ($\tau_{F_1} / \tau_{F_1\,MIN} \approx 2.0$) indicating that a very intense mixing process existed. The fact that the density distribution for the vortex configuration without superimposed axial flow is so different is indicative of a basic difference in the flow patterns with and without superimposed axial flow. The containment data provide further evidence of this difference; for the same light-to-heavy-gas flow rate ratio, the containment parameter and the heavy-gas density ratio were approximately one order of magnitude larger for the configuration without axial flow than for the configuration with axial flow.

Effect of Vortex Tube Length-to-Diameter Ratio

Results of tests conducted to determine the effect of vortex tube length-to-diameter ratio on heavy-gas containment are presented on Fig. 17. The multiple-fixed-port vortex tube with L/D = 1.0 was used in these tests (see TABLE I). Also shown on Fig. 17 is a faired curve from Fig. 15 which represents the previously dis-

15

cussed data for the vortex tubes having L/D = 3.0. The results of these tests are similar to the results for L/D = 3.0; the containment parameter was independent of axial-flow Reynolds number and decreased with increasing heavy-gas density ratio. However, for a given heavy-gas density ratio, the containment parameter was approximately 2 to 3 times larger for L/D = 1.0 than for L/D = 3.0 (Fig. 17). Or, stated another way, for a given ratio of light-to-heavy-gas weight flow rates (shown by the lines of constant W_P/W_F), both the containment parameter and the heavy-gas density ratio were approximately 2 to 3 times larger for L/D = 1.0 than for L/D = 3.0. Thus, the containment is improved with decreasing length-to-diameter ratio.

The effect of length-to-diameter ratio on the radial distribution of heavy-gas density is presented in Fig. 18. The distributions shown are for a light-to-heavy-gas flow rate ratio of approximately 23. The shapes of the two distributions are similar and indicate that, although the containment parameter and heavy-gas density ratio are larger for L/D = 1.0 than for L/D = 3.0 (see Fig. 17), no well-defined fuel containment region existed in either case. In each distribution, the variation of heavy-gas density with radius is small, indicating that substantial mixing between the light and heavy gases existed throughout the vortex tube for both L/D = 1.0 and L/D = 3.0.

Results of Tests with Directed-Wall-Jet Vortex Tubes

Results of containment tests reported in Ref. 8 indicated that substantial improvements in heavy-gas containment were obtained with a directed-wall-jet light-gas injection configuration. For this configuration, the light gas is injected with an axial velocity component to reduce the axial pressure gradient required to accelerate the flow toward the axial-flow end wall. Tests were conducted in the high Reynolds number facility to determine whether the increased containment parameters and heavy-gas density ratios reported in Ref. 8 can be maintained or improved when the axial-flow Reynolds number is increased and when the vortex tube length-to-diameter ratio is changed.

Effects of Light-gas Injection Area and Axial-flow Reynolds Number

Tests to determine the effects of changes in light-gas injection area, A_j , and axial-flow Reynolds number $Re_{z,w}$, on heavy-gas containment were conducted using the directed-wall-jet vortex tube having a length-to-diameter ratio of 3.0. The light-gas injection angle, β_j , varied from 0 deg (i.e., no axial velocity component) at the nonaxial-flow end wall to 63.5 deg at the axial-flow end wall. This distribution was chosen based upon the results from Ref. 8. TABLE I presents further details of the vortex tube geometry which was employed.

16

Heavy-gas containment data obtained from tests using the directed-wall-jet vortex tube having light-gas injection areas, A_j, equal 11.0 and 32.2 sq in. are presented in Figs. 19 and 20, respectively. In Fig. 21 the data from Figs. 19 and 20 are summarized. The data shown in Figs. 19 and 20 indicate that the containment parameter was essentially independent of the axial flow Reynolds number for the two light-gas injection areas; a result consistent with that obtained from the multiple-fixed-port vortex tubes. Further, Fig. 21 shows that the containment parameter and heavy-gas density ratios were also independent of the light-gas injection area. The containment parameters ranged from a value of approximately 7 at a heavy-gas density ratio of 0.036 (corresponding to a light-to-heavy-gas flow rate ratio of 194) to a value of approximately 1.5 at a heavy-gas density ratio of 0.46 (corresponding to a light-to-heavy-gas flow rate ratio of 3.3).

Radial distributions of heavy-gas density within the directed-wall-jet vortex tubes were similar to those in the multiple-fixed-port vortex tubes (see Fig. 16). The variation of heavy-gas density with radius was small.

Effect of Vortex Tube Length-to-Diameter Ratio

Results of tests conducted to determine the effect of vortex tube length-to-diameter ratio on heavy-gas containment are presented in Fig. 22. Data were obtained for vortex tubes having length-to-diameter ratios of 1.0 and 2.0 to compare with the data for L/D = 3.0 from Fig. 21. The results indicate that the containment parameters increased as L/D was decreased from 3.0 to 1.0. The containment parameter was essentially independent of axial-flow Reynolds number and decreased with increases in heavy-gas density ratio for both the L/D = 1.0 and L/D = 2.0 vortex tube configurations.

Comparison of Results of Containment Tests Employing Multiple-Fixed-Port and Directed-Wall-Jet Vortex Tubes

Figure 23 summarizes results of tests with both multiple-fixed-port and directed wall-jet vortex tubes. The curves indicate that for a vortex tube length-to-diameter-ratio equal to 1.0, the containment parameter increased from approximately 3.5 to 10 as the ratio of the light-gas weight flow rate to the heavy-gas weight flow rate was increased from 7 to 50. The corresponding heavy-gas density ratio decreased from 0.5 to 0.2. The containment parameter was found to be essentially independent of the axial-flow Reynolds number, the tangential injection Reynolds number, the axial component of the light-gas injection velocity, and light-gas injection area and geometry. However, Fig. 23 also shows that the containment parameter decreased as the vortex tube length-to-diameter ratio was increased. For example, with a ratio of light-gas weight flow rate to heavy-gas flow rate of 50, the containment parameter

decreased from approximately 10 to 5 and the heavy-gas density ratio decreased from 0.2 to 0.1 as the vortex tube length-to-diameter ratio was increased from 1.0 to 3.0.

Included in Fig. 23 is a line representing results of tests of a vortex tube configuration without superimposed axial flow. (Further descriptions of tests with this configuration are presented in APPENDIX I.) The containment parameters and density ratios obtained from these tests were approximately 8 to 10 times those obtained from tests of comparable configurations with axial flow. The low values of containment parameter obtained from tests of axial-flow configurations are believed to be due to mixing between the fluid near the outer region of the vortex tube and the fluid in the central, or heavy-gas-containment, region. Such mixing results from the presence of the large amounts of superimposed axial flow near the vortex tube peripheral wall. Further verification and discussion of this mixing problem is contained in Ref. 8.

Results of heavy-gas containment tests discussed in the preceding paragraphs indicate that the axial-flow vortex configuration will not provide the values of containment parameter and heavy-gas density ratio presently estimated to be required for an economically practical open-cycle vortex-stabilized gaseous nuclear rocket engine. Experimentally determined containment parameters reported herein for vortexes with radial outflow and large superimposed axial flows are between one and two orders of magnitude lower than those which are presently estimated for such an engine.

Results of Tests Employing Different Simulated Fuels

A series of tests employing different density gases was conducted in the high Reynolds number test facility. To avoid confusion between the terms heavy gas and light gas, the gas injected at the vortex centerline (previously called the heavy gas) will be referred to as the simulated fuel and the gas injected at the vortex peripheral wall (previously called the light gas) will be referred to as the simulated propellant in this section of the report. Simulated fuels were used that had densities at injection of less than, approximately equal to, and greater than the simulated-propellant density at injection. The directed-wall-jet vortex tube had a light-gas injection area of 11.0 sq in. and a length-to-diameter ratio of 1.0. The injection direction of the simulated propellant (air) varied from 0 deg at the nonaxial-flow end wall to 63.5 deg at the axial-flow end wall. Simulated fuels, either helium, nitrogen, or sulphur hexafluoride, were injected at the center of the nonaxial-flow end wall. Small amounts of iodine vapor were added to each simulated fuel as a tracer. The molecular weights of the mixture were approximately 6, 30, and 148, respectively.

Figures 24, 25, and 26 present the results of containment tests with each of the three simulated fuels: the data are summarized in Fig. 27. Data were obtained at three axial-flow Reynolds numbers and several simulated-fuel flow rates. No significant effect on the containment parameter of variations in axial-flow Reynolds number can be seen except when helium was employed as the simulated fuel at low axial-flow Reynolds numbers. Figure 27 shows that the use of a simulated fuel whose density at injection was less than that of the simulated propellant (helium) resulted in a substantial increase in the containment parameter for some cases. Use of simulated fuels with densities equal to or greater than the simulated propellant density (nitrogen or sulphur hexafluoride) resulted in essentially the same values of containment parameter as were previously noted (e.g., compare Figs. 27 and 23). The increase in containment parameter when helium was used as the simulated fuel is also apparent in basic vortex tube tests described in APPENDIX II. This suggests that the favorable density gradient that occurs when helium was used as the simulated fuel may be suppressing some of the turbulent mixing that normally occurs in a radial-outflow vortex.

Figure 28 presents the radial distribution of simulated-fuel density (normalized by the simulated-propellant density at injection) for three of the tests whose results are presented in Fig. 27. The density distributions obtained with nitrogen and sulphur hexafluoride are identical but that obtained with helium is quite different. The helium density is approximately constant inside a radius of 0.75 r_1, whereas the nitrogen and sulphur hexafluoride distributions continue to increase inside this radius.

The data of Fig. 28 are replotted in Fig. 29 to show the radial distribution of the local partial pressure of the simulated fuel (it was assumed for this data that the static pressure in the vortex was constant and equal to the simulated-propellant pressure at the peripheral wall). A simulated-fuel partial pressure equal to approximately 65 percent of the simulated-propellant injection pressure was obtained over a substantial volume of the vortex tube (i.e., inside a radius of 0.8 r_1). This occurred only when the simulated fuel had a density at injection that was less than that of the simulated propellant. The local simulated-fuel partial pressure was substantially lower whenever the simulated-fuel density at injection was equal to or greater than that of the simulated propellant.

Figure 30 shows the radial distribution of local density in the vortex for the conditions of Figs. 28 and 29. The density in the central region of the vortex with helium as the simulated fuel was less than 50 percent of the density at the peripheral wall and was relatively constant over three quarters of the radius. The effect of the large favorable density gradient (i.e., increasing density with increasing radius) on the turbulence level was probably the cause of the increased simulated-fuel containment that existed for this case (see Fig. 27).

19

The radial variation of density within a vortex and its effect on the fuel containment is an important consideration in gaseous nuclear rockets. As described in Ref. 9, the closed-cycle gaseous nuclear rocket engine (i.e., the nuclear light bulb engine) may have a density distribution simular to that shown for the helium simulated fuel in Fig. 30. The flow between the transparent wall of the nuclear light bulb engine and the nuclear fuel will consist of a coolant gas, probably neon. Since neon is essentially transparent to thermal radiation, the density of the neon coolant very near the wall will in all probability be greater than the density of the gaseous nuclear fuel. Thus, the density gradient near the transparent wall should be favorable (i.e., increasing density with increasing radius). It is anticipated that this favorable density gradient will minimize the turbulent diffusion of fuel to the peripheral wall of the vortex tube.

In contrast, the open-cycle engine will have hot hydrogen that is nearly opaque to thermal radiation surrounding the nuclear fuel. Thus, with the exception of a very thin region near the peripheral wall, no favorable density gradient exists within this vortex flow and, hence, no similar turbulence suppressing mechanism exists in the open-cycle engine.

REFERENCES

1. McLafferty, G. H.: Analytical Study of the Performance Characteristics of Vortex-Stabilized Gaseous Nulcear Rocket Engines. United Aircraft Research Laboratories Report D-910091-7, prepared under Contract NASw-847, September 1965. To be issued as NASA CR report.

2. Travers, A.: Experimental Investigation of Peripheral-Wall Injection Techniques in Water Vortex Tube. United Aircraft Research Laboratories Report D-910091-7, prepared under Contract NASw-847, September 1965. To be issued as NASA CR report.

3. Travers, A. and B. V. Johnson: Measurements of Flow Characteristics in an Axial-Flow Vortex Tube. United Aircraft Research Laboratories Report C-910091-3, prepared under Contract NASw-847, September 1964. Also issued as NASA CR-277.

4. Mensing, A. E. and J. S. Kendall: Experimental Investigation of Containment of a Heavy Gas in a Jet-Driven Light-Gas Vortex. United Aircraft Research Laboratories Report D-910091-4, prepared under Contract NASw-847, March 1965. To be issued as NASA CR report.

5. Mensing, A. E. and J. S. Kendall: Experimental Investigation of the Effect of Heavy-to-Light-Gas Density Ratio on Two-Component Vortex Tube Containment Characteristics. United Aircraft Research Laboratories Report D-910091-9, prepared under Contract NASw-847, September 1965. To be issued as NASA CR report.

6. Kendall, J. S. and A. E. Mensing: Experimental Investigation of the Effect of Heavy-to-Light-Gas Density Ratio on Vortex Containment Characteristics. United Aircraft Research Laboratories Report UAR-E54, prepared under Contract NASw-847, April 1966. Paper presented at AIAA Second Propulsion Joint Specialists Conference, Colorado Springs, Colo., June 13-17, 1966.

7. Travers, A.: Experimental Investigation of Flow Patterns in Radial-Outflow Vortexes Using a Rotating-Peripheral-Wall Vortex Tube. United Aircraft Research Laboratories Report F-910091-10, prepared under Contract NASw-847, May 1967. To be issued as NASA CR report.

8. Johnson, B. V.: Exploratory Flow and Containment Experiments in a Directed-Wall-Jet Vortex Tube with Radial Outflow and Moderate Superimposed Axial Flows. United Aircraft Research Laboratories Report F-910091-11, prepared under Contract NASw-847, May 1967. To be issued as NASA CR report.

REFERENCES (Cont'd)

9. Clark, J. W., B. V. Johnson, J. S. Kendall, A. E. Mensing, and A. Travers: Summary of Gaseous Nuclear Rocket Fluid Mechanics Research Conducted under Contract NASw-847. United Aircraft Research Laboratories Report F-910091-13, prepared under Contract NASw-847, May 1967. To be issued as NASA CR report.

10. McLafferty, G. H., H. E. Bauer and D. E. Sheldon: Preliminary Conceptual Design Study of a Specific Vortex-Stabilized Gaseous Nuclear Rocket Engine. United Aircraft Research Laboratories Report E-910093-29, prepared under Contract NASw-847, September 1966. To be issued as NASA CR report.

11. McLafferty, G. H.: Summary of Investigations of a Vortex-Stabilized Gaseous Nuclear Rocket Concept. Air Force Systems Command Report RTD-TDR-63-1097, prepared by United Aircraft Research Laboratories, November 1963.

12. Mensing, A. E., and J. S. Kendall: Experimental Investigation of Containment of Gaseous Iodine in Jet-Driven Vortex. Air Force Systems Command Report RTD-TDR-63-1092, prepared by United Aircraft Research Laboratories, November 1963.

13. Anderson, O. L.: Theoretical Solutions for the Secondary Flow on the End Wall of a Vortex Tube. United Aircraft Research Laboratories Report R-2494-1, November 1961.

LIST OF SYMBOLS

A_j Light-gas injection area at vortex tube periphery, sq ft or sq in.

D Diameter of vortex tube, $2r_1$, ft or in.

h_s Vortex tube light-gas injection slot height (APPENDIX II), ft or in.

I Intensity of light transmitted through test section during a test, candles.

I_0 Intensity of light transmitted through test section immediately prior to the injection of iodine vapor into vortex tube, candles.

L Length of vortex tube, ft or in.

L/D Vortex tube length-to-diameter ratio, dimensionless.

p Partial pressure, lb/ft^2 or atm.

P Static pressure, lb/ft^2 or atm.

Q Volumetric flow rate, ft^3/sec.

Q_{P_1} Volumetric flow rate of light gas at vortex tube peripheral wall, ft^3/sec.

Q_z Volumetric flow rate through axial-flow annulus, ft^3/sec.

$\left(Q_F/Q_P\right)_{INJ}$ Heavy-to-light-gas volume flow rate ratio at injection, dimensionless.

r Radial distance from vortex tube centerline, ft or in.

r_1 Radius of vortex tube, ft or in.

Re_r Radial Reynolds number, $W_{P_{TF}}/2\pi\mu_{P_1}L$, dimensionless.

$Re_{t,j}$ Light-gas tangential injection Reynolds number, $\left(\rho_{P_1} V_{\phi,j} r_1\right)/\mu_{P_1}$, dimensionless.

$Re_{z,w}$ Axial-flow Reynolds number or equivalent axial-flow Reynolds number, $\left(\rho_{P_1} \bar{V}_{z,w} r_1\right)/\mu_{P_1}$, dimensionless.

t Time (APPENDIX III), sec.

t_I — Iodine time constant (APPENDIX III), sec.

t_{FC-77} — FC-77 time constant (APPENDIX III), sec.

t_F — Heavy-gas time constant (i.e., average heavy-gas dwell time), sec.

$t_{F_{MIN}}$ — Heavy-gas time constant for fully mixed flow (i.e., minimum average heavy-gas dwell time), $V/\left[Q_{P_1}\left\{ 1 + (Q_F/Q_P)_{INJ}\right\}\right]$, sec.

T — Temperature, deg F or deg R.

T_{P_1} — Temperature of light gas at injection into vortex tube (APPENDIX IV), deg F or deg R.

T_{F_1} — Temperature of heavy gas at injection into vortex tube (APPENDIX IV), deg F or deg R.

$V_{\phi,j}$ — Average tangential component of light-gas injection velocity, $W_{P_1} \cos \beta_j / \rho_{P_1} A_j$, ft/sec.

$\overline{V}_{z,w}$ — Average velocity through equivalent axial-flow annulus, $Q_z/(7/16)\pi r_1^2$ ft/sec.

V — Volume of vortex tube, $\pi r_1^2 L$, ft^3.

W — Weight flow rate, lb/sec.

W_P/W_F — Light-to-heavy-gas weight flow rate ratio, dimensionless.

$\mathcal{W}$ — Weight of gas stored in vortex tube, lb.

β_j — Angle between r-ϕ plane and centerline of directed-wall-jet insert (see sketch TABLE I), deg.

μ_{P_1} — Viscosity of light gas or simulated propellant at injection, lb/(sec-ft).

ρ — Density, lb/ft^3.

LIST OF SYMBOLS (Cont'd)

$\left(\bar{\rho}_{F_1}/\rho_{P_1}\right)_{MAX}$ Maximum value of heavy gas density ratio, dimensionless.

$\rho_{F_{INJ}}$ Density of heavy gas or simulated fuel at injection, lb/ft^3 (APPENDIX IV).

$\rho_{I_{STD}}$ Density of iodine vapor at 273 K and 760 mm Hg, assuming iodine vapor is a perfect gas, ($0.707\ lb/ft^3$).

ρ_{P_1} Density of light gas or simulated propellant at injection, lb/ft^3.

$\bar{\rho}_{F_1}$ Average density of heavy gas within vortex tube, $W_F/\pi r_1^2 L$, lb/ft^3.

$\bar{\rho}_{F_1}/\rho_{P_1}$ Heavy-gas or simulated-fuel density ratio, dimensionless.

T Total time for one vertical traverse of axial light beam (see APPENDIX III).

τ_{F_1} Dimensionless heavy-gas or simulated-fuel time constant, $t_F\ \mu_{P_1}/\rho_{P_1}\ r_1^2$, dimensionless.

$\tau_{F_1\ MIN}$ Dimensionless heavy-gas or simulated-fuel time constant for fully mixed flow, $t_{F_{MIN}}\mu_{P_1}/\rho_{P_1}\ r_1^2$, dimensionless.

$\tau_{F_1}/\tau_{F_1\ MIN}$ Heavy-gas containment parameter, dimensionless.

ϕ Azimuthal angle, deg.

Station Subscripts

1 Outer radius of vortex tube.

6 Edge of fuel-containment region.

INJ Injection location.

TF Thru-flow exhaust ducts.

LIST OF SYMBOLS (Cont'd)

Other Subscripts

F   Heavy gas or simulated fuel.

FC-77   Fluorocarbon.

I   Iodine vapor.

P   Light gas or simulated propellant.

APPENDIX I

SUMMARY OF TESTS OF BASIC VORTEX TUBES HAVING
MULTIPLE-FIXED-PORT LIGHT-GAS INJECTION

A description of containment tests for vortex flows having no superimposed axial flow is presented in this APPENDIX. Results are presented for both radial-outflow and radial-inflow vortex configurations.

Radial-Outflow Tests

Containment tests of vortexes with radial outflow in a basic vortex tube were conducted to provide a comparison with results of similar tests in an axial-flow vortex tube.

A multiple-fixed-port vortex tube having 4284 holes of 0.078-in.-dia was installed in the high Reynolds number test facility for these tests (Fig. 31). The light gas (air) was injected through two-thirds of the holes and was exhausted through the remaining one-third into four exhaust plenums spaced 90 deg apart around the peripheral wall (see Fig. 31). The heavy gas consisted of a mixture of FC-77 and iodine vapor and was injected into the vortex from a 1.0-in.-dia porous tube located on the vortex tube centerline.

Tests were conducted at tangential injection Reynolds numbers of $Re_{t,j} = 1.1 \times 10^5$, 1.9×10^5 and 2.8×10^5 with corresponding equivalent axial-flow Reynolds numbers of $Re_{z,w} = 4.0 \times 10^4$, 7.6×10^4 and 11.0×10^4. Results of heavy-gas containment tests are presented on Fig. 32 as the variation of containment parameter with heavy-gas density ratio. The containment parameter $(\tau_{F_1}/\tau_{F_1 MIN})$ increases with increasing equivalent axial-flow Reynolds number, i.e., with increasing light-gas weight flow rate (W_p is directly proportional to the equivalent axial-flow Reynolds number). These results are different from those reported in the main text of the report for vortexes with radial outflow and large superimposed axial flow; results of those tests showed that the containment parameter was independent of axial-flow Reynolds number and, hence, independent of light-gas weight flow (e.g., Figs. 12, 13 and 14). Comparable results from tests of a vortex configuration with radial outflow and no superimposed axial flow, but with single-slot light-gas injection (Ref. 4) are also presented in Fig. 32.

Radial-Inflow Tests

Containment tests were also conducted using a vortex with radial inflow and no superimposed axial flow. The primary purpose of these tests was to determine the maximum amount of heavy gas that can be stably contained in a vortex of this type. Results of previous tests (see Ref. 4) showed that, for some flow conditions, an instability occurred which caused a complete breakdown of the vortex flow pattern.

The high Reynolds number test facility was used for these tests, and the vortex tube employed was identical to that described in the preceeding paragraphs. Figure 33 presents a sketch and a photograph of the vortex-tube geometry for the radial-inflow tests. The radial-inflow configuration was different from the radial-outflow configuration in two respects: (1) in the radial-inflow configuration, a fraction of the total injected flow was withdrawn through ports located at the center of one or both end walls, whereas in the radial-outflow configuration, all of the injected flow was withdrawn through the peripheral wall; and (2) in the radial-inflow configuration, heavy gas was injected into the vortex tube through twelve 1/2-in.-long x 0.096-in.-ID tubes which were located around the periphery at the axial mid-plane of the vortex tube (see Fig. 33), whereas for the radial-outflow configuration, the heavy gas was injected through a porous tube located along the vortex tube centerline.

For tests employing a radial-inflow vortex configuration, the light-gas flow condition is specified in terms of the equivalent axial-flow Reynolds number $Re_{z,w}$, the tangential injection Reynolds number $Re_{t,j}$, and the radial Reynolds number Re_r. The radial Reynolds number is a measure of the weight flow rate of light gas removed through the thru-flow ports located at the centers of the end walls of the vortex tube (see Fig. 33). The radial Reynolds number, Re_r, is defined as

$$Re_r = \frac{W_{TF}}{2\pi \mu_{P_l} L} \tag{I-1}$$

where W_{TF} is the total light-gas weight flow through the thru-flow ports.

Results of tests to determine the effect of radial Reynolds number on the heavy-gas containment characteristics of vortexes with thru-flow removal at one or both ends of the vortex tube are presented in Fig. 34. For these tests, the tangential injection Reynolds number was 170,000 and the heavy-gas flow rate was approximately constant at 0.034 lb/sec. The results indicate that the differences between the data for thru-flow removal through one end wall and through both end walls were small for radial Reynolds numbers less than approximately 100. For radial Reynolds numbers greater than 150 and configurations having thru-flow re-

moval at only one end of the vortex tube, the measured values of containment para-
meter were approximately 15 percent greater than those obtained from the configura-
tion having two thru-flow ports.

The effect of radial Reynolds number on the radial distribution of heavy-gas
density is presented in Fig. 35 for tests with Re_r = 25, 50, 75 and 100. The
density distributions shown were obtained from the configuration with thru-flow re-
moval through one end wall (containment data for these tests were presented in
Fig. 34). For these tests, the heavy-gas flow rate was held constant. Different
radial distributions of heavy gas obtained at different radial Reynolds numbers can
be attributed to changes in the vortex convective flow patterns. The data presented
for radial Reynolds numbers of 25 and 50 indicate that the heavy gas was distributed
in an annular region between radius ratios of approximately 0.5 and 1.0. When the
radial Reynolds number was increased to 75, the heavy-gas annulus extended into the
central region of the vortex tube; increasing the radial Reynolds number to a value
of 100 resulted in more heavy gas stored near the center of the vortex tube and
less stored near the peripheral wall. The total heavy gas stored for Re_r equal to
75 and 100 was approximately the same.

Observations of a flow instability were reported in Ref. 4 for some flow con-
ditions employing a radial-inflow vortex. In the present program, tests were con-
ducted at Reynolds numbers which approximated those at which the instability was
observed (i.e., $Re_{t,j}$ = 170,000 and Re_r = 60). Visual observations of the
heavy-gas annulus in the vortex were made. An instability similar to that reported
in Ref. 4 was not observed. However, the vortex tube geometry employed in these
tests was not identical to that employed in the study of Ref. 4; a multiple-fixed-
port vortex tube was used in the present program and a single-slot-injection vortex
tube was used in Ref. 4. It is possible that the occurrence of this instability
was in some way related to the single-slot geometry which was employed in Ref. 4.

Additional radial-inflow tests were conducted with a radial Reynolds number of
100 and a tangential injection Reynolds number of 170,000. For these tests, the
primary variable was the heavy-gas weight flow rate. Results of these tests are
presented in Fig. 36 along with data from Ref. 4. The data presented in Fig. 36
indicate that the density ratios obtained with the vortex tube geometry used in the
present investigation were larger than those reported in Ref. 4.

29

APPENDIX II

SUMMARY OF TESTS OF VORTEX TUBES HAVING SINGLE-SLOT
LIGHT-GAS INJECTION

Description of Tests

The experiments described in this APPENDIX were conducted with vortex tubes having single-slot light gas injection. Most of the vortex test equipment used in these tests has been described in Refs. 4 and 5. The flow configuration employed was a radial-outflow vortex without superimposed axial flow. Five series of tests were conducted and included in the following:

1. Tests in the basic 10-in.-dia vortex tube to investigate the effect of the light-gas (i.e., simulated propellant) injection slot height on heavy-gas containment.

2. Tests in the basic 10-in.-dia vortex tube to investigate the effects of different density heavy gases (i.e., simulated fuel) on heavy-gas containment.

3. Tests in the 10-in.-dia vortex tube to investigate the effects of heavy-gas injection with and without a centerline porous tube on heavy-gas containment.

4. Tests in the basic 8-in.-dia vortex tube to investigate the effect of vertical and horizontal positioning of the vortex tube axis on heavy-gas containment.

5. Tests in a newly constructed 30-in.-dia vortex tube to investigate the effect of a large change in tube length-to-diameter ratio on heavy-gas containment.

Tests using the 10-in.-dia Vortex Tube

This vortex tube consisted of a cylindrical metal tube 30-in. long, to which end walls were attached. A sketch of the vortex tube is presented in Fig. 37. The light gas was injected through a tangential injection slot extending the entire length of the vortex tube; both light and heavy gases were withdrawn through a screen on the peripheral wall just upstream of the injection slot. Further details of this configuration are given in Ref. 4.

30

Previous tests (Refs. 4 and 5) in this vortex tube had been conducted with a light-gas injection slot height of 0.182 in. To determine if the injection slot height has any appreciable effect on the heavy gas containment characteristics additional tests were conducted with slot heights of 0.060 in. and 0.440 in. For each of the new configurations, heavy-gas time constants were determined at several values of tangential injection Reynolds number; at each Reynolds number several values of injected heavy-gas weight flow were used. For these tests the heavy gas was injected through a 1 1/4-in.-OD porous tube positioned concentric with the vortex tube (see Fig. 37).

Heavy-gas containment data from these tests along with data from Ref. 5 obtained with a 0.182-in.-high injection slot are presented in Fig. 38. These data show the variation of the containment parameter with the equivalent axial-flow Reynolds number.

The equivalent axial-flow Reynolds number is defined as that value of $Re_{z,w}$ that would exist if all the injected light gas were removed through an annulus extending from $r = 0.75 \, r_l$ to $r = r_l$ in one end wall. The relationship between the equivalent axial-flow Reynolds number and the tangential Reynolds number for the single injection slot vortex tube is,

$$Re_{z,w} = Re_{t,i} \left(\frac{h_s L}{(7/16) \pi r_l^2} \right) \tag{II-1}$$

The data presented in Fig. 38 were obtained for two different heavy-gas weight flow rates and at three different injection slot heights. It is evident from Fig. 38 that, for a given equivalent axial-flow Reynolds number, the containment parameter increased as the slot height decreased. Moreover, data obtained with the smaller injection slot heights showed an increase in heavy-gas containment with increasing Reynolds number. The reasons for this are not fully understood at present, but may be associated with an increase in tangential velocity (and hence circulation and circulation gradient) that occurs with decreasing slot heights at a given equivalent axial-flow Reynolds number.

A second series of tests was conducted to determine the containment characteristics of a vortex having small heavy-gas weight flows of different density heavy gases. The vortex configuration employed in these tests had a single, 0.18-in.-high light-gas injection slot; the heavy gas (i.e., simulated fuel) was injected through a 1 1/4-in.-dia porous tube positioned on the vortex tube centerline. These tests were similar to those discussed previously in this report (subsection entitled;

Results of Tests Employing Different Simulated Fuels in DISCUSSION OF RESULTS) except that the basic vortex tube configuration was used. The results of the tests are presented in Fig. 39 as the variation of the heavy-gas containment parameter with heavy-gas density ratio. The simulated fuel employed in these tests consisted of a mixture of iodine vapor and one of four other gases: viz., FC-75 (molecular weight of 416), sulphur hexafluoride (molecular weight of 146), nitrogen (molecular weight of 28), and helium (molecular weight of 4).

The most significant result shown by Fig. 39 is that, where overlapping occurred in the weight flows of two different density heavy gases, very little difference in the containment parameters was noted. Also, the containment parameter increased as the weight flow of the heavy gases was decreased. Values of the containment parameter of approximately 75 were achieved for some test configurations. In addition, visual observation of the vortex flow in the tests employing helium as the simulated fuel indicated a larger and less turbulent heavy-gas containment region.

In a third series of tests conducted in the 10-in.-dia, single-slot vortex tube, the heavy gas (FC-75 and iodine vapor) was injected directly into the vortex through 1.0-in.-dia holes at the centers of both end walls. Again the basic vortex tube configuration was used. The variation of heavy-gas containment parameter with heavy-gas density ratio for these tests is presented in Fig. 40, and for comparison, some data from Fig. 39 have been included. The data presented in Fig. 40 indicate that for this configuration (i.e., no superimposed axial flow) the containment parameters obtained from tests with heavy-gas injection through a centerline porous tube were 20 to 80 percent larger than those obtained with heavy-gas injection through the end walls.

Tests in the 8-in.-dia Vortex Tube

A series of tests were conducted to investigate the effects of vortex tube orientation on heavy-gas containment characteristics. For radial-outflow vortexes, the buoyancy force due to gravity may have an adverse effect on the heavy-gas containment characteristics. To investigate this possibility, tests using the vortex tube shown in Fig. 41 were conducted with the axis of the vortex tube both vertical and horizontal. (Additional details of the vortex tube employed in these tests are given in Ref. 12, the instrumentation techniques are described in Ref. 4.) The heavy gas was a mixture of FC-75 and iodine vapor and was injected through a 1 1/4-in.-OD porous tube located on the vortex tube centerline.

Tests were made at several heavy-gas flow rates and at several light-gas injection Reynolds numbers. The results of these tests are presented in Fig. 42 and, within the scatter of the data, no change in the heavy-gas containment character-

istics due to the orientation of the vortex tube is evident. This result is in agreement with a similar result reported in Ref. 8 for a directed-wall-jet vortex tube with superimposed axial flow.

Tests using a 30-in.-dia Vortex Tube

A series of tests were conducted in a specially constructed 30-in.-dia vortex tube. This vortex tube was formed by separating the 10-in.-dia vortex tube from the light-gas injection plenum and replacing it with a piece of sheet metal rolled into a 30-in.-dia tube. Plexiglass end walls were clamped to the end of the rolled sheet metal tube. The light-gas injection and exhaust system used in the 10-in.-dia vortex tube were also employed with this vortex tube. A photograph of the 30-in.-dia vortex tube is shown in Fig. 43.

The primary objective of using these tests was to determine the effect of vortex tube diameter on heavy-gas containment characteristics. The tests were conducted with air as the light gas injected through a 0.190-in.-high slot at the periphery and with the heavy gas injected through a 1 1/4-in.-OD porous tube positioned concentric with the vortex tube. The air was injected at a velocity of 135 ft/sec resulting in an injection Reynolds number of 530,000. (In a 10-in.-dia vortex tube this velocity corresponded to an injection Reynolds number of 180,000.) The variation of containment parameter with heavy-gas density ratio for these tests is presented in Fig. 44. The results are similar to those obtained from previous tests. However, the containment parameters are somewhat less than those from comparable tests with the 10-in.dia vortex tube.

Based on visual observations of the heavy-gas cloud, the velocities near the center of the vortex were extremely low for the 30-in.-dia vortex, and hence buoyancy forces caused by gravity were adversly effecting the heavy-gas distribution in the central region of the vortex. Since this phenomena was not observed in the 10-in.-dia vortexes, it is possible that the lower values of the heavy-gas containment parameter were caused by combined effects of low angular velocity and gravity.

APPENDIX III

DETERMINATION OF THE AMOUNT OF HEAVY GAS STORED WITHIN THE VORTEX TUBE

A data acquisition system based on the principle of light absorption by iodine vapor was used to determine the total amount of heavy gas stored within the vortex tube during containment tests.

Description of Axial Absorptometer

The principal components of the axial absorptometer are shown schematically in Fig. 7. It consists of a 100 watt zirconium arc lamp located at the focal plane of two 6-in.-dia f/8 parabolic mirrors, a beam selector and scanner, plane mirrors on each of the vortex-tube end walls, a 15-in.-dia f/1.5 focusing lens, an interference filter (40 $\overset{\circ}{A}$ half-width with peak transmission at 5250 $\overset{\circ}{A}$), and an RCA 6655A photo-multiplier tube. Light from the arc lamp reflects from the parabolic mirrors to form two 6-in.-dia parallel light beams. The light beams strike the beam selector, a flat plate on the scanner which has two small (approximately 3/16-in.-dia) holes drilled $5\frac{1}{2}$ in. apart. Light passing through this plate is in two narrow collimated light beams. The diameter of each light beam can be adjusted by an iris on the plate, and a sliding shutter is used to alternately block the light of each beam. The narrow light beams pass axially through the vortex tube and the focusing lens to the photomultiplier tube.

The scanner consists of an electric motor with a gear reduction unit that drives a cam upon which the selector plate rides. The cam (shown in Fig. 45) was designed such that a uniform angular displacement results in vertical motion of the selector plate proportional to the square of the distance traveled. Figure 45 shows the vertical displacement of the selector plate as a function of the angular displacement of the cam. In this way, the two narrow light beams passing through the plate traverse radially with a speed proportional to the square of their radial distance from the vortex tube centerline. The scanner is adjusted so that one light beam traverses along a vertical radius above the centerline; its shutter is then closed, the other light beam shutter opens, and this beam traverses along a vertical radius below the centerline. The process is then repeated. The light beam shutters are opened and closed automatically by a signal from an auxiliary photomultiplier tube. The optical system was aligned such the narrow light beams were parallel to the vortex tube centerline at all times.

Analysis

As the light beam passes through the vortex tube, its intensity will be reduced due to absorption by the iodine vapor present in the optical path. In Ref. 12, the expression relating the density of the iodine vapor to the fraction of light transmitted is shown to be

$$\rho_I = \left(\frac{-\rho_{I_{STD}}}{1 - e^{-553/T}} \right) \left(\frac{\ln I/I_0}{3660L} \right) \qquad \text{(III-1)}$$

where I is the intensity of light transmitted through the vortex tube during a test and I_0 is the intensity of light transmitted immediately prior to the injection of iodine vapor. The iodine density calculated from Eq. (III-1) is an average density over the length, L. The iodine vapor does not have to be uniformly distributed along the optical path length because the fraction of light transmitted is proportional only to the total number of absorbing iodine molecules in the optical path.

The radial variation of light intensity was obtained by traversing the light beam radially and recording the subsequent photomultiplier tube output (which was proportional to the light intensity). For the data reported herein the variation of I_0 with radius was obtained by traversing the light beams across the vortex tube without iodine present, but with the light-gas flow established (see section entitled TEST PROCEDURES). The intensity of the light beam with iodine present, I, was then obtained in the same manner, with heavy gas flowing. Figure 46 presents typical photomultiplier output records as the light beams were traversed radially. From the known relationship between the cam rotation and radial position of the light beam (i.e., from Fig. 45) and the traces of I and I_0, the axially averaged iodine density as a function of radius can be obtained using Eq. (III-1).

The amount of iodine vapor stored within the vortex, $\mathcal{W}_I$, is

$$\mathcal{W}_I = \int_V \rho_I \, dv$$

and since

$$\mathcal{W}_I = \pi L \int_{r=0}^{r=r_1} \rho_I \, d(r^2) \qquad \text{(III-2)}$$

35

Combining Eqs. (III-1) and (III-2),

$$W_I = -\frac{\pi}{3660}\left(\frac{\rho_{I_{STD}}}{1-e^{-553/T}}\right)\int_{r=0}^{r=r_1}(\ln I/I_0)\,d(r^2)$$

or

$$W_I = -\frac{\pi}{3660}\left(\frac{\rho_{I_{STD}}}{1-e^{-553/T}}\right)\left\{\int_{r=0}^{r=r_1}(\ln I)\,d(r^2)-\int_{r=0}^{r=r_1}(\ln I_0)\,d(r^2)\right\} \qquad \text{(III-3)}$$

Since uniform angular displacement of the cam on the scanner produces a displacement of the light beam proportional to the square of its radial location, and since the cam turns at constant speed, then the time of travel as a function of radial position is

$$t = ar^2 + b$$

with conditions that at $t = 0$, $r = r_1$ and at $t = T$, $r = 0$, where T is the total time of traverse. Thus,

$$t = T\left[1-\left(\frac{r}{r_1}\right)^2\right]$$

Then

$$d(r^2) = -\frac{r_1^2}{T}\,dt \qquad \text{(III-4)}$$

Substituting Eq. (III-4) into Eq. (III-3),

$$W_I = \frac{\pi r_1^2}{3660T}\left(\frac{\rho_{I_{STD}}}{1-e^{-553/T}}\right)\left\{\int_{t=0}^{t=T}(\ln I_0)\,dt-\int_{t=0}^{t=T}(\ln I)\,dt\right\} \qquad \text{(III-5)}$$

The advantage of expressing W_I in the form given by Eq. (III-5) is that the integration can now be performed electronically. Signals from the photomultiplier tube (i.e., first I_0, then I) go into a log amplifier. The output signal then goes into an electronic integrator and the integrator

36

output signal is recorded. Starting and stopping of the integrators is done by the auxiliary photomultiplier tube which is also used to control the light beam shutters. Thus, by knowing the time of integration (which can be set by controlling the cam speed), the amount of iodine vapor stored within the vortex is proportional to the difference of the two integrals (see Eq. (III-3)).

To calculate the iodine time constant, t_I , both the amount of iodine vapor stored within the vortex and the iodine vapor flow rate must be determined. The former is obtained from Eq. (III-5), and the iodine vapor flow rate is obtained from an iodine absorptometer positioned on the heavy-gas injection duct just upstream of the vortex tube. The iodine absorptometer is similar to that described in APPENDIX I of Ref. 4, but differs in that the one employed in this study had an optical path length of 1.125-in. and the gas flowing through the duct was only heavy gas. For most tests the heavy gas was a mixture of FC-77 and iodine vapor (see text).

The density of iodine vapor passing through the absorptometer is (from APPENDIX I of Ref. 4)

$$\rho_I = \left(\frac{-\rho_{I_{STD}}}{1 - e^{-553/T}} \right) \left(\frac{\ln I/I_0}{344} \right) \qquad \text{(III-6)}$$

where I/I_0 is the fraction of light transmitted through the iodine vapor.

Since the iodine vapor and FC-77 vapor were premixed (see text), the volume flow rate of each flowing through the duct were equal. Thus,

$$w_I = \rho_I \left(\frac{w_{FC-77}}{\rho_{FC-77}} \right) \qquad \text{(III-7)}$$

w_{FC-77} is the weight flow rate of the FC-77 and is measured by a turbine flow meter prior to mixing with the iodine vapor. ρ_{FC-77} is the density of FC-77 as it flows through the absorptometer; and, since the partial pressure of the iodine vapor in the duct is small, ρ_{FC-77} is calculated from the measured pressure and temperature in the duct at the absorptometer.

The iodine vapor time constant is calculated from Eqs. (III-5) and (III-7). It is assumed that the heavy-gas time constant is equal to the iodine time constant (there are no forces to cause any appreciable separation between the iodine vapor and the FC-77 once they are mixed together).

Then,

$$t_F = t_I = t_{FC-77}$$

and
$$\mathscr{W}_F = t_F \, w_F = t_I \left(w_I + w_{FC-77} \right)$$

or
$$\mathscr{W}_F = \mathscr{W}_I \left(1 + \frac{w_{FC-77}}{w_I} \right) \qquad\qquad (III-8)$$

$\mathscr{W}_I$ is obtained from Eq. (III-5), w_I from Eq. (III-7), and w_{FC-77} is measured. Eq. (III-8) gives the total amount of heavy gas stored within the vortex tube during steady-state operation.

APPENDIX IV

RELATIONS BETWEEN DIMENSIONLESS AND DIMENSIONAL VORTEX FLOW PARAMETERS

The data described in the present report were obtained in vortex tubes with a constant peripheral-wall radius and with L/D ratios of 1, 2 and 3. The length and volume for these vortex tubes are:

L/D	Radius, r_l	Length, L	Volume, V
1	0.416 ft	0.833 ft	0.45 ft^3
2	0.416 ft	1.667 ft	0.91 ft^3
3	0.416 ft	2.500 ft	1.36 ft^3

The approximate properties of the simulated-propellant and simulated-fuel gases at injection into the vortex tube are:

Property	Simulated-Propellant	Simulated Fuel
Gas	Air	Fluorocarbon, FC-77
Temperature	$T_{P_l} = 300$ F	$T_{F_l} = 320$ F
Pressure	P = 13.5 psia	P = 13.5 psia
Density	$\rho_{P_l} = 0.048$ lb/ft^3	$\rho_{F_{INJ}} = 0.643$ lb/ft^3
Viscosity	$\mu_{P_l} = 1.57 \times 10^{-5}$ lb/sec ft	

To use these model performance results in full-scale engine performance studies and to compare the present results with previous and concurrent heavy-gas containment tests, the containment results for a given configuration are presented in terms of three dimensionless parameters. Typical values from test data for a vortex tube with L/D = 1.0 are:

Heavy-gas density ratio, $\bar{\rho}_{F_l}/\rho_{P_l} = 0.2$
Containment parameter, $\tau_{F_l}/\tau_{F_l \, MIN} = 10$
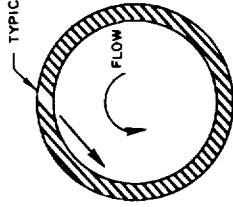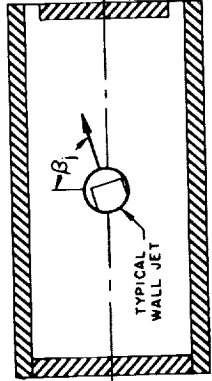Axial-flow Reynolds number, $Re_{z,w} = 300,000$

These dimensionless parameters are converted to dimensional parameters in the following table.

Symbol	Parameter	Equation for Conversion	Sample Calculation
$\mathcal{W}_P$	Light gas stored	$\approx V \rho_{P_l}$	$(0.45)(0.048) = 0.022$ lb
$\mathcal{W}_F$	Heavy gas stored	$(\bar{\rho}_{F_l}/\rho_{P_l}) V \rho_{P_l}$	$(0.2)(0.45)(0.048) = 0.0043$ lb
w_P	Light-gas-flow rate	$Re_{z,w}\left[(7/16)\pi r_l \mu_{P_l}\right]$	$300{,}000\left[(7/16)\pi(0.416)1.57 \times 10^{-5}\right] = 2.69$ lb/sec
w_F	Heavy-gas flow rate	$\left[(\bar{\rho}_{F_l}/\rho_{P_l})/(\tau_{F_l}/\tau_{F_{l\,MIN}})\right] w_P$	$\dfrac{0.2}{10}\ (2.69) = 0.054$ lb/sec
w_P/w_F	Ratio of light-gas flow rate to heavy-gas flow rate	$(\tau_{F_l}/\tau_{F_{l\,MIN}})/(\bar{\rho}_{F_l}/\rho_{P_l})$	$\dfrac{10}{0.2} = 50$
$\mathcal{W}_F/\mathcal{W}_P$	Ratio of heavy gas stored to light gas stored	$\approx \bar{\rho}_{F_l}/\rho_{P_l}$	$0.2 = 0.2$
$t_{F_{MIN}}$	Approximate dwell time of simulated propellant	$V \rho_{P_l} / w_P$	$(0.45)(0.048)/(2.69)$ $= 0.008$ sec
t_F	Dwell time of simulated fuel	$(\tau_{F_l}/\tau_{F_{l\,MIN}}) t_{MIN}$	$(10)(0.008) / 0.08$ sec

40

TABLE I

Summary of Vortex Tube Geometries
Employed in Tests Discussed in Main Text
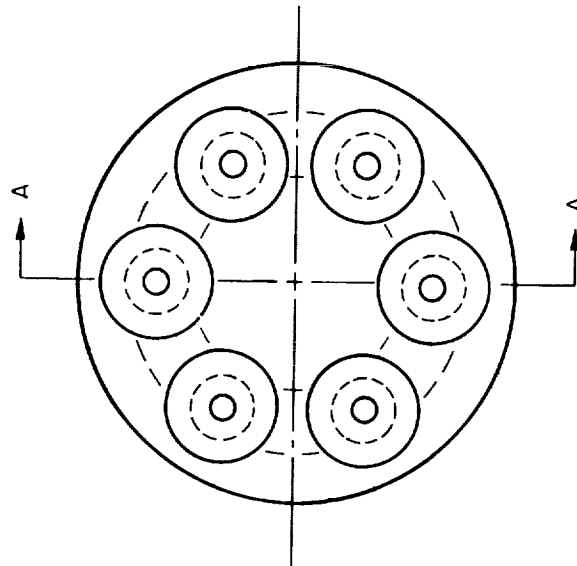
Diameter of Vortex Tubes, D = 10 in.

VORTEX TUBE PERIPHERAL WALL CONFIGURATION	DESCRIPTION OF INJECTION CONFIGURATION	TOTAL INJECTION AREA, AJ - SQ IN.	LENGTH-TO-DIAMETER RATIO, L/D
MULTIPLE-FIXED-PORT See Fig. 9 (r-φ PLANE) TYPICAL PORT, FLOW	1) 4284 ports (36 lengthwise rows of 119 ports), dia = 0.062 in., β_j = 0 deg	13.1	3.0
	2) 4284 ports (36 lengthwise rows of 119 ports), dia = 0.078 in., β_j = 0 deg	20.5	3.0
	3) 4284 ports (36 lengthwise rows of 119 ports), dia = 0.108 in., β_j = 0 deg	40.2	3.0
	4) 1428 ports (36 lengthwise rows of 40 ports), dia = 0.108 in., β_j = 0 deg	13.3	1.0
DIRECTED-WALL-JET See Figs. 10 and 11 (r-z PLANE) TYPICAL WALL JET	1) 300 directable wall jets (10 lengthwise rows of 30 jets) β_j = 0 to 63.5 deg, slot width = 0.5 in., slot height = 0.045 to 0.100 in.	11.0	3.0
	2) 900 directable wall jets (30 lengthwise rows of 30 jets) β_j = 0 to 63.5 deg, slot width = 0.5 in., slot height = 0.045 to 0.100 in.	32.2	3.0
	3) 600 directable wall jets (20 lengthwise rows of 30 jets) β_j = 0 to 63.5 deg, slot width = 0.5 in., slot height = 0.045 to 0.100 in.	21.5	2.0
	4) 300 directable wall jets (10 lengthwise rows of 30 jets) β_j = 0 to 63.5 deg, slot width = 0.5 in., slot height = 0.045 to 0.100 in.	11.0	1.0

41

SCHEMATIC OF VORTEX-STABILIZED OPEN-CYCLE GASEOUS NUCLEAR ROCKET ENGINE

FIG. I

PRESSURE SHELL NOT SHOWN

MODERATOR-REFLECTOR

EXHAUST NOZZLE
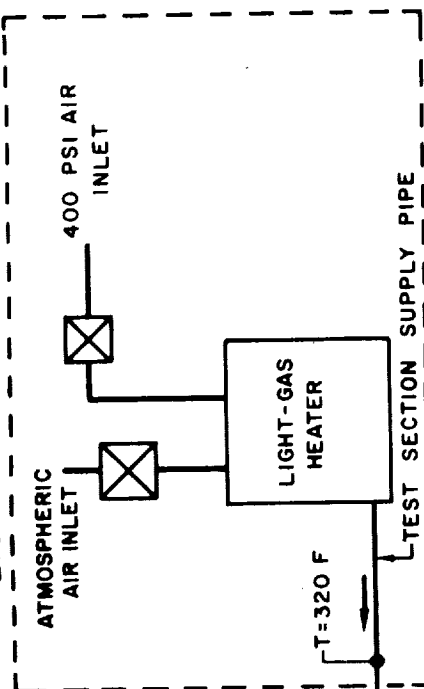
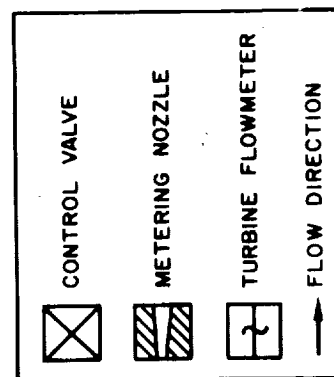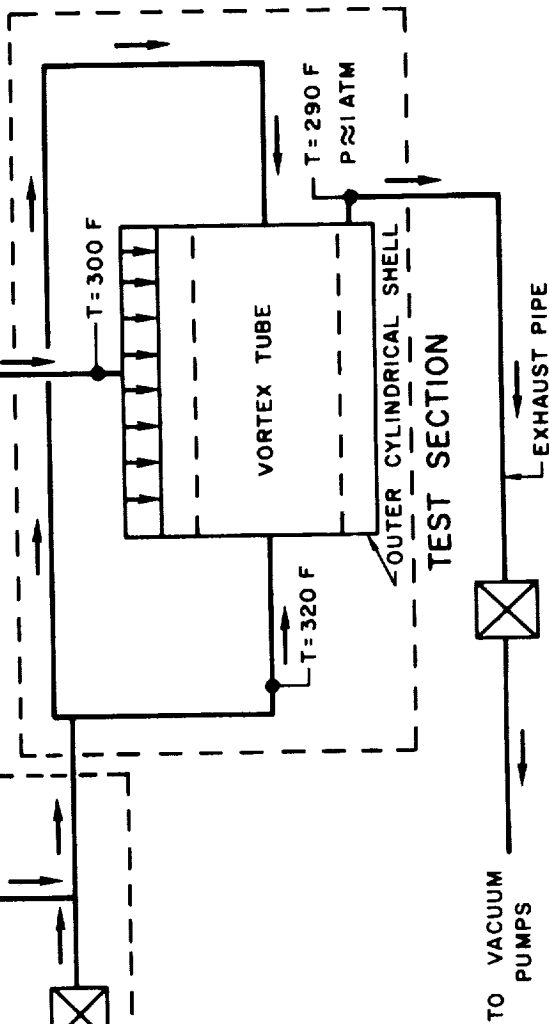PROPELLANT REGION

FUEL INJECTION PORT

FUEL REGION

SECTION A-A

42
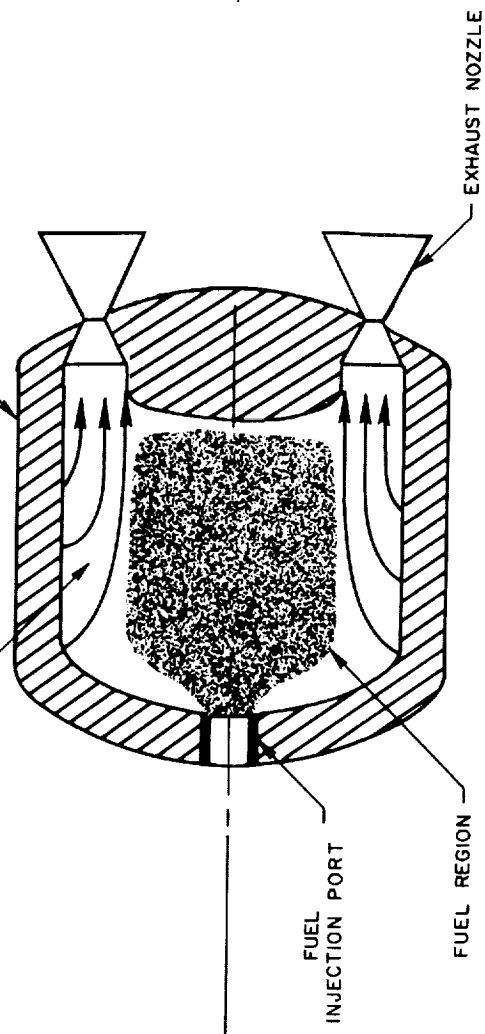
FIG. 2

SCHEMATIC DIAGRAM OF FLOW SYSTEM
IN HIGH REYNOLDS NUMBER TEST FACILITY

Legend:
- CONTROL VALVE
- METERING NOZZLE
- TURBINE FLOWMETER
- FLOW DIRECTION

LIGHT-GAS SUPPLY SYSTEM

400 PSI AIR INLET

ATMOSPHERIC AIR INLET

LIGHT-GAS HEATER

TEST SECTION SUPPLY PIPE

T=320 F

T=300 F

T=290 F
P≈1 ATM

VORTEX TUBE

OUTER CYLINDRICAL SHELL

TEST SECTION

T=320 F

EXHAUST PIPE

TO VACUUM PUMPS

CARRIER-GAS SUPPLY SYSTEM

HEAVY-GAS SUPPLY SYSTEM

HEAVY-GAS BOILER
T=325 F

IODINE BOILER

43

FIG. 3
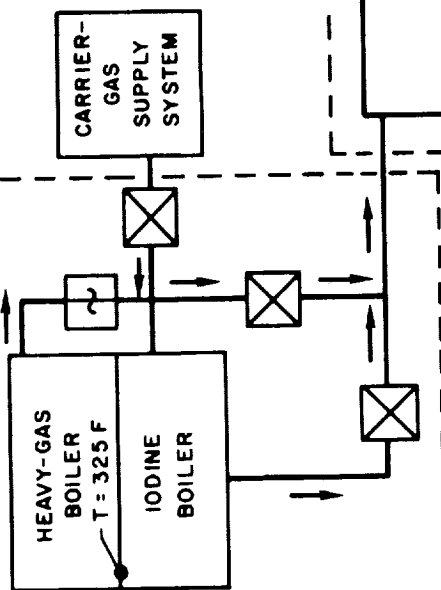
PHOTOGRAPH OF LIGHT-GAS SUPPLY SYSTEM
SEE FIG. 2 FOR SCHEMATIC DIAGRAM

400 PSI AIR INLET

LIGHT-GAS HEATER

TEST SECTION SUPPLY

CONTROL VALVE

ATMOSPHERIC AIR INLET
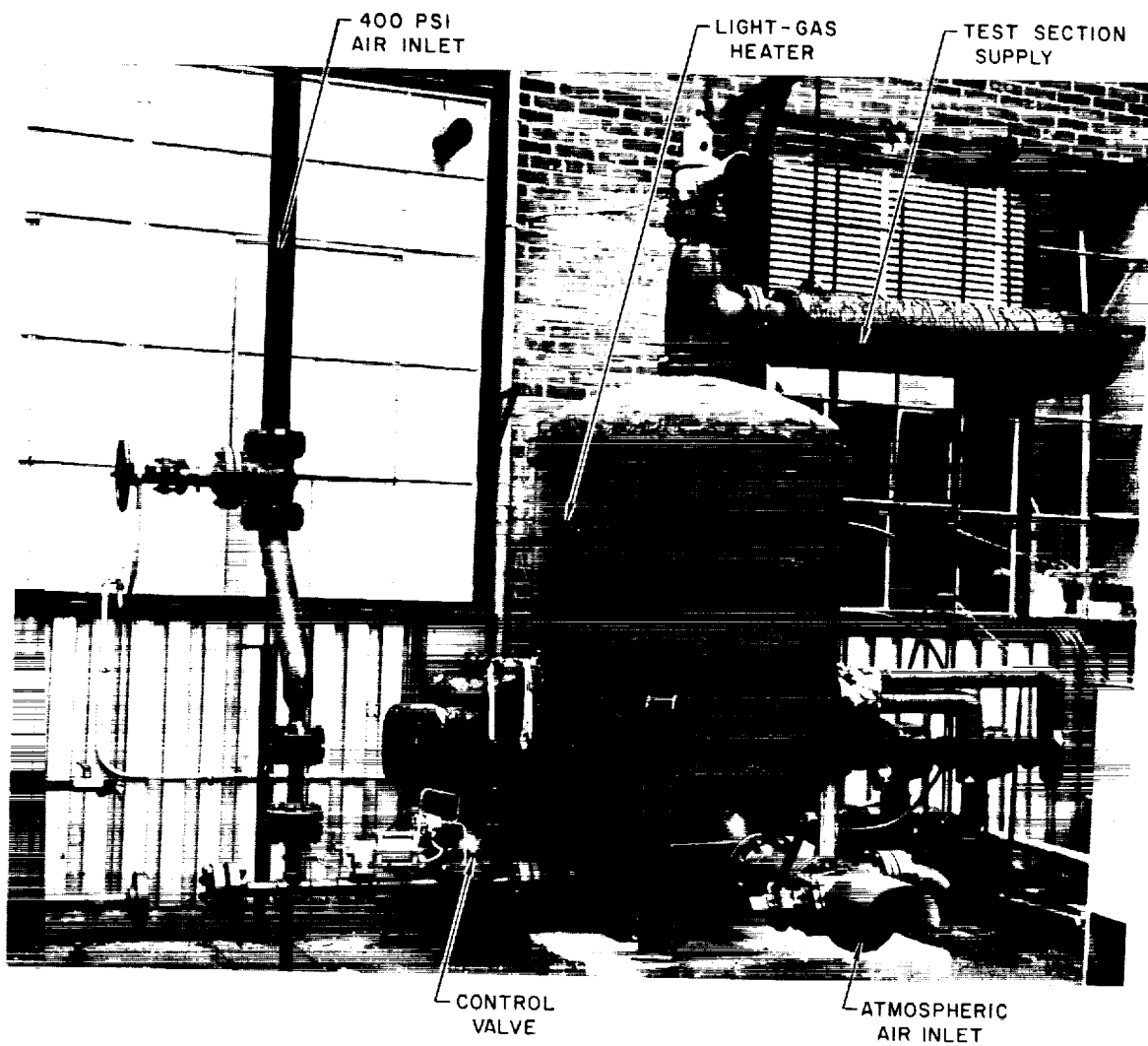
FIG. 4

PHOTOGRAPH OF HEAVY-GAS SUPPLY SYSTEM

SEE FIG 2 FOR SCHEMATIC DIAGRAM

CONTROL VALVES

IODINE BOILER

TURBINE FLOWMETERS

HEAVY-GAS BOILER

20"
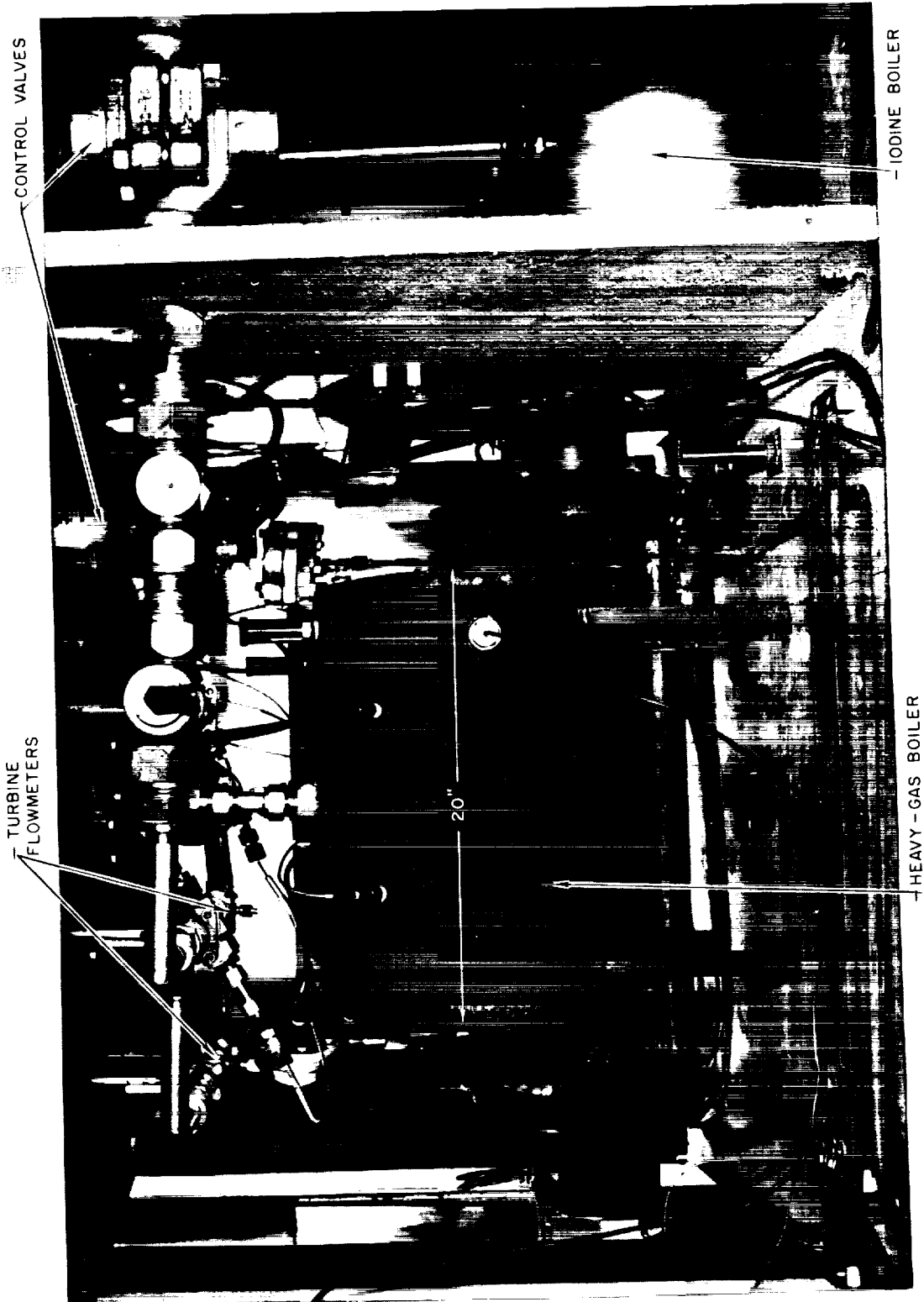
PHOTOGRAPH OF TEST SECTION

SEE FIG. 2 FOR SCHEMATIC DIAGRAM

BASIC VORTEX CONFIGURATION (NO SUPERIMPOSED AXIAL FLOW)

EXHAUST PIPES

TEST SECTION SUPPLY PIPES

POROUS TUBE (USED FOR SOME TESTS)

VORTEX TUBE

OUTER CYLINDRICAL SHELL

FIG. 5

46

FIG. 6

PHOTOGRAPH OF HIGH REYNOLDS NUMBER
TEST FACILITY CONTROL CONSOLE

9 FT
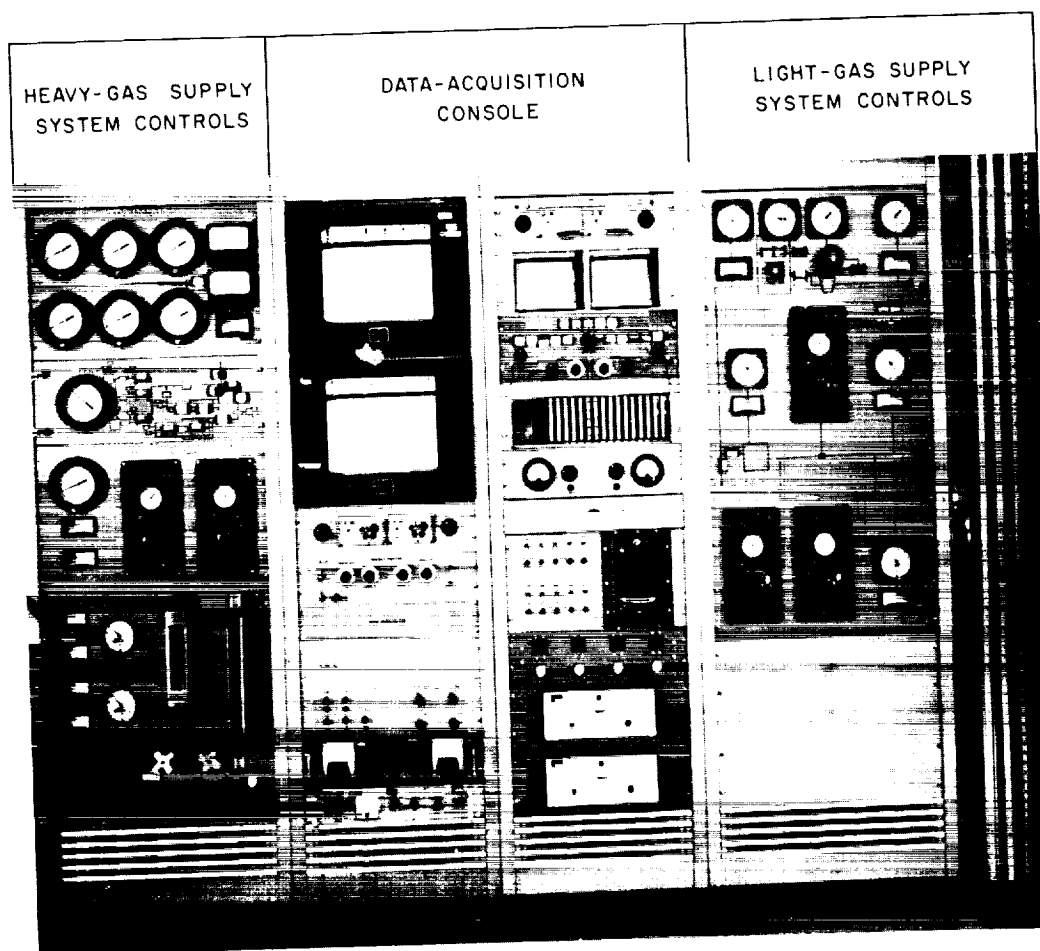
SCHEMATIC DIAGRAM OF AXIAL ABSORPTOMETER

AXIAL-FLOW VORTEX CONFIGURATION

LIGHT BEAM TRAVERSES PERPENDICULAR TO PLANE OF THIS VIEW

TOP VIEW

FIG. 7

48
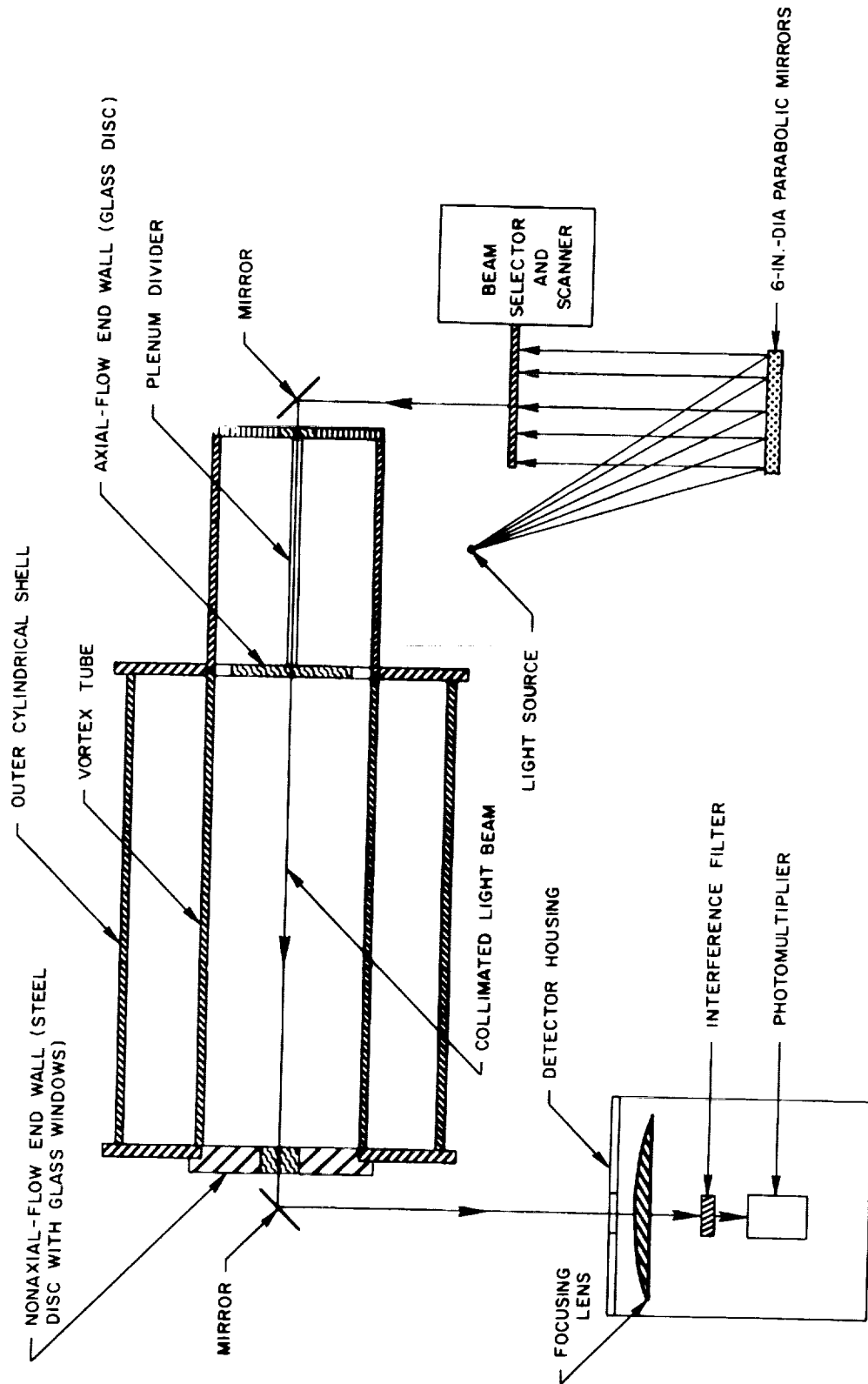
GEOMETRY OF AXIAL-FLOW VORTEX CONFIGURATION

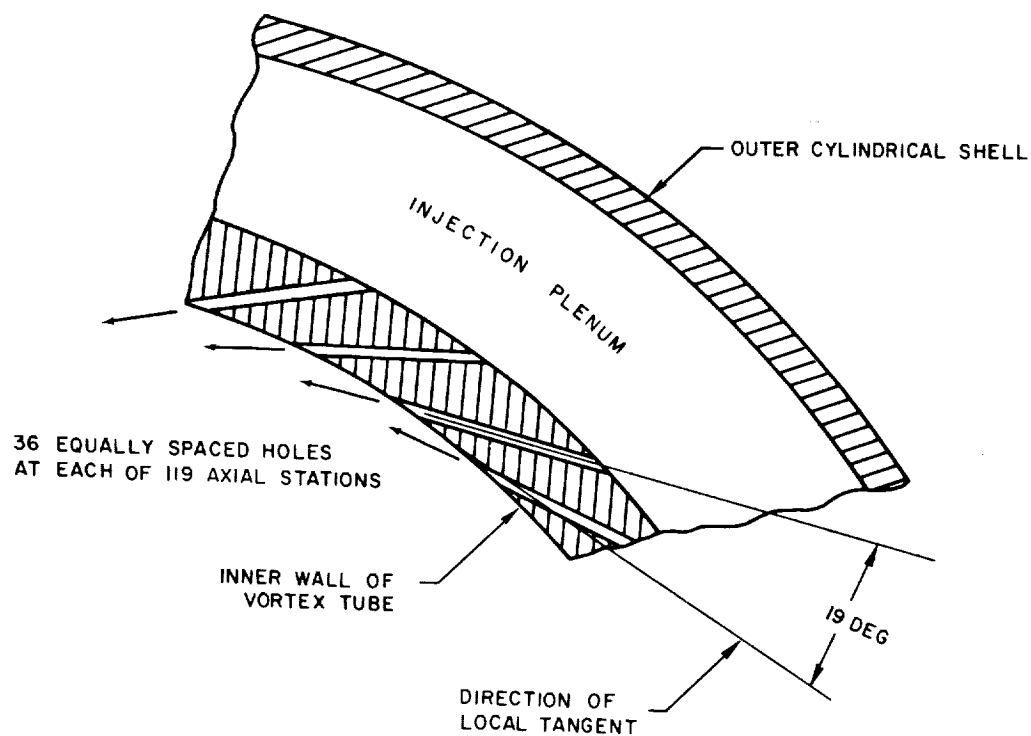DETAILS OF LIGHT-GAS INJECTION GEOMETRY NOT SHOWN; SEE FIGS. 9 AND 10
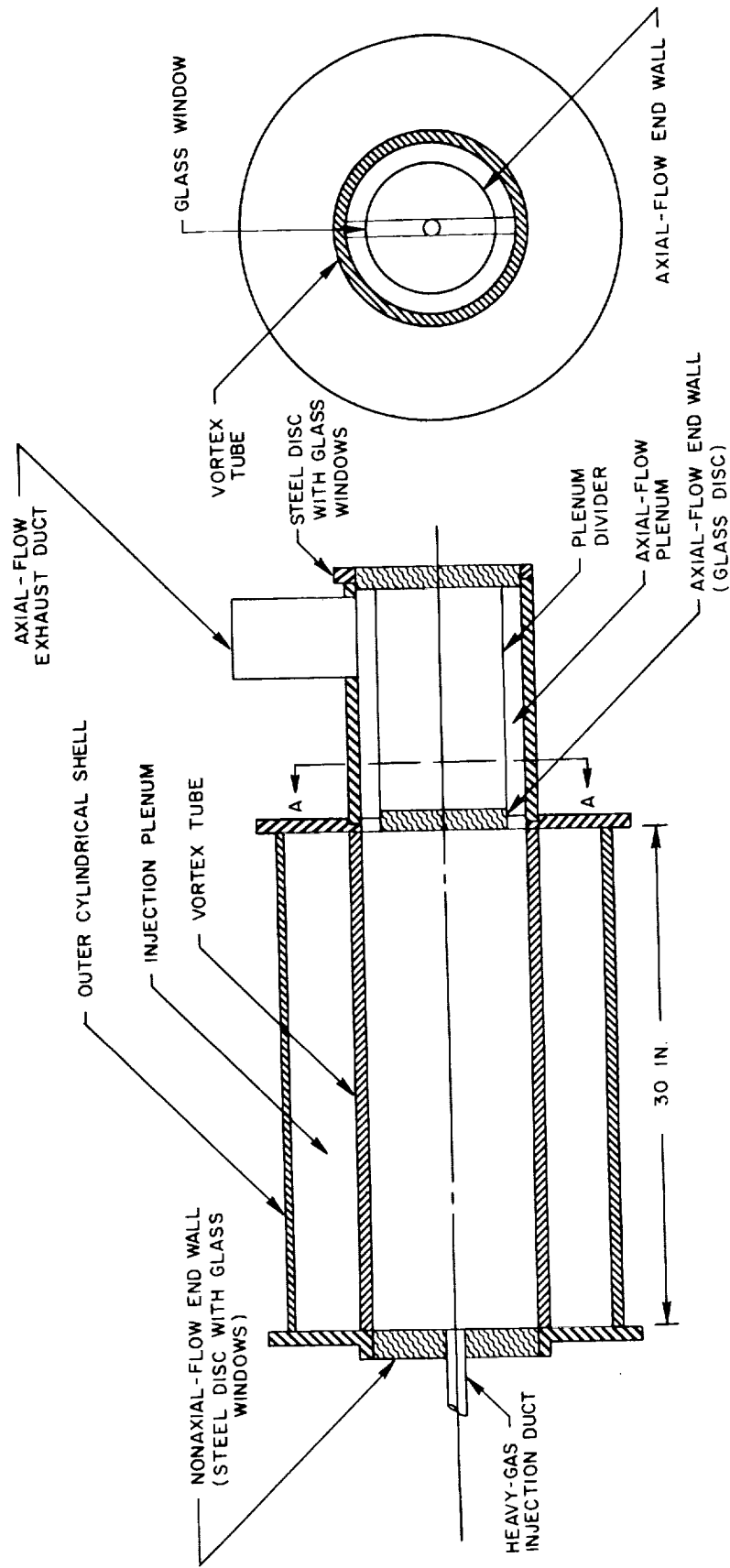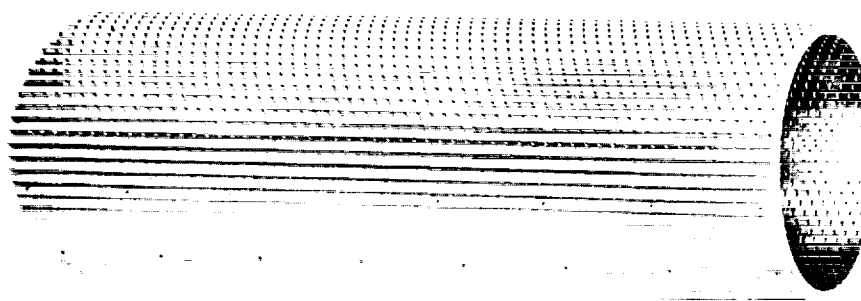
FIG. 8

SECTION A-A

SIDE VIEW

49

FIG. 9

LIGHT-GAS INJECTION GEOMETRY FOR MULTIPLE-FIXED-PORT VORTEX TUBES

a) SCHEMATIC OF INJECTION GEOMETRY

OUTER CYLINDRICAL SHELL

INJECTION PLENUM

36 EQUALLY SPACED HOLES
AT EACH OF 119 AXIAL STATIONS

INNER WALL OF
VORTEX TUBE

19 DEG

DIRECTION OF
LOCAL TANGENT

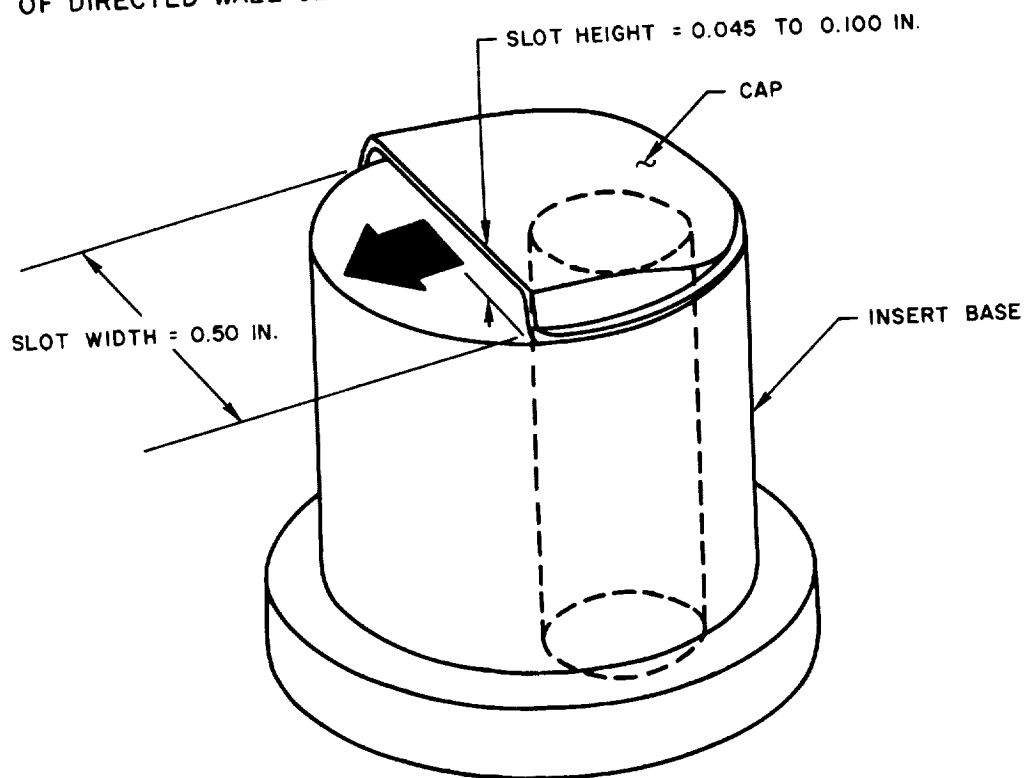b) PHOTOGRAPH OF TYPICAL MULTIPLE-FIXED-PORT VORTEX TUBE

LENGTH, L = 30 IN.

DIAMETER, D = 10 IN.

50

FIG. 10

LIGHT-GAS INJECTION GEOMETRY FOR DIRECTED-WALL-JET VORTEX TUBE

a) SCHEMATIC OF INJECTION GEOMETRY

DIRECTED-WALL-JET INSERT

OUTER CYLINDRICAL SHELL

INJECTION

PLENUM

INNER WALL OF
VORTEX TUBE

INSERT MAY BE ROTATED
FULL 360 DEG
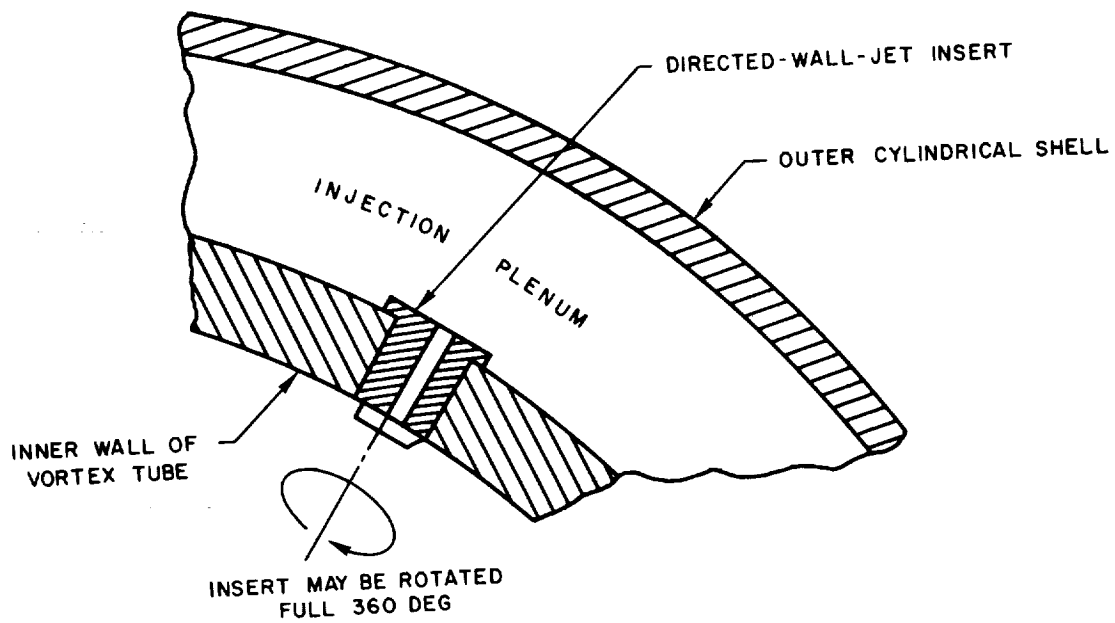
b) DETAILS OF DIRECTED-WALL-JET INSERT

SLOT HEIGHT = 0.045 TO 0.100 IN.

CAP

SLOT WIDTH = 0.50 IN.

INSERT BASE

51

FIG. II

PHOTOGRAPH OF DIRECTED-WALL-JET VORTEX TUBE
PARTIALLY ASSEMBLED

INJECTION PLENUM DIVIDER

DIRECTED-WALL-JET INSERTS

AXIAL-FLOW EXHAUST

AXIAL-FLOW PLENUM

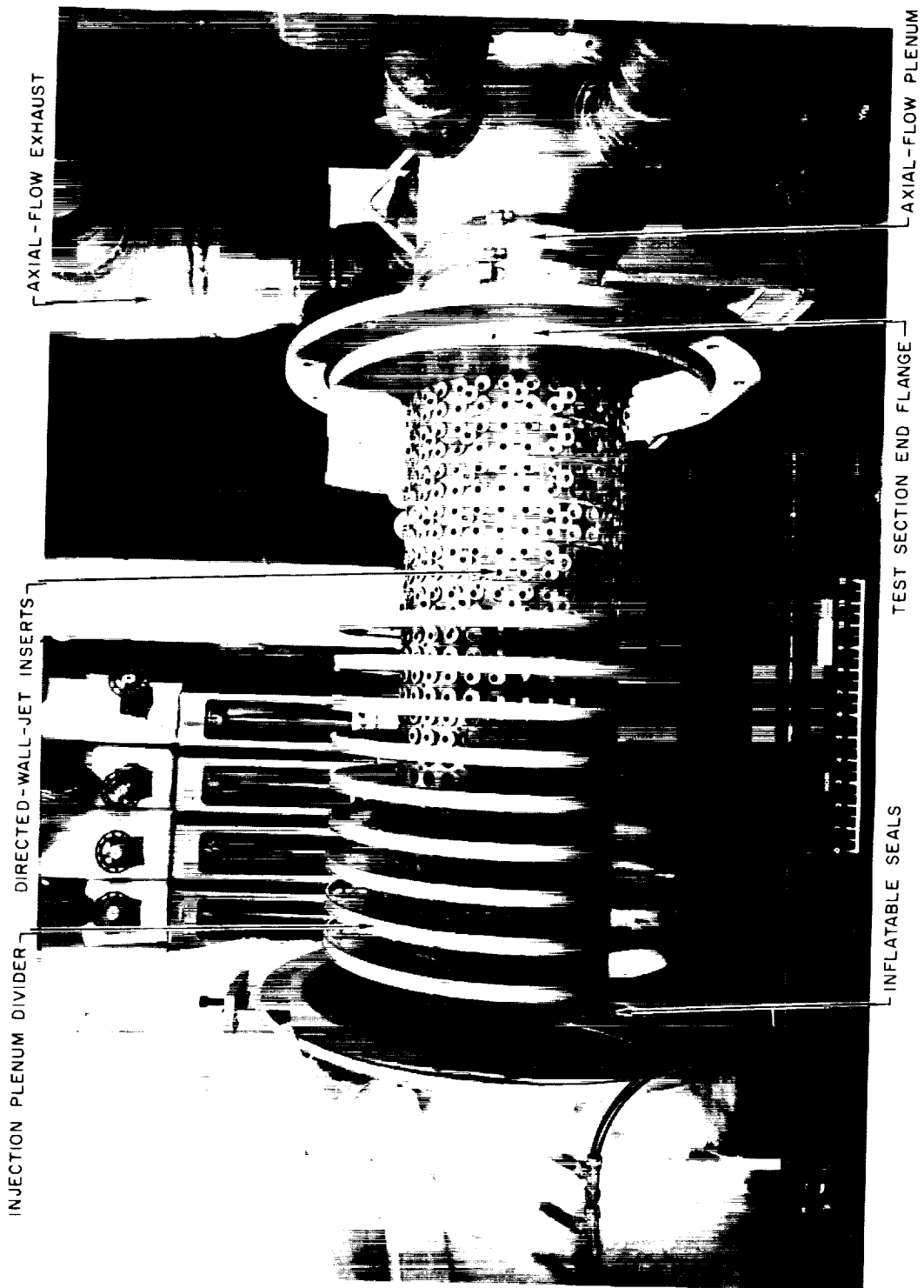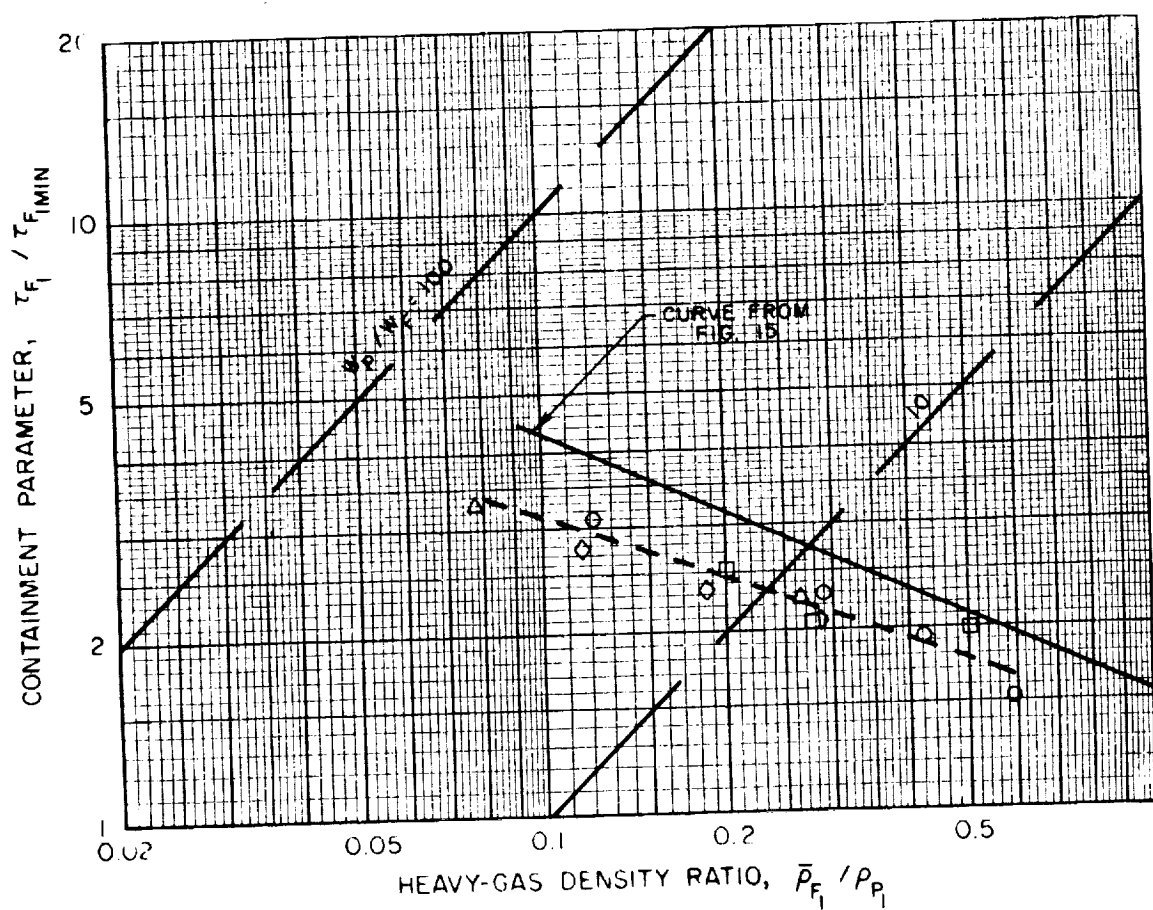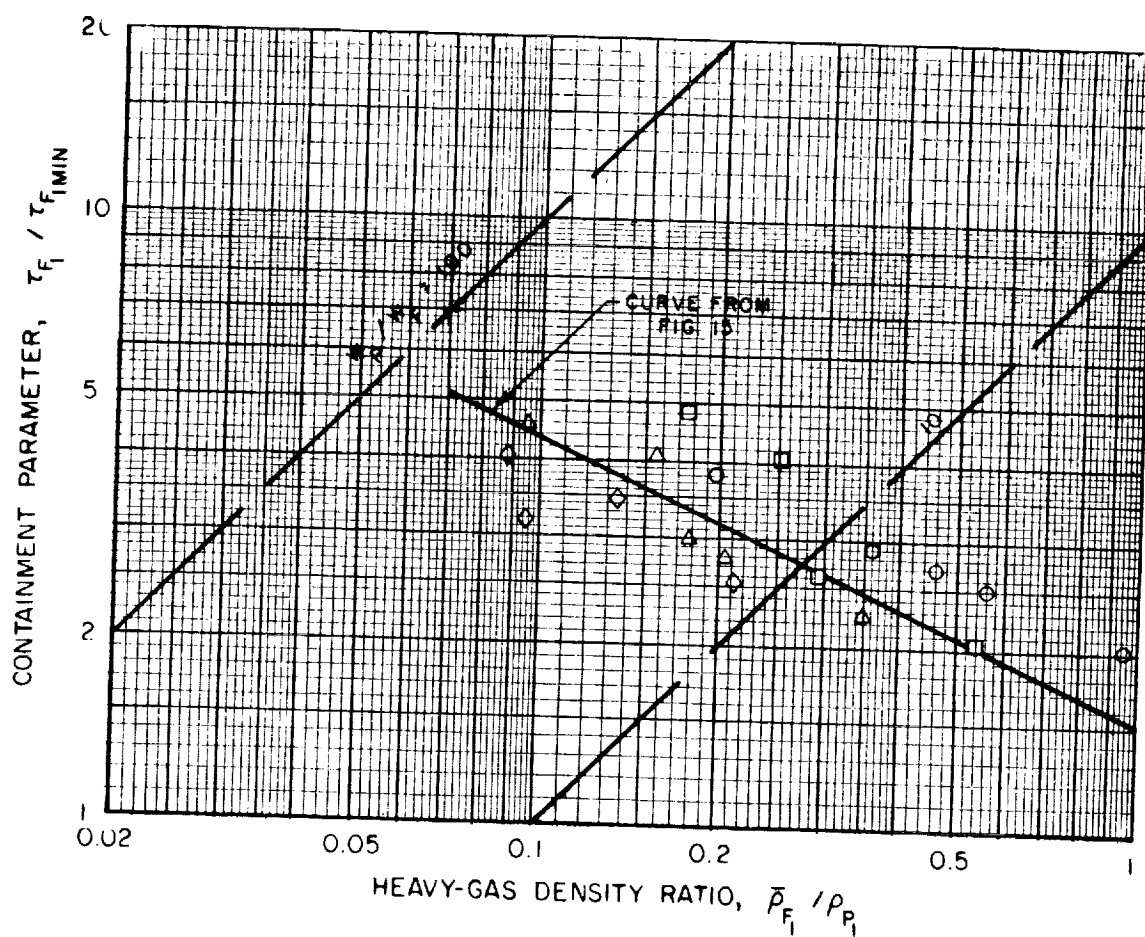TEST SECTION END FLANGE

INFLATABLE SEALS

52

FIG. 12

VARIATION OF CONTAINMENT PARAMETER WITH HEAVY-GAS DENSITY RATIO FOR THE MULTIPLE-FIXED-PORT VORTEX TUBE HAVING $A_j = 13.1$ SQ IN. AND $L/D = 3.0$

SYMBOL	$Re_{z,w}$	$Re_{t,j}$	$\tau_{F_{1MIN}}$
○	46,000	121,000	0.00029
□	73,600	194,000	0.00018
△	92,600	244,000	0.00015
◇	133,000	350,000	0.00010

CONTAINMENT PARAMETER, $\tau_{F_1}/\tau_{F_{1MIN}}$

HEAVY-GAS DENSITY RATIO, $\bar{\rho}_{F_1}/\rho_{P_1}$

53

FIG. 13

VARIATION OF CONTAINMENT PARAMETER WITH HEAVY-GAS DENSITY RATIO FOR THE MULTIPLE-FIXED-PORT VORTEX TUBE HAVING $A_j = 20.5$ SQ IN. AND $L/D = 3.0$

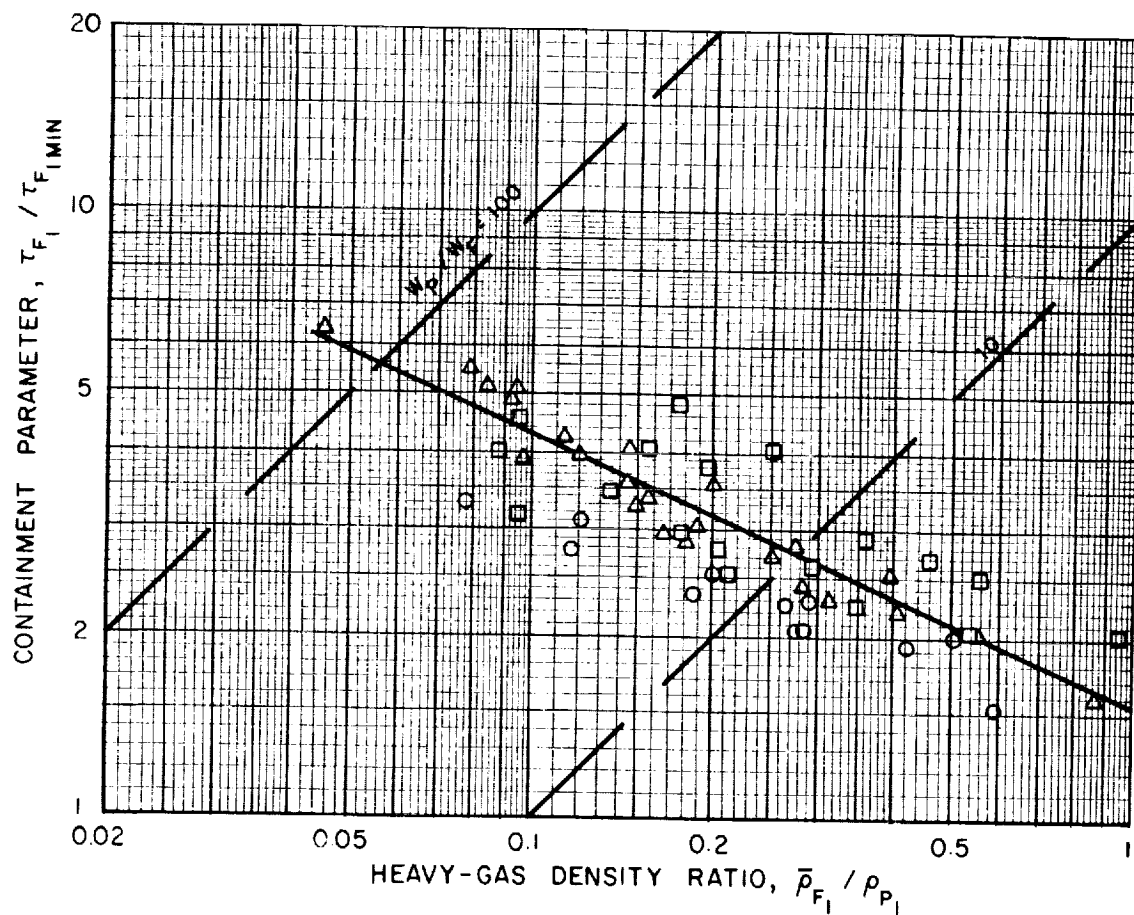| SYMBOL	$Re_{z,w}$	$Re_{t,j}$	$\tau_{F_{1MIN}}$
O	49,000	81,600	0.000270
□	101,000	169,000	0.000130
△	158,000	263,000	0.000086
◊	287,000	478,000	0.000048

FIG. 14

VARIATION OF CONTAINMENT PARAMETER WITH HEAVY-GAS DENSITY RATIO FOR THE MULTIPLE-FIXED-PORT VORTEX TUBE HAVING $A_j = 40.2$ SQ IN. AND $L/D = 3.0$

SYMBOL	$Re_{z,w}$	$Re_{t,i}$	$\tau_{F_{iMIN}}$
○	48,600	41,900	0.000280
□	100,000	86,100	0.000140
△	194,000	167,000	0.000071
◇	285,000	247,000	0.000048
◁	481,000	415,000	0.000029

HEAVY-GAS DENSITY RATIO, $\bar{P}_{F_i}/P_{P_i}$

CONTAINMENT PARAMETER, $\tau_{F_i}/\tau_{F_{iMIN}}$

$W_g/W_F = 100$

CURVE FROM FIG. 15

FIG. 15
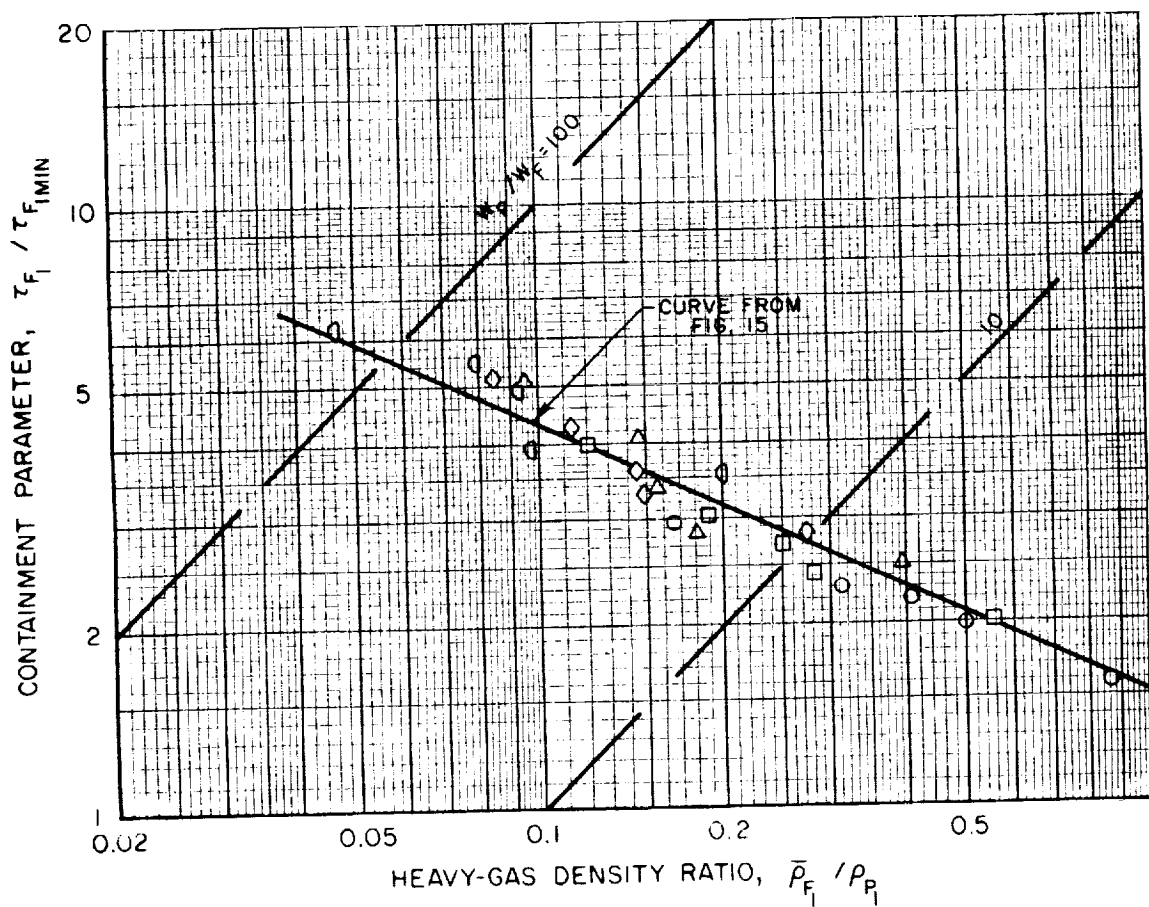
SUMMARY OF DATA FOR MULTIPLE-FIXED-PORT VORTEX TUBES
HAVING A_j =13.1,20.5 AND 40.2 SQ IN. AND L/D =3.0

SYMBOL	A_j - SQ IN.	DATA FROM FIG.
O	13.1	12
□	20.5	13
△	40.2	14

CONTAINMENT PARAMETER, $\tau_{F_1} / \tau_{F_1 MIN}$

HEAVY-GAS DENSITY RATIO, $\bar{\rho}_{F_1} / \rho_{P_1}$

FIG. 16

TYPICAL RADIAL DISTRIBUTIONS OF HEAVY-GAS DENSITY IN MULTIPLE-FIXED-PORT VORTEX TUBES WITH AND WITHOUT SUPERIMPOSED AXIAL FLOW

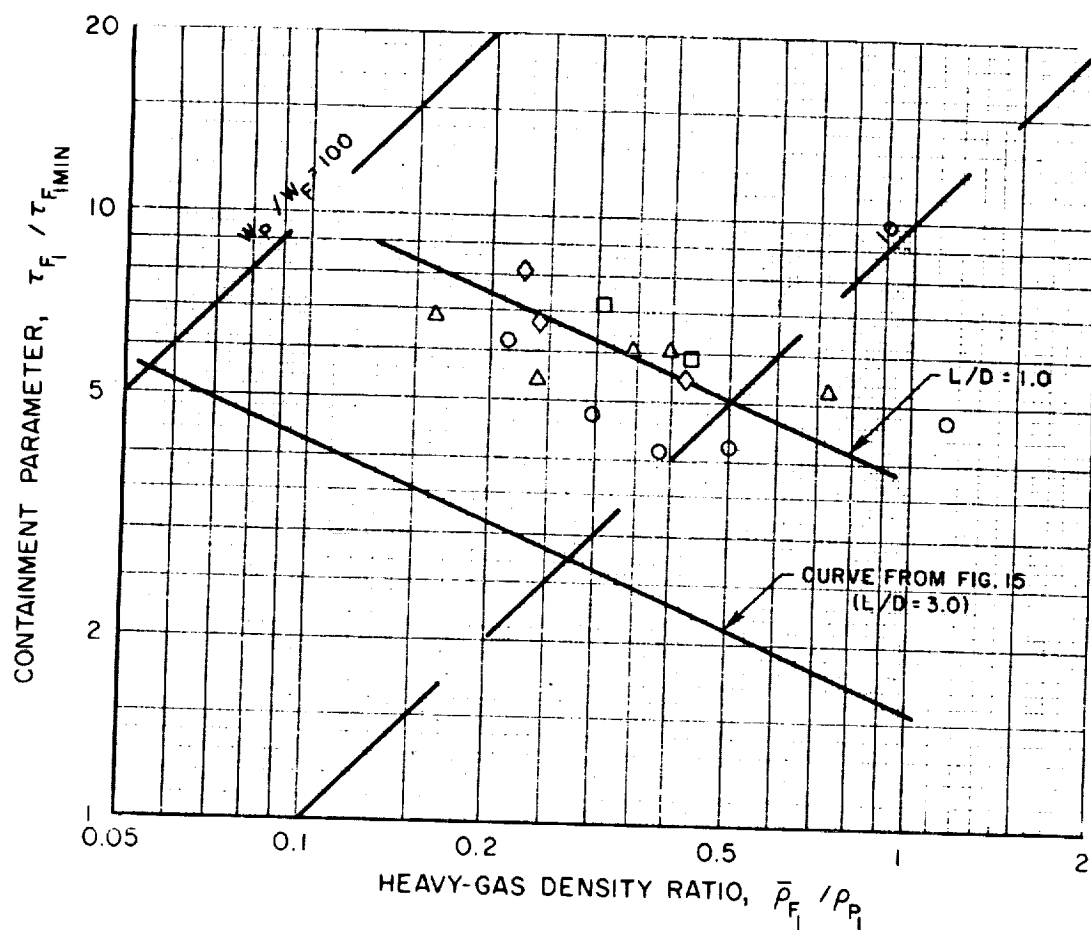| SYMBOL	A_j - SQ IN.	W_P / W_F	$Re_{z,w}$	$\tau_{F_{1MIN}}$	$\tau_{F_1} / \tau_{F_{1MIN}}$	$\bar{\rho}_{F_1} / \rho_{P_1}$
O	13.3	10.5	112,000	0.00012	28.00	2.670
□	13.1	8.5	92,600	0.00014	2.24	0.264
△	20.5	13.3	158,000	0.00008	2.84	0.205
◇	40.2	10.4	285,000	0.00005	2.88	0.276
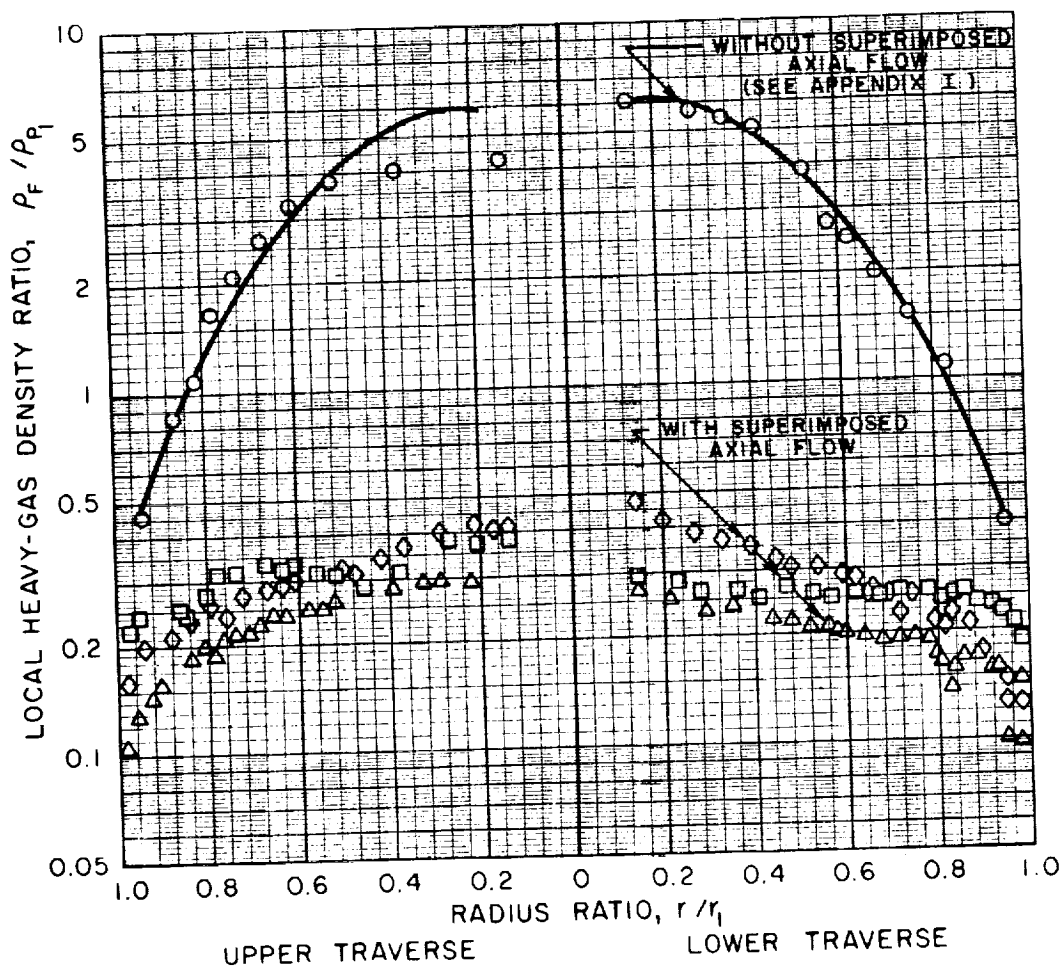
FIG. 17

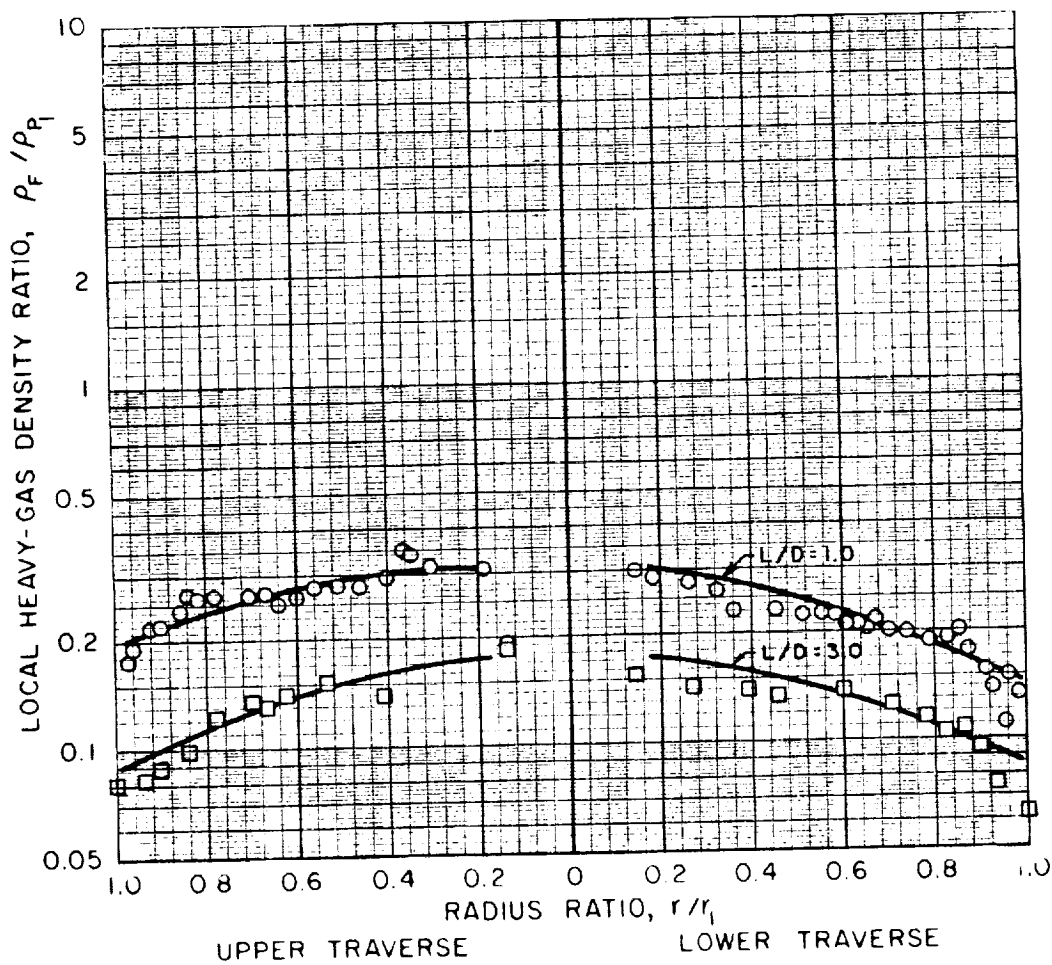VARIATION OF CONTAINMENT PARAMETER WITH HEAVY-GAS
DENSITY RATIO FOR THE MULTIPLE-FIXED-PORT VORTEX TUBE
HAVING $A_j = 13.3$ SQ IN. AND $L/D = 1.0$

SYMBOL	$Re_{z,w}$	$Re_{t,j}$	$\tau_{F_{1MIN}}$
○	100,000	258,000	0.000045
□	157,000	406,000	0.000029
△	197,000	510,000	0.000023
◇	348,000	902,000	0.000013

CONTAINMENT PARAMETER, $\tau_{F_i} / \tau_{F_{1MIN}}$

$W_P / W_F = 100$

L/D = 1.0

CURVE FROM FIG. 15
(L/D = 3.0)

HEAVY-GAS DENSITY RATIO, $\bar{\rho}_{F_i} / \rho_{P_i}$

TYPICAL RADIAL DISTRIBUTIONS OF HEAVY-GAS DENSITY
IN MULTIPLE-FIXED-PORT VORTEX TUBES
HAVING L/D = 1.0 AND 3.0

FIG. 18

SYMBOL	A_j - SQ IN.	L/D	W_P/W_F	$Re_{z,w}$	$\tau_{F_{1MIN}}$	$\tau_{F_1}/\tau_{F_{1MIN}}$	$\bar{\rho}_{F_1}/\rho_{P_1}$
O	13.3	1.0	23.9	157,000	0.000029	6.24	0.30
□	13.1	3.0	22.8	133,000	0.000103	2.74	0.12

59

FIG. 19

VARIATION OF CONTAINMENT PARAMETER WITH HEAVY-GAS DENSITY RATIO FOR THE DIRECTED-WALL-JET VORTEX TUBE HAVING A_j = 11.0 SQ IN. AND L/D = 3.0

SYMBOL	$Re_{z,w}$	$Re_{t,i}$	$\tau_{F_{I \, MIN}}$
O	97,000	220,000	0.000141
□	151,000	343,000	0.000090
△	211,000	479,000	0.000065
◇	307,000	698,000	0.000044
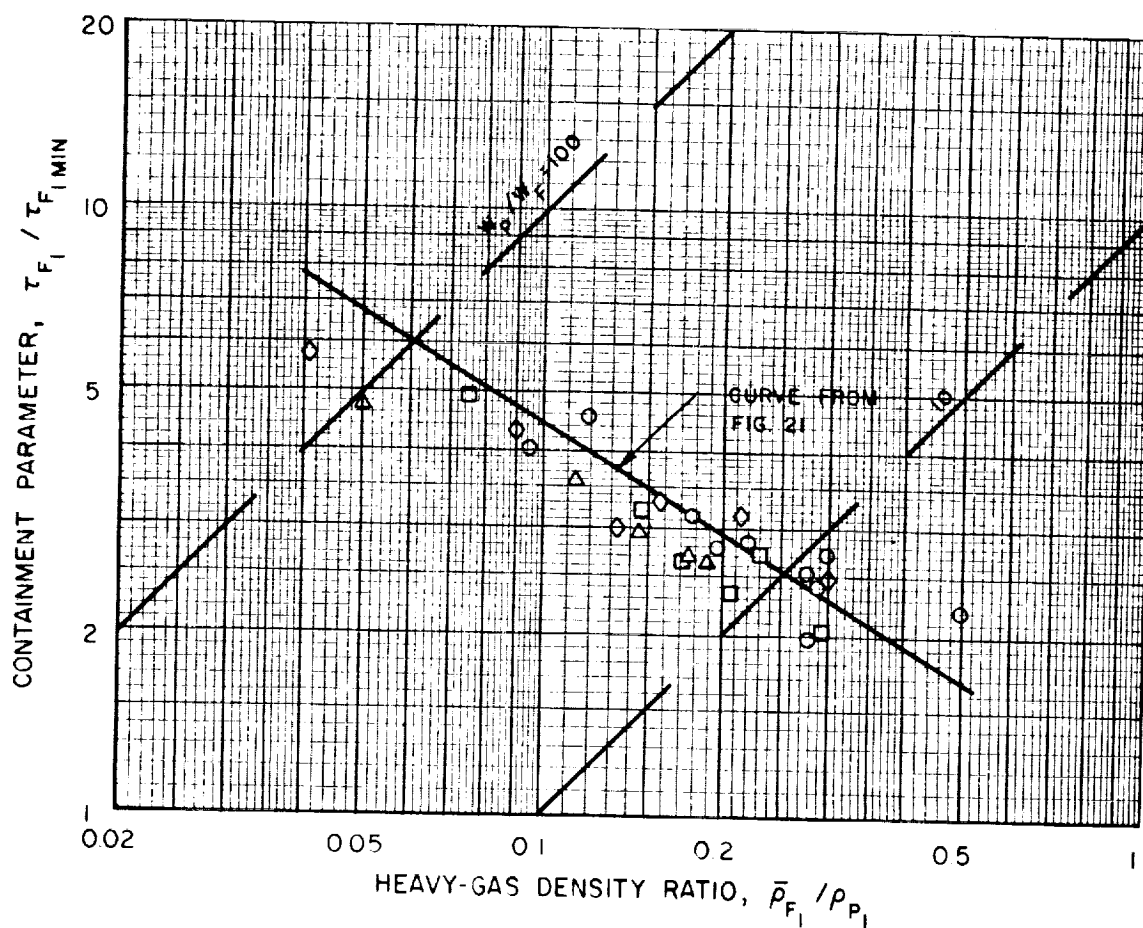
FIG. 20

VARIATION OF CONTAINMENT PARAMETER WITH HEAVY-GAS
DENSITY RATIO FOR THE DIRECTED-WALL-JET VORTEX TUBE
HAVING A_j = 32.2 SQ IN. AND L/D = 3.0

| SYMBOL	$Re_{z,w}$	$Re_{t,j}$	$\tau_{F_1 MIN}$
O	90,500	69,100	0.000150
□	205,000	156,000	0.000067
△	325,000	248,000	0.000042
◇	462,000	353,000	0.000030
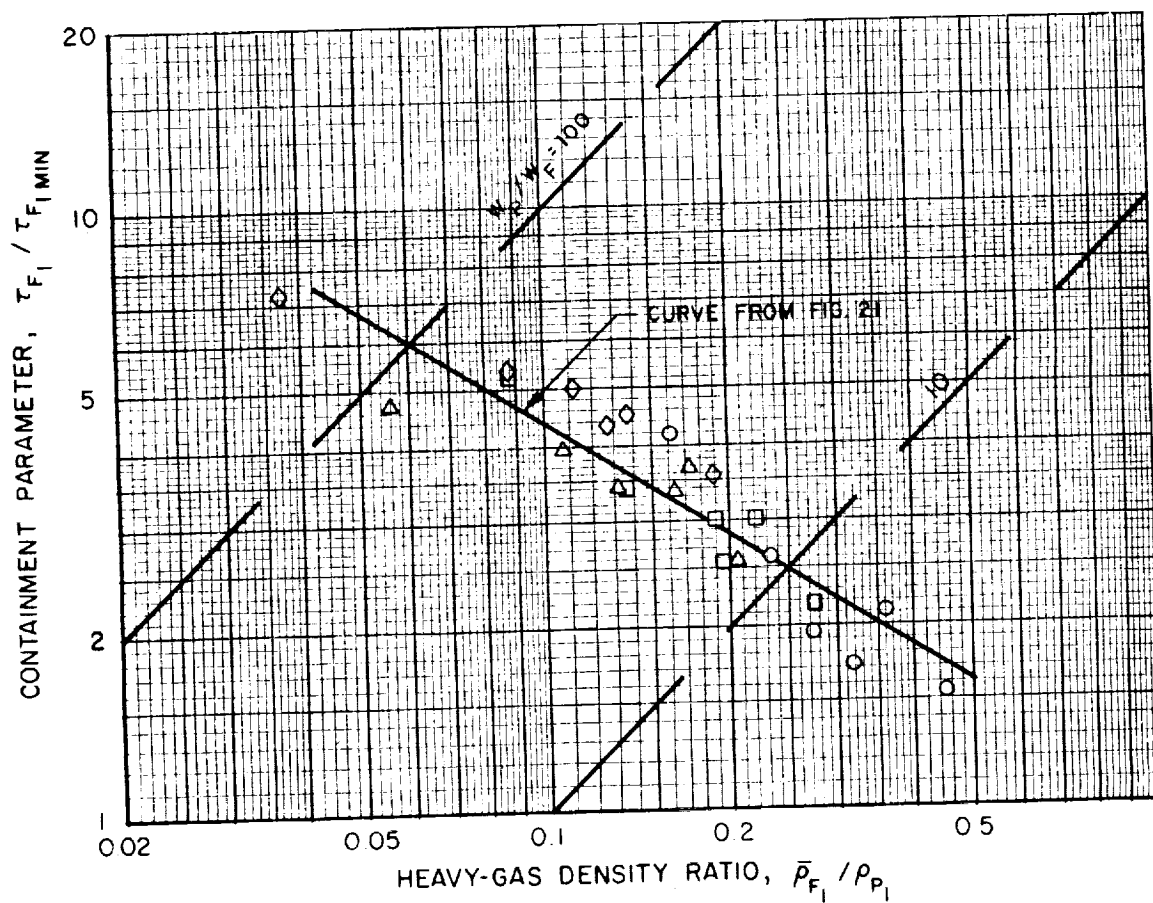
FIG. 21

SUMMARY OF DATA FOR DIRECTED-WALL-JET VORTEX TUBES
HAVING A_j = 11.0 AND 32.2 SQ IN. AND L/D = 3.0

SYMBOL	A_j - SQ IN.	DATA FROM FIG.
O	11.0	19
▢	32.2	20

CONTAINMENT PARAMETER, $\tau_{F_1} / \tau_{F_{1 MIN}}$

HEAVY-GAS DENSITY RATIO, $\bar{\rho}_{F_1} / \rho_{P_1}$

FIG 22
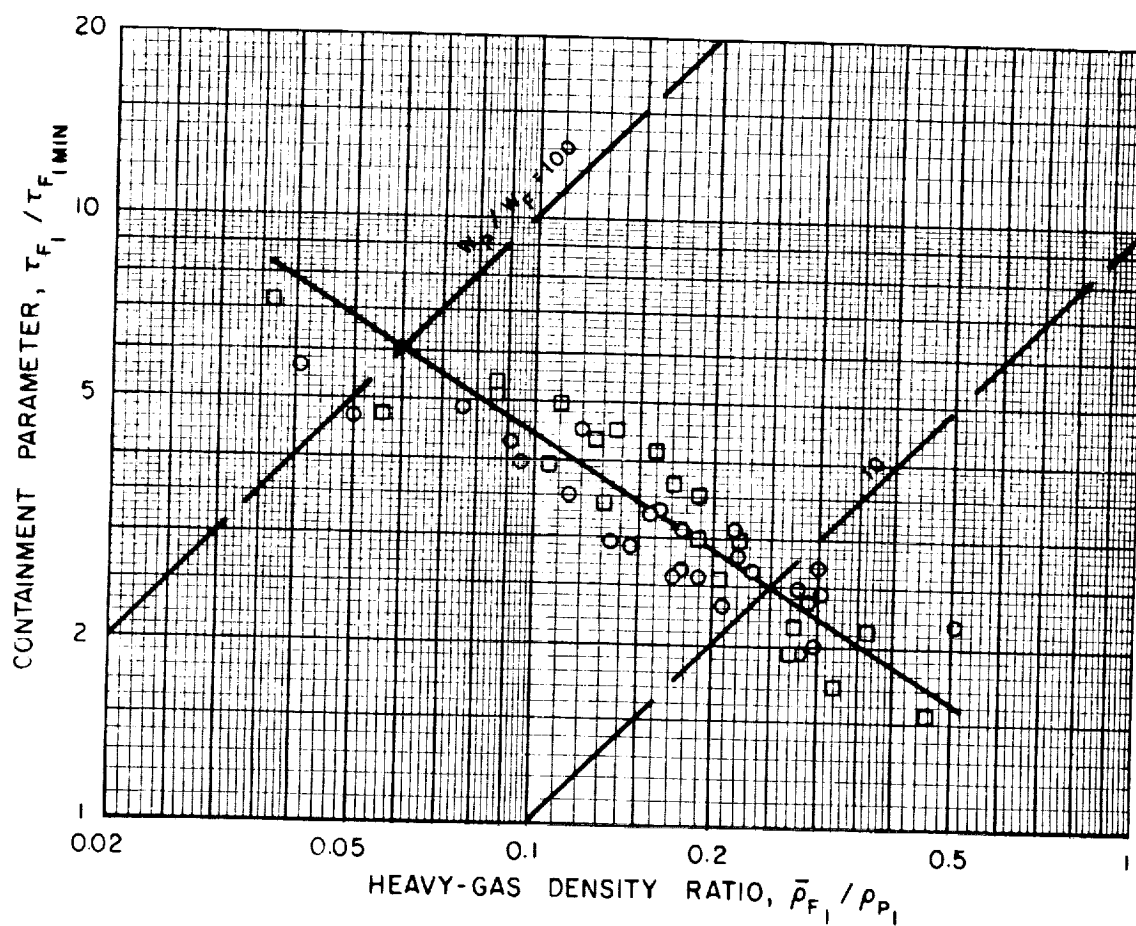
SUMMARY OF DATA FOR DIRECTED-WALL-JET VORTEX TUBES
HAVING A_j = 11.0 AND 21.5 SQ IN. AND L/D = 1.0 AND 2.0

SYMBOL	A_j - SQ IN	L/D	$Re_{z,w}$	$Re_{t,i}$	$\tau_{F_1 MIN}$
O	11.0	1.0	143,000	326,000	0.000032
□	11.0	1.0	223,000	510,000	0.000020
△	11.0	1.0	268,000	614,000	0.000017
◇	21.5	2.0	161,000	184,000	0.000056
D	21.5	2.0	224,000	287,000	0.000040
▽	21.5	2.0	334,000	383,000	0.000027

63

FIG 23
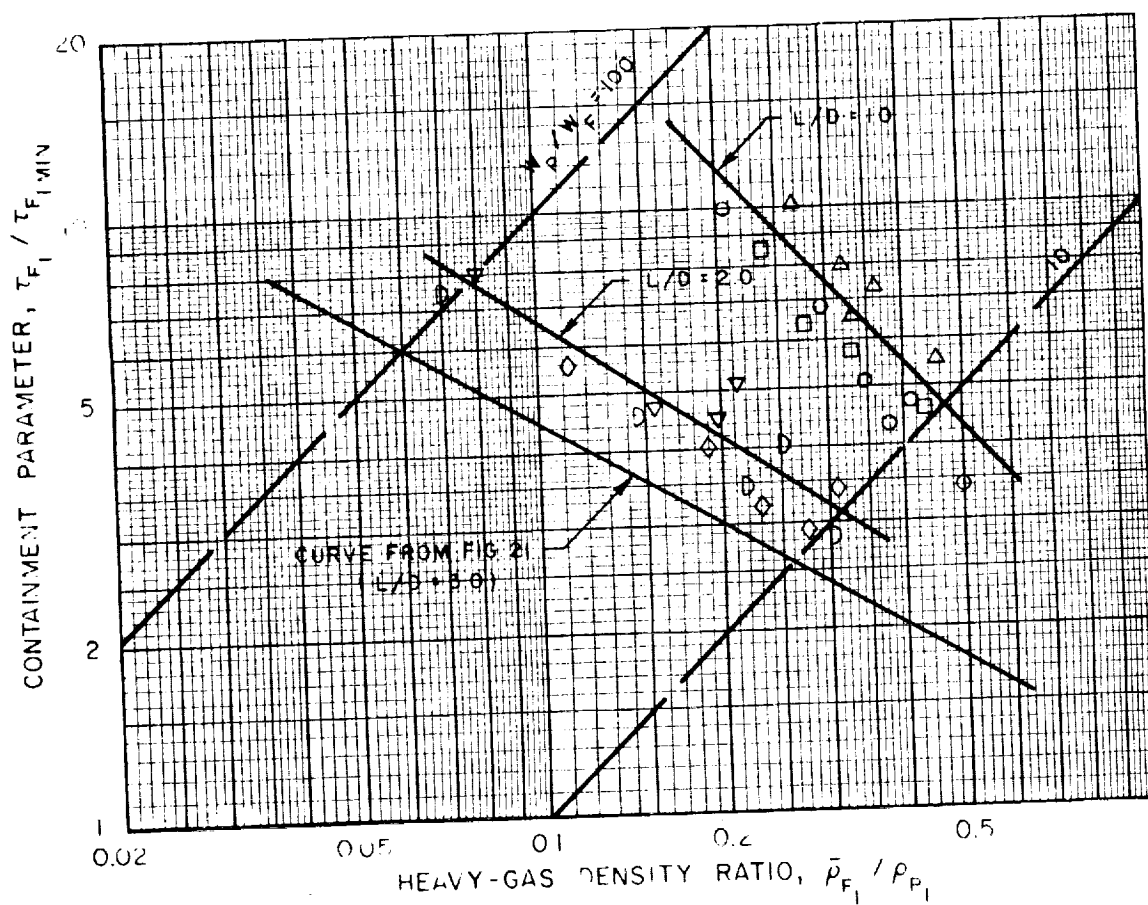
COMPARISON OF RESULTS OF TESTS WITH MULTIPLE-FIXED-PORT AND DIRECTED-WALL-JET VORTEX TUBES

LINE	VORTEX TUBE	L/D	CURVE FROM FIG
————	MFP	1.0	17
— — —	DWJ	1.0	22
— —— —	MFP	3.0	15
— · —	DWJ	3.0	21
— ·· —	MFP	3.0	SEE APP. I

FIG. 24
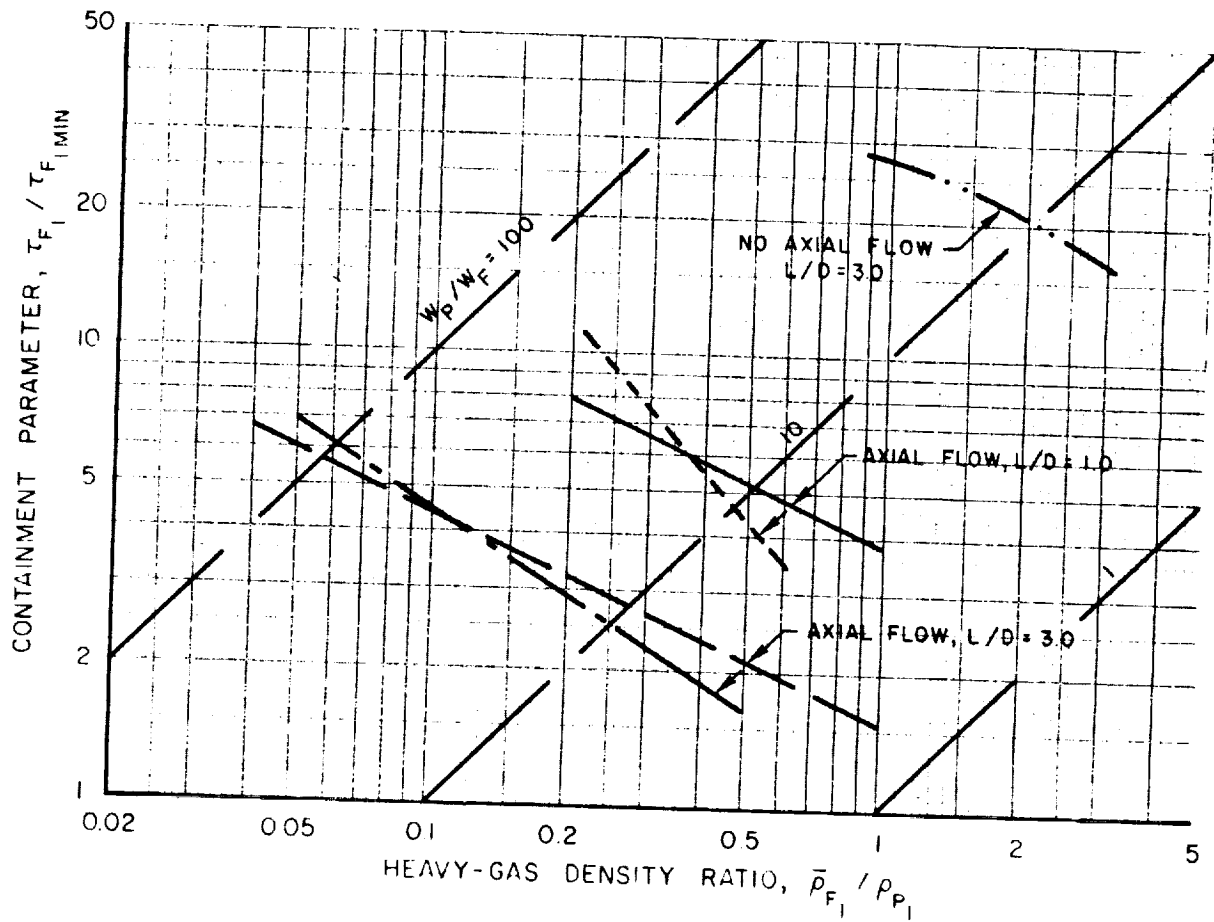
VARIATION OF CONTAINMENT PARAMETER WITH HEAVY-GAS DENSITY RATIO FOR TESTS USING HELIUM AS THE SIMULATED FUEL

DIRECTED-WALL-JET VORTEX TUBE, $A_j = 11.0$ SQ IN AND $L/D = 1.0$

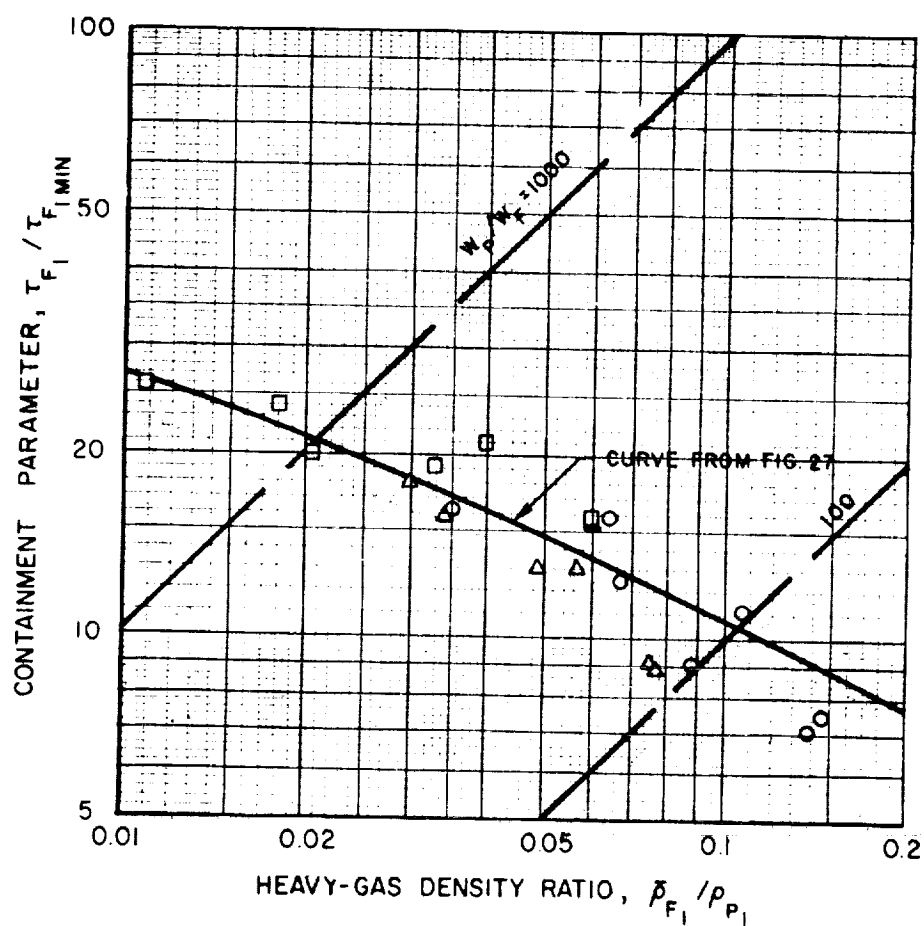| SYMBOL	$Re_{z,w}$	$Re_{t,j}$	$\tau_{F_{1 MIN}}$	SIMULATED FUEL
O	60,000	140,000	0.000076	HELIUM AND IODINE; $(\rho_F / \rho_P)_{INJ} = 0.15$
□	148,000	344,000	0.000031	
△	319,000	742,000	0.000014	

FIG. 25
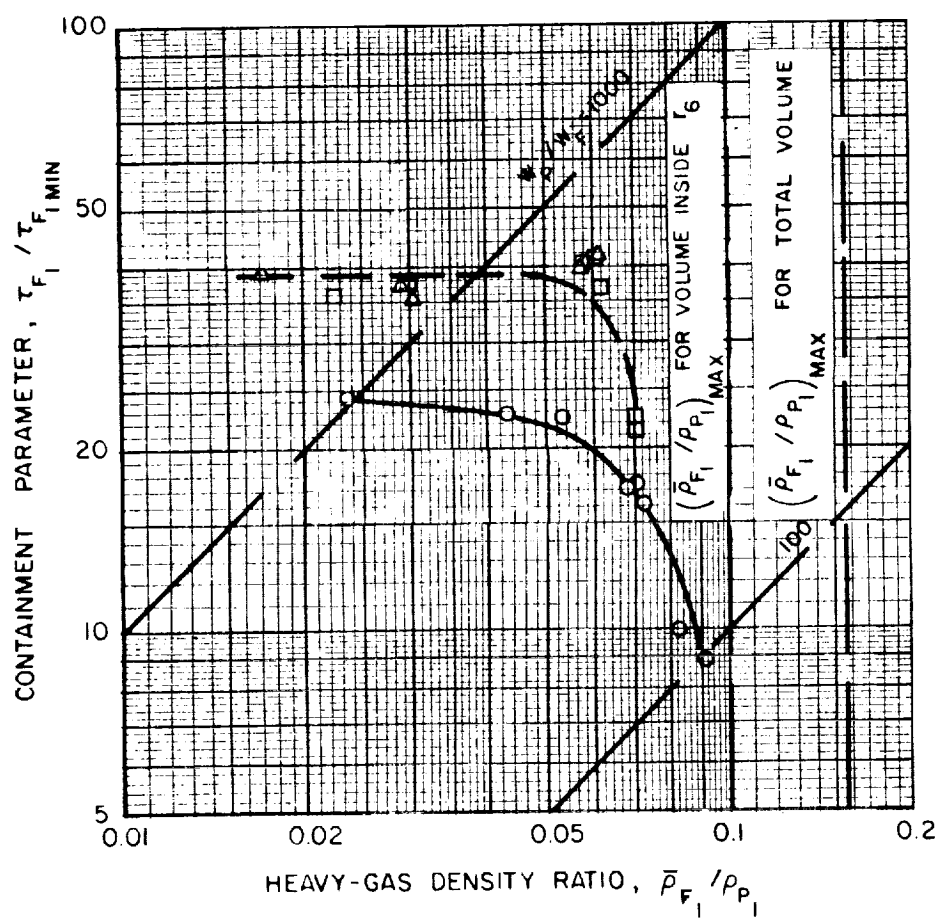
VARIATION OF CONTAINMENT PARAMETER WITH HEAVY-GAS DENSITY RATIO FOR TESTS USING NITROGEN AS THE SIMULATED FUEL

DIRECTED-WALL-JET VORTEX TUBE, $A_j = 11.0$ SQ IN. AND $L/D = 1.0$
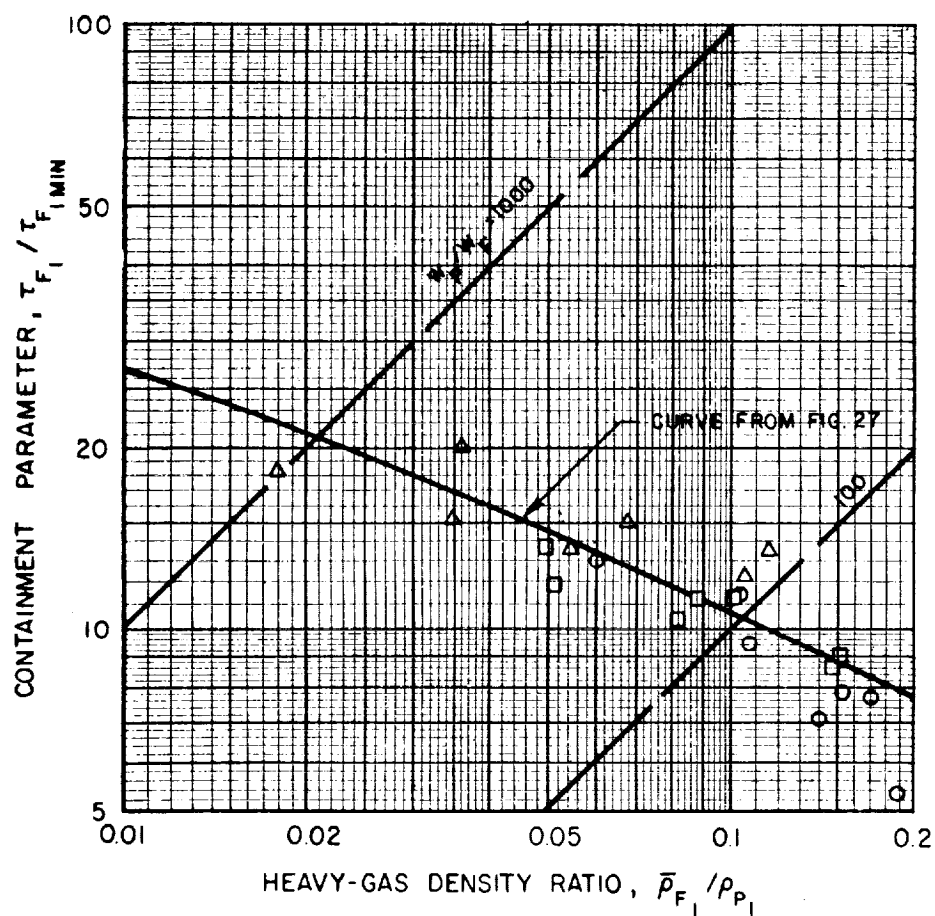
SYMBOL	$Re_{z,w}$	$Re_{t,j}$	$\tau_{F_{1\,MIN}}$	SIMULATED FUEL
O	60,000	140,000	0.000076	NITROGEN AND IODINE;
□	148,000	344,000	0.000031	$\left(\rho_F/\rho_P\right)_{INJ} = 1.0$
△	319,000	742,000	0.000014	

CONTAINMENT PARAMETER, $\tau_{F_1}/\tau_{F_{1\,MIN}}$ vs. HEAVY-GAS DENSITY RATIO, ρ_{F_1}/ρ_{P_1}

FIG. 26

VARIATION OF CONTAINMENT PARAMETER WITH HEAVY-GAS DENSITY RATIO FOR TESTS USING SULPHUR HEXAFLUORIDE AS THE SIMULATED FUEL

DIRECTED-WALL-JET VORTEX TUBE, $A_j = 11.0$ SQ IN. AND L/D = 1.0

SYMBOL	$Re_{z,w}$	$Re_{t,j}$	$\tau_{F_{I\,MIN}}$	SIMULATED FUEL
O	60,000	140,000	0.000076	SULPHUR HEXAFLUORIDE
□	148,000	344,000	0.000031	AND IODINE ;
△	319,000	742,000	0.000014	$(P_F / P_P)_{INJ} = 5.0$

67

FIG. 27

FIG. 29

EFFECT OF SIMULATED-FUEL DENSITY AT INJECTION ON THE RADIAL DISTRIBUTION OF SIMULATED-FUEL PARTIAL PRESSURE IN THE VORTEX TUBE

DIRECTED-WALL-JET VORTEX TUBE, $A_j = 11.0$ SQ IN., AND L/D = 1.0

$Re_{z,w} = 60,000$

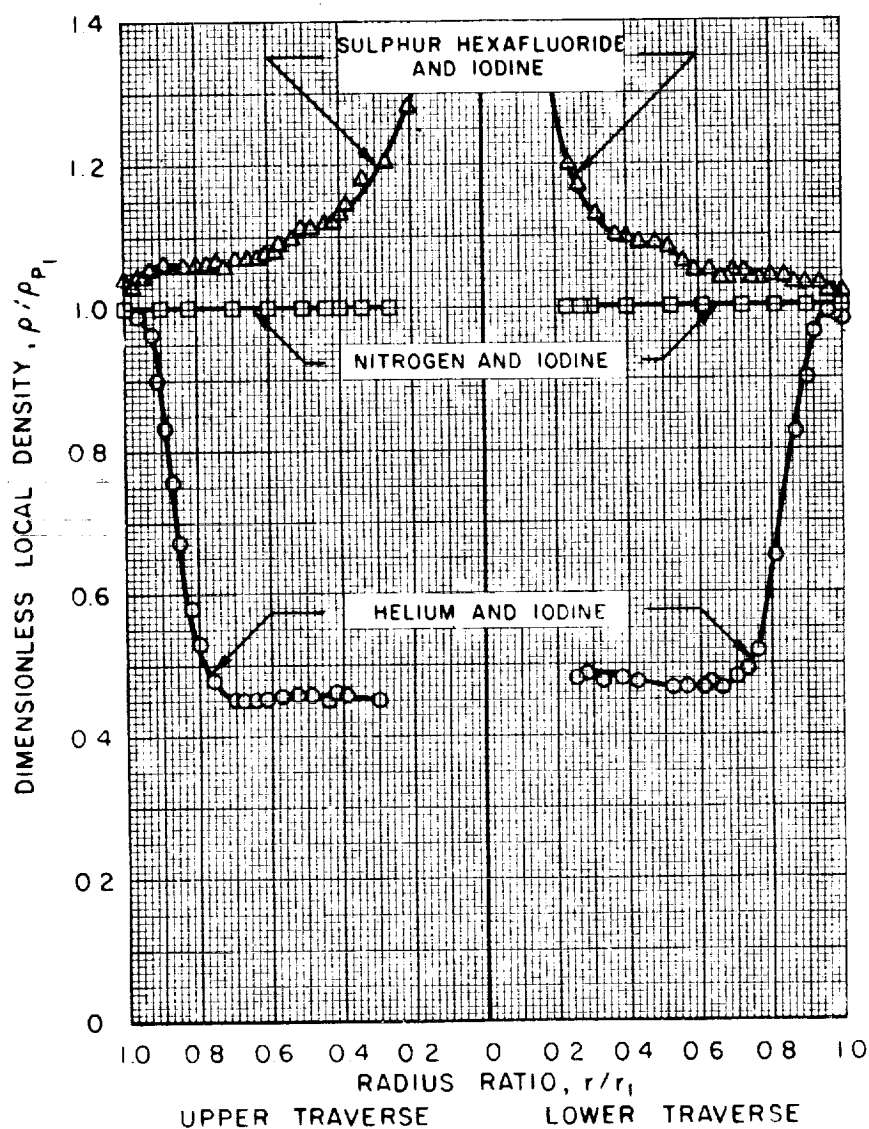| SYMBOL	$(\rho_F/\rho_P)_{INJ}$	W_P/W_F	$\tau_{F_1}/\tau_{F_1 MIN}$	$\bar{P}_{F_1}/\rho_{P_1}$	SIMULATED FUEL
O	0.155	91	8.9	0.098	HELIUM AND IODINE
□	1.030	91	10.8	0.119	NITROGEN AND IODINE
△	5.050	112	11.7	0.104	SULPHUR HEXAFLUORIDE AND IODINE

FIG. 30

EFFECT OF SIMULATED-FUEL DENSITY AT INJECTION ON THE RADIAL DISTRIBUTION OF LOCAL DENSITY IN THE VORTEX TUBE
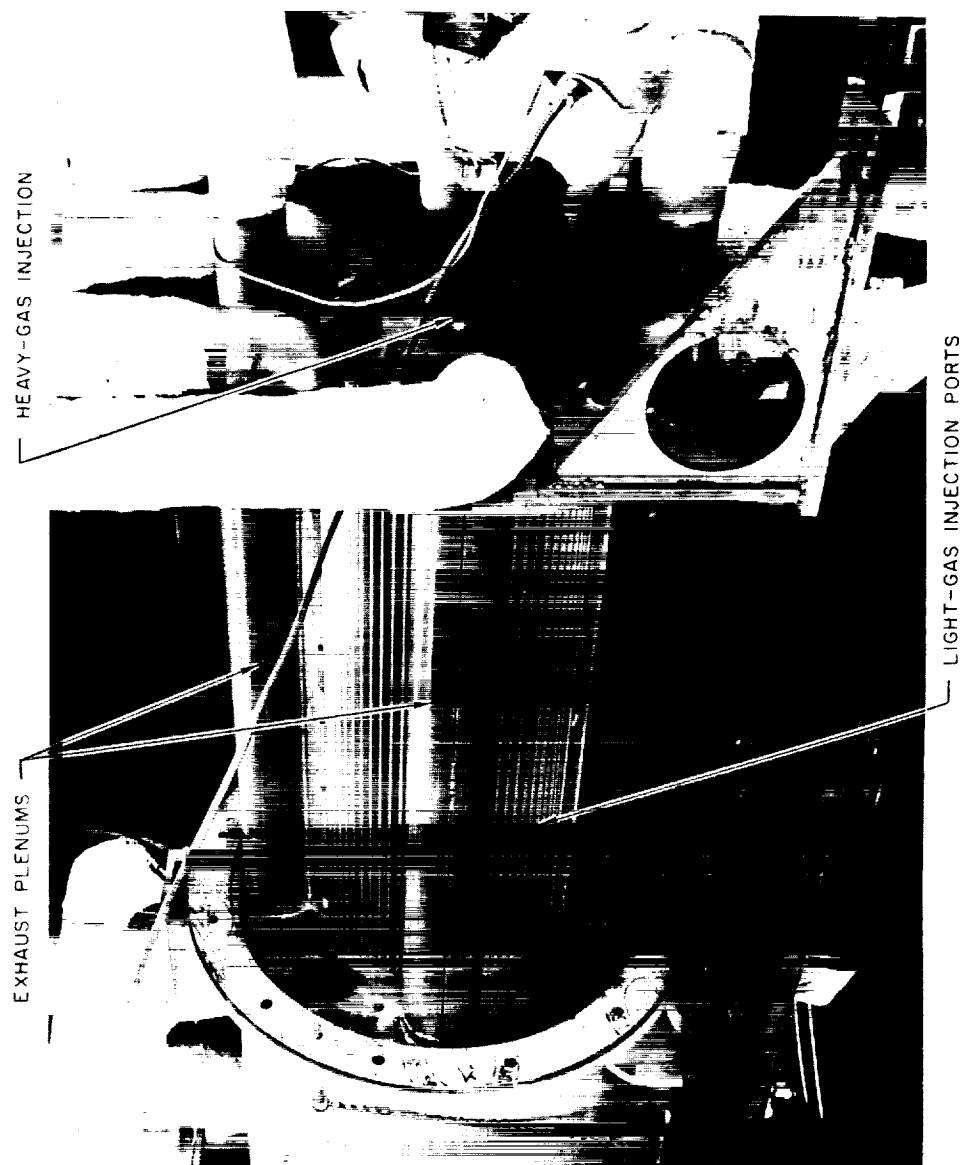
DIRECTED-WALL-JET VORTEX TUBE, $A_j = 11.0$ SQ IN. AND $L/D = 1.0$

$Re_{z,w} = 60,000$

SYMBOL	$(\rho_F/\rho_P)_{INJ}$	W_P/W_F	$\tau_{F_1}/\tau_{F_{1MIN}}$	$\bar{\rho}_{F_1}/\rho_{P_1}$	SIMULATED FUEL
O	0.155	91	8.9	0.098	HELIUM AND IODINE
□	1.030	91	10.8	0.119	NITROGEN AND IODINE
Δ	5.050	112	11.7	0.104	SULPHUR HEXAFLUORIDE AND IODINE

SULPHUR HEXAFLUORIDE AND IODINE

NITROGEN AND IODINE

HELIUM AND IODINE

DIMENSIONLESS LOCAL DENSITY, ρ'/ρ_{P_1}

RADIUS RATIO, r/r_1

UPPER TRAVERSE   LOWER TRAVERSE

71

PHOTOGRAPH OF VORTEX TUBE FOR TESTS WITH RADIAL OUTFLOW AND NO SUPERIMPOSED AXIAL FLOW

HEAVY-GAS INJECTION

LIGHT-GAS INJECTION PORTS

EXHAUST PLENUMS

FIG. 31

72

FIG. 33

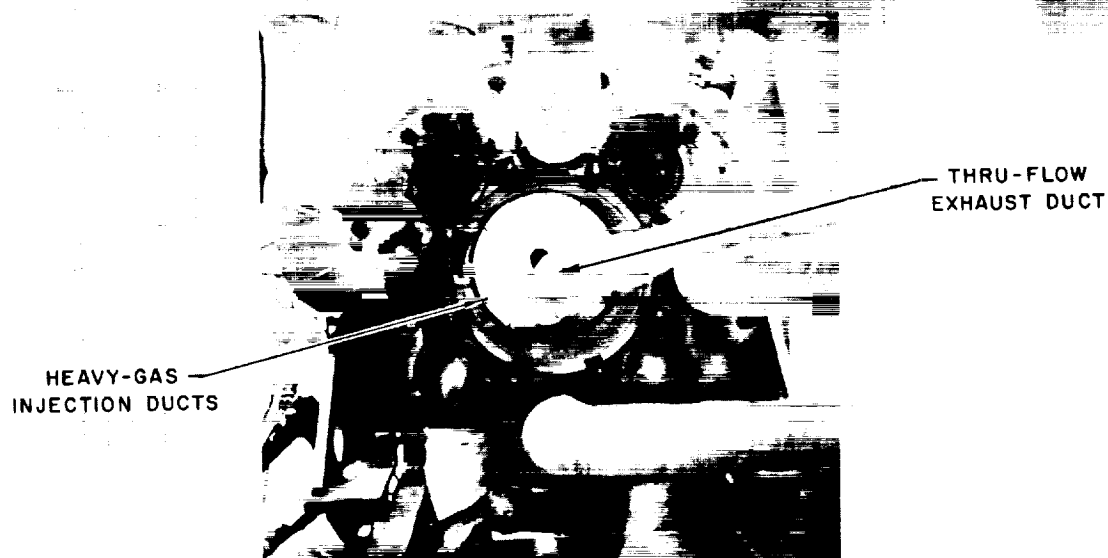# GEOMETRY OF VORTEX TUBE FOR TESTS WITH RADIAL INFLOW AND NO SUPERIMPOSED AXIAL FLOW

a) SKETCH OF VORTEX TUBE AND END WALLS

SECTION A-A

MULTIPLE-FIXED-PORT VORTEX TUBE

THRU-FLOW EXHAUST DUCT (1.0 IN. DIA)

10"

BYPASS-FLOW PLENUM
HEAVY-GAS INJECTION DUCTS

30"
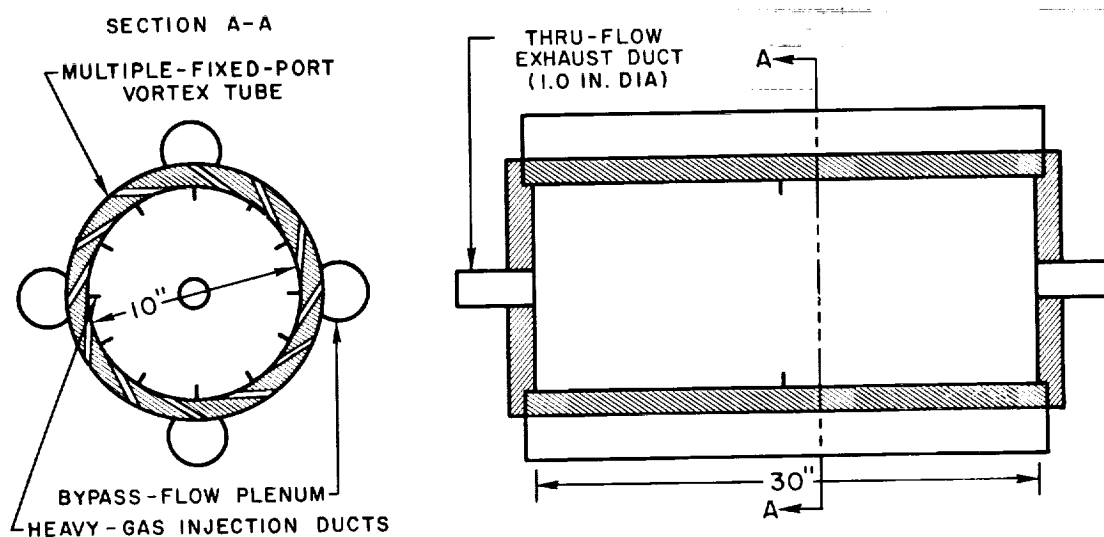
b) PHOTOGRAPH OF VORTEX TUBE INSTALLED IN TEST SECTION

THRU-FLOW EXHAUST DUCT

HEAVY-GAS INJECTION DUCTS

FIG. 32

VARIATION OF CONTAINMENT PARAMETER WITH HEAVY-GAS DENSITY RATIO FOR VORTEXES WITH RADIAL OUTFLOW AND NO SUPERIMPOSED AXIAL FLOW

SEE FIG. 31 FOR VORTEX TUBE GEOMETRY
HEAVY-GAS INJECTION THROUGH CENTERLINE POROUS TUBE

SYMBOL OR LINE	$Re_{z,w}$	$Re_{t,i}$	A_j - SQ IN.	LIGHT-GAS INJECTION GEOMETRY
O	40,000	110,000	13.5	MULTIPLE-FIXED-PORT
□	76,000	190,000	13.5	MULTIPLE-FIXED-PORT
△	110,000	280,000	13.5	MULTIPLE-FIXED-PORT
— — —	27,000	180,000	5.5	SINGLE-SLOT (SEE REF. 5)
—·—·—	65,000	430,000	5.5	SINGLE-SLOT (SEE REF. 5)

73

FIG. 34
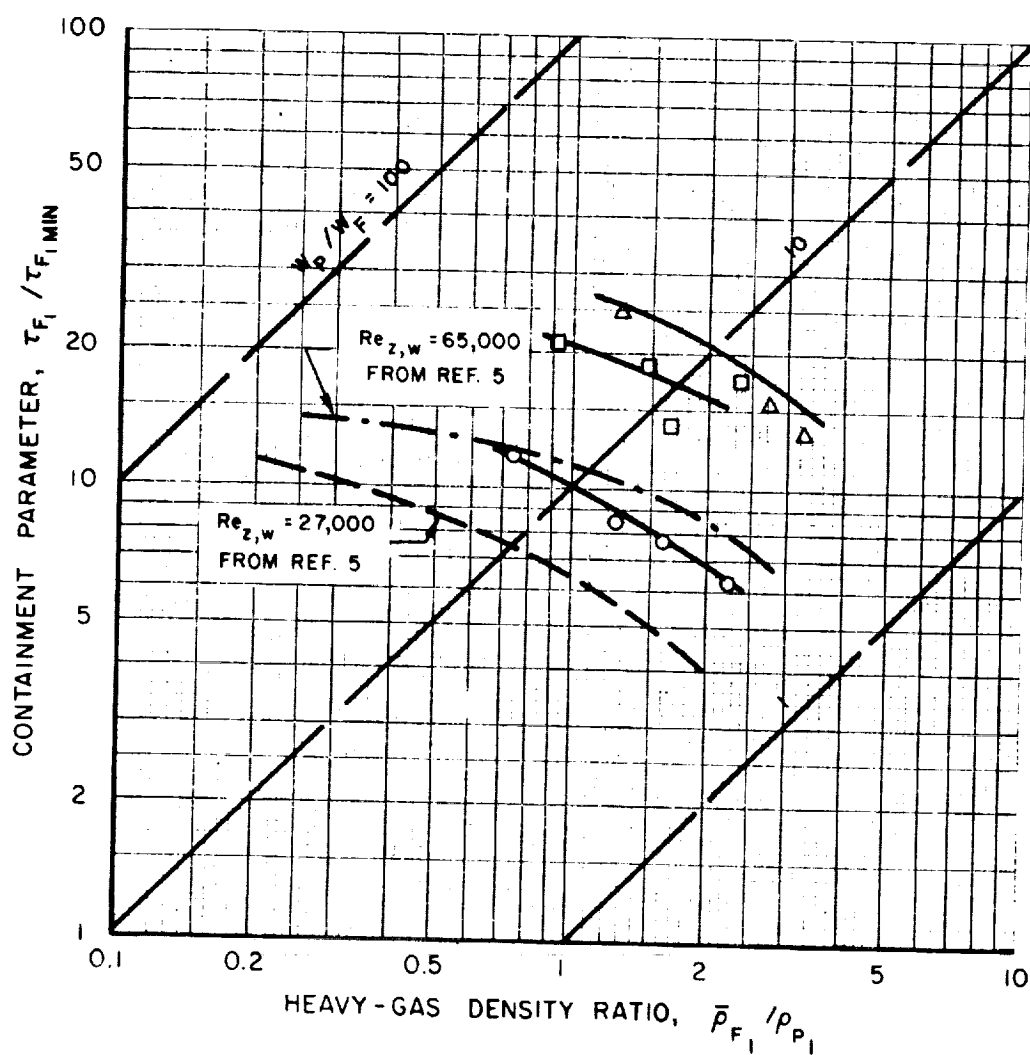
VARIATION OF CONTAINMENT PARAMETER WITH RADIAL REYNOLDS NUMBER FOR VORTEXES WITH RADIAL INFLOW AND NO SUPERIMPOSED AXIAL FLOW

SEE FIG. 33 FOR VORTEX TUBE GEOMETRY

$Re_{t,j} = 170,000, \quad Re_{z,w} = 65,000$

SYMBOL	A_j – SQ IN.	W_P/W_F	$\tau_{F_{1 MIN}}$	THRU-FLOW REMOVAL
O	13.6	16.5	0.00021	BOTH END WALLS
●	13.6	18.0	0.00021	ONE END WALL

75

FIG. 35
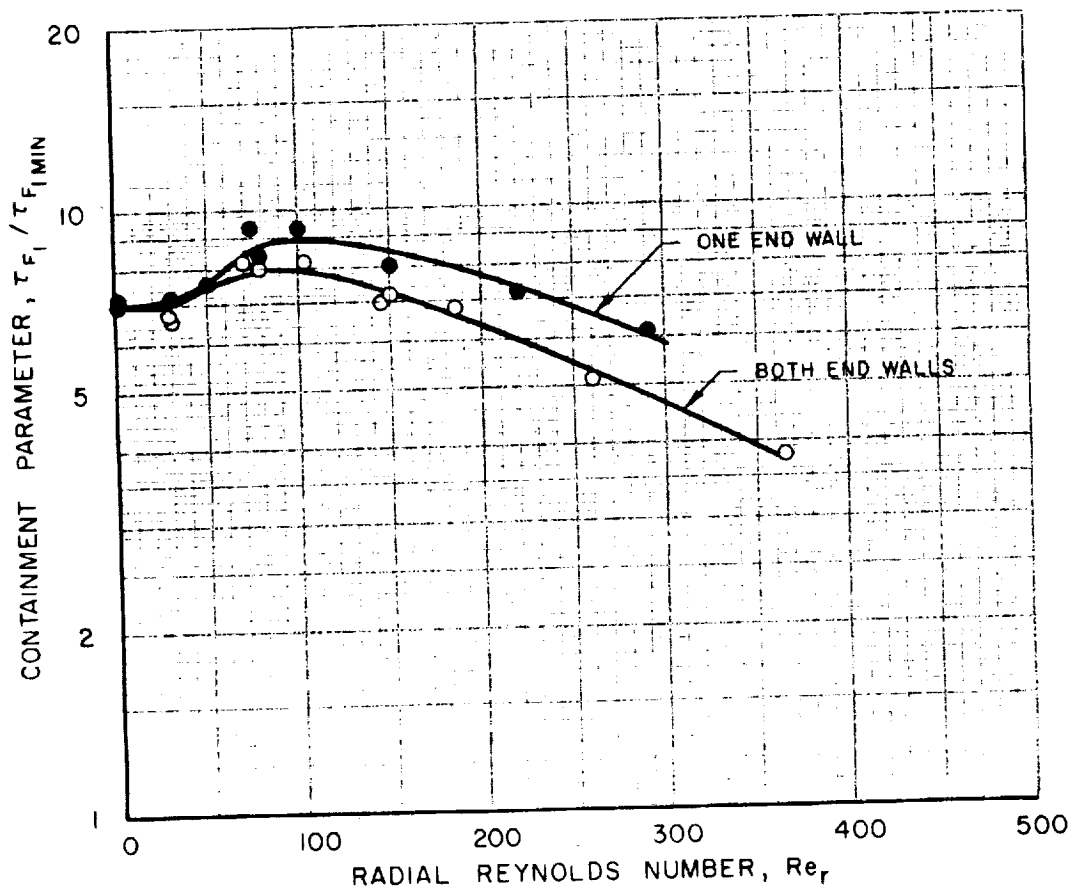
EFFECT OF RADIAL REYNOLDS NUMBER ON THE RADIAL DISTRIBUTION OF HEAVY-GAS DENSITY FOR VORTEXES WITH RADIAL INFLOW AND NO SUPERIMPOSED AXIAL FLOW

VORTEX TUBE GEOMETRY SPECIFIED IN FIG. 33
OTHER CONDITIONS SPECIFIED IN FIG. 34
THRU-FLOW REMOVAL THROUGH ONE END WALL
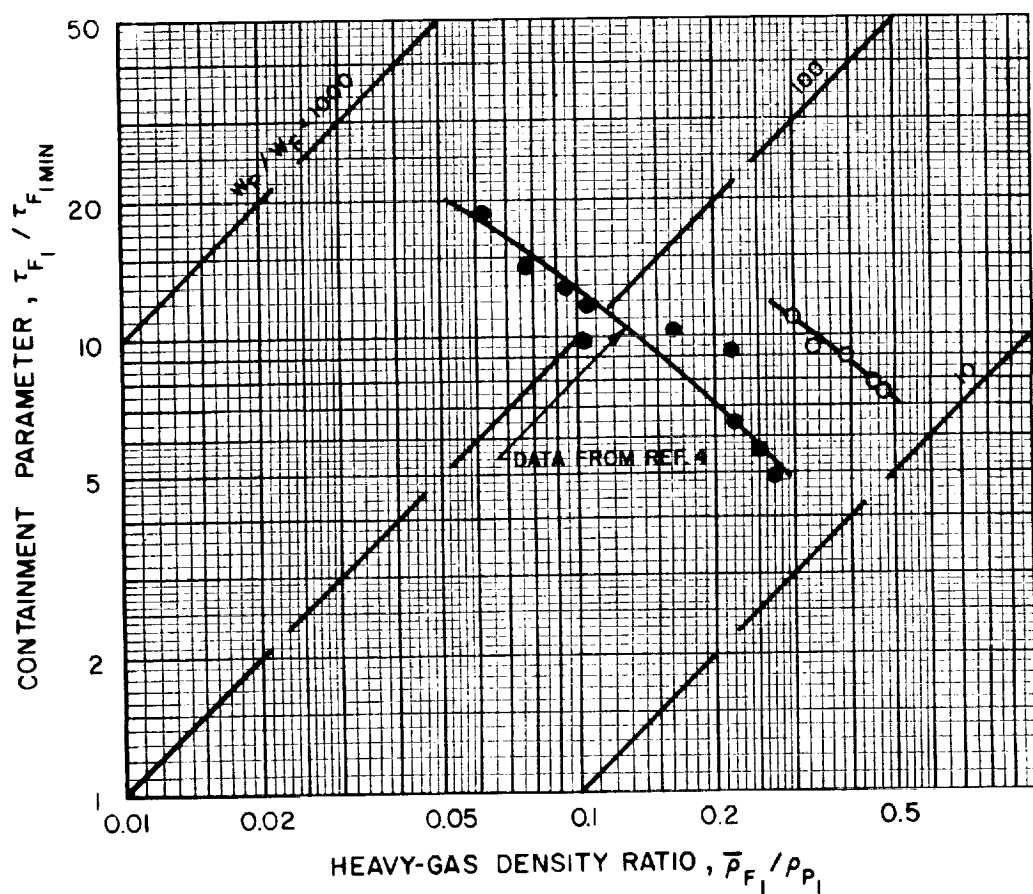$Re_{t,j} = 170,000$, $Re_{z,w} = 65,000$

SYMBOL	Re_r	$\tau_{F_I} / \tau_{F_{I\,MIN}}$	$\bar{\rho}_{F_I} / \rho_{P_I}$
O	100	9.21	0.506
□	75	9.53	0.521
△	50	7.79	0.428
◇	25	7.24	0.395
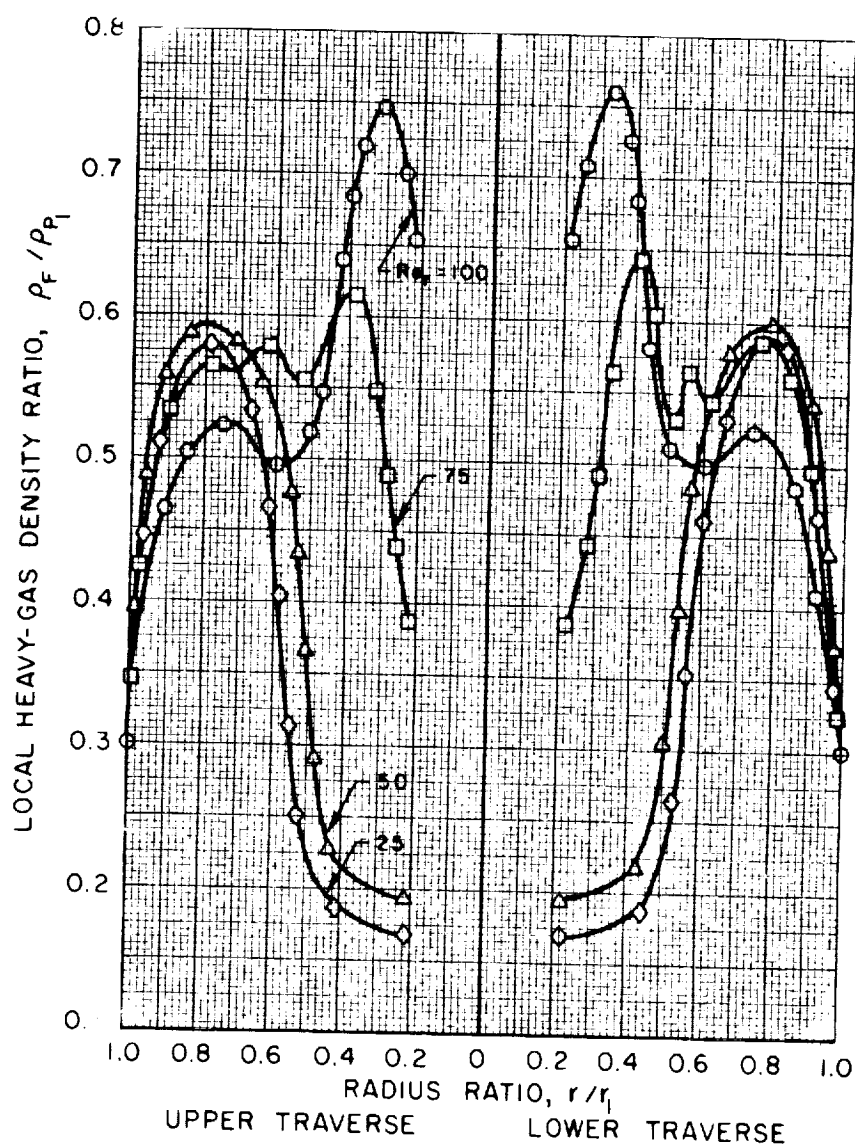
LOCAL HEAVY-GAS DENSITY RATIO, ρ_F / ρ_{P_I}

RADIUS RATIO, r/r_I

UPPER TRAVERSE   LOWER TRAVERSE

FIG. 36

VARIATION OF CONTAINMENT PARAMETER WITH HEAVY-GAS DENSITY RATIO FOR VORTEXES WITH RADIAL INFLOW AND NO SUPERIMPOSED AXIAL FLOW

SEE FIG.33 FOR VORTEX TUBE GEOMETRY
THRU-FLOW REMOVED AT CENTERS OF EACH END WALL
$Re_r = 100$

SYMBOL	A_j-SQ IN.	$Re_{z,w}$	$Re_{t,j}$	$\tau_{F_{1}MIN}$	LIGHT-GAS INJECTION CONFIGURATION	HEAVY-GAS INJECTION CONFIGURATION
O	13.3	65,000	170,000	0.00021	MULTIPLE-FIXED-PORT WITH PERIPHERAL BYPASS	12 0.125-IN.-DIA DUCTS AT AXIAL MIDPLANE
●	5.4	27,000	180,000	0.00050	SINGLE-SLOT WITH PERIPHERAL BYPASS - SEE REF. 4	1 0.125-IN.-DIA DUCTS AT AXIAL MIDPLANE

DATA FROM REF. 4

CONTAINMENT PARAMETER, $\tau_{F_1}/\tau_{F_{1}MIN}$

HEAVY-GAS DENSITY RATIO, $\overline{\rho}_{F_1}/\rho_{P_1}$

GEOMETRY OF 10-IN.-DIA SINGLE-SLOT VORTEX TUBE

FIG. 37

HEAVY-GAS
INJECTION DUCT

L = 30 IN.

1 1/4-IN. OD POROUS TUBE

HEAVY-GAS
INJECTION
DUCT

DIA = 10 IN.

LIGHT-GAS
INJECTION
SLOT HEIGHT
0.182 ± 0.005 IN.
(FOR MOST TESTS)

INJECTION PLENUM
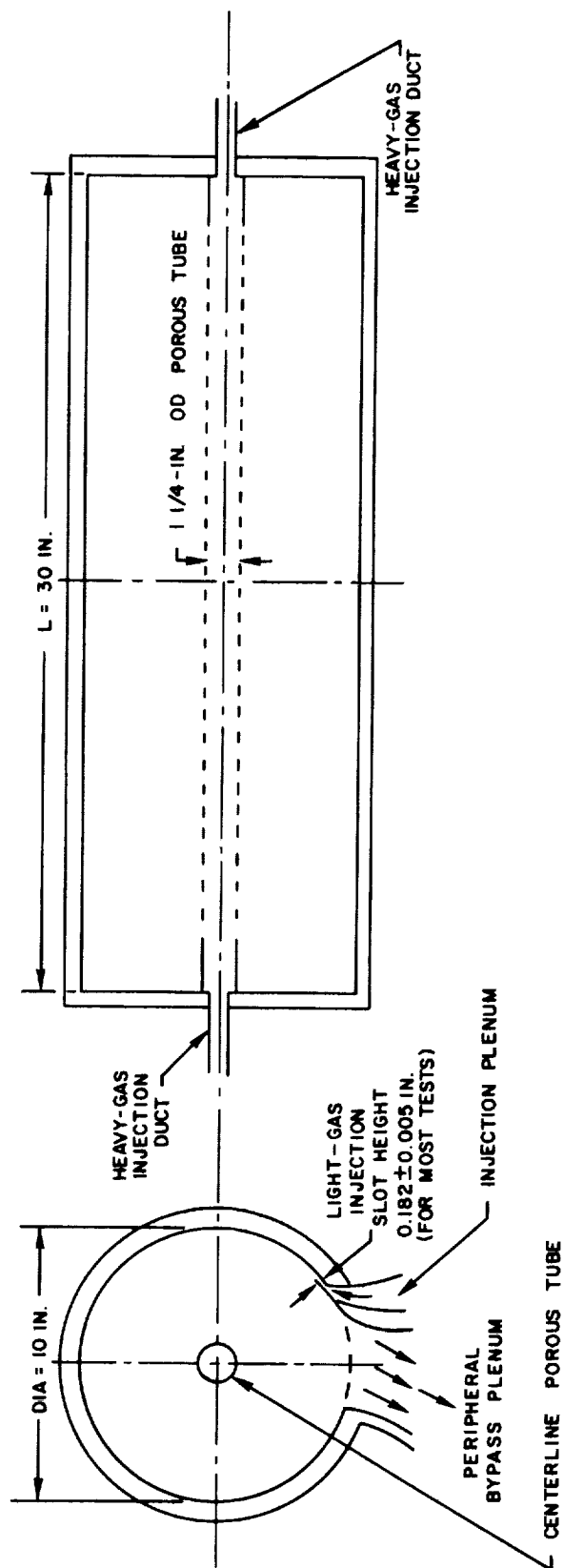
PERIPHERAL
BYPASS PLENUM

CENTERLINE POROUS TUBE

FIG. 39

VARIATION OF CONTAINMENT PARAMETER WITH HEAVY-GAS DENSITY RATIO FOR A RADIAL-OUTFLOW VORTEX WITH CENTERLINE-POROUS-TUBE HEAVY-GAS INJECTION

NO SUPERIMPOSED AXIAL FLOW
SEE FIG. 37 FOR GEOMETRY OF VORTEX TUBE
$Re_{t,j} = 180,000$, $Re_{z,w} = 27,000$

SYMBOL	HEAVY-GAS COMPOSITION
○	HELIUM AND IODINE
□	NITROGEN AND IODINE
△	SULPHUR HEXAFLUORIDE AND IODINE
◇	FC-75 AND IODINE

FIG. 38
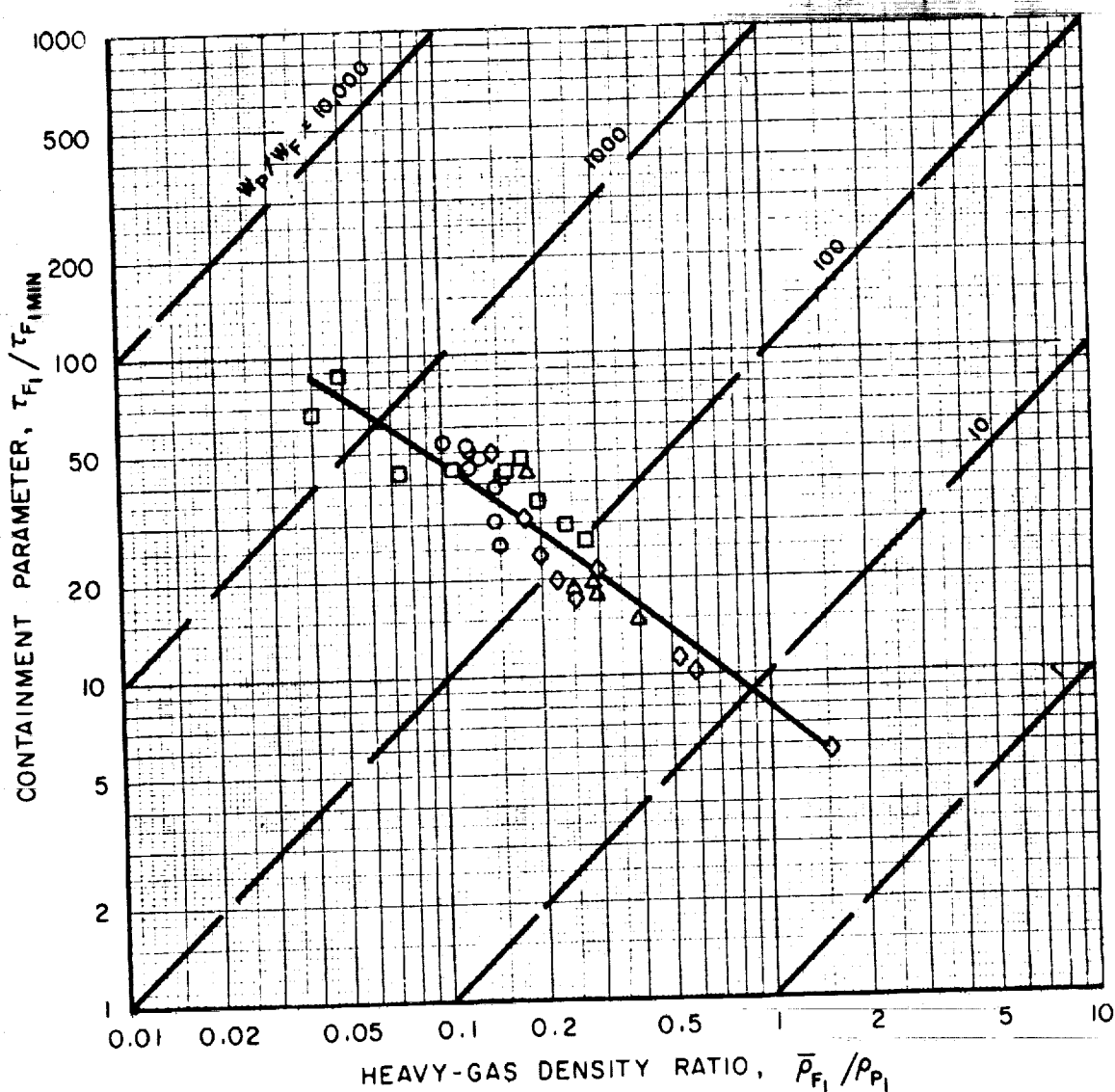
EFFECT OF LIGHT-GAS INJECTION SLOT HEIGHT ON CONTAINMENT PARAMETER

SEE FIG. 37 FOR GEOMETRY OF VORTEX TUBE
RADIAL OUTFLOW AND NO SUPERIMPOSED AXIAL FLOW
HEAVY-GAS COMPOSITION, FC-75 AND IODINE

LINE	W_F-LB/SEC
———	0.01
- - - -	0.10

EQUIVALENT AXIAL-FLOW REYNOLDS NUMBER, $Re_{z,w}$

79

FIG. 40
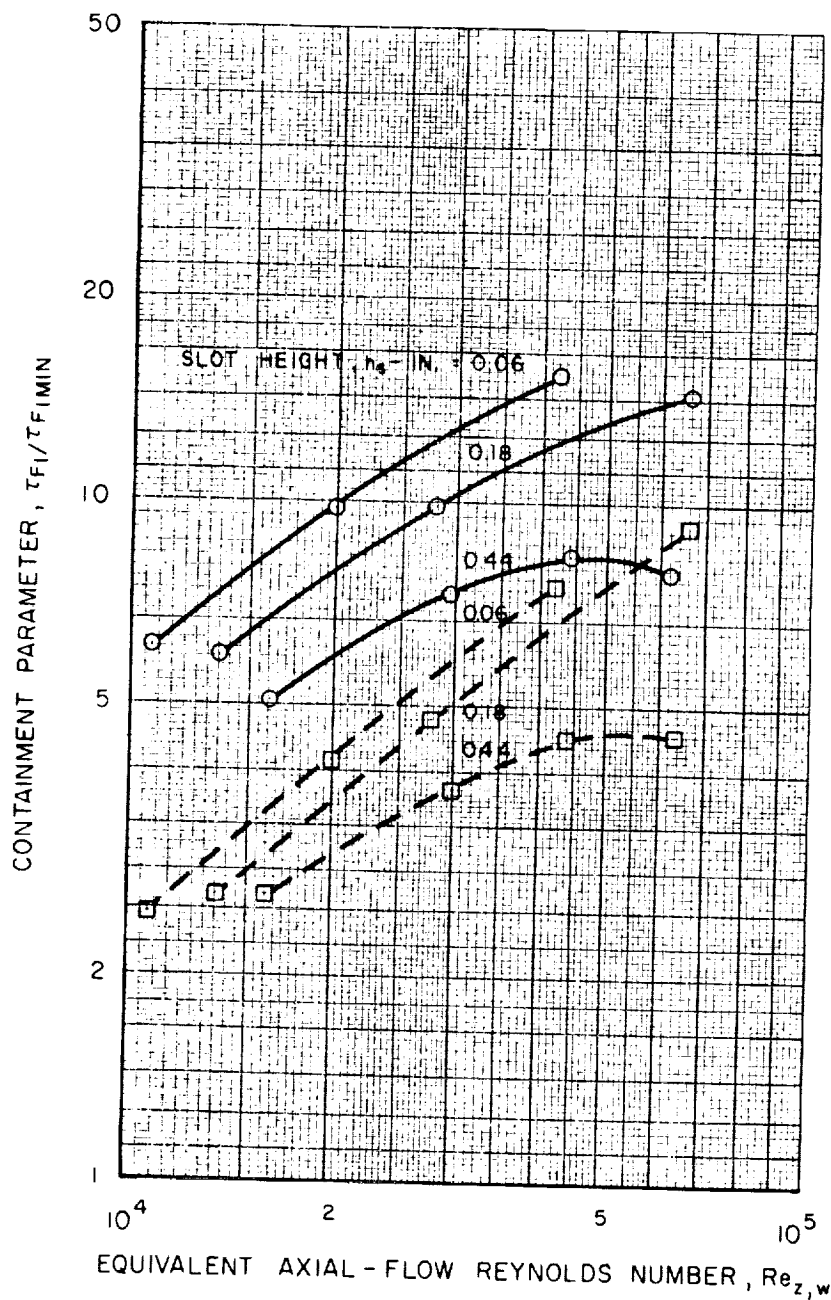
EFFECT OF HEAVY-GAS INJECTION CONFIGURATION
ON CONTAINMENT PARAMETER FOR A RADIAL-OUTFLOW VORTEX
WITH NO SUPERIMPOSED AXIAL FLOW

SEE FIG. 37 FOR GEOMETRY OF VORTEX TUBE
HEAVY-GAS COMPOSITION, FC-75 AND IODINE
$Re_{t,i} = 180,000$, $Re_{z,w} = 27,000$

SYMBOL	HEAVY-GAS INJECTION CONFIGURATION
O	1.0-IN.-DIA PORT AT CENTERS OF BOTH END WALLS
△	1.25-IN.-DIA POROUS TUBE AT VORTEX TUBE CENTERLINE
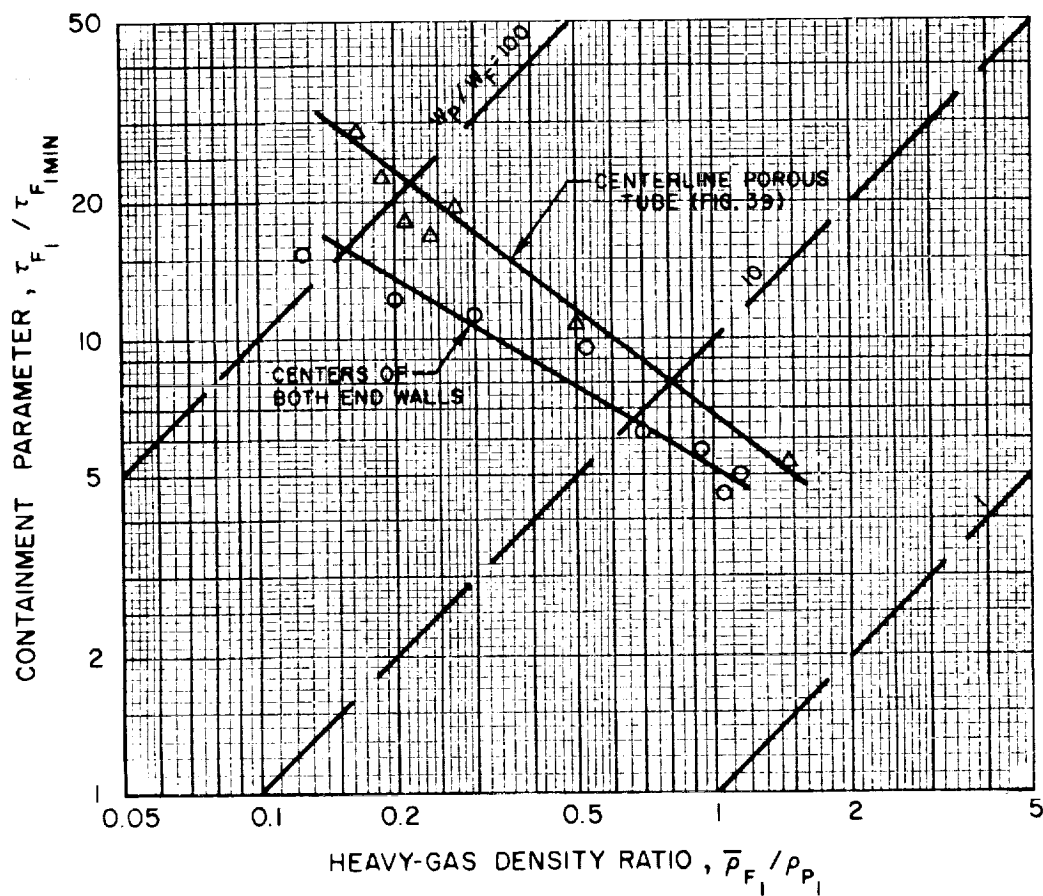
PHOTOGRAPHS OF 8-IN.-DIA SINGLE-SLOT VORTEX TUBE

TOP VIEW

LIGHT-GAS INJECTION DUCT
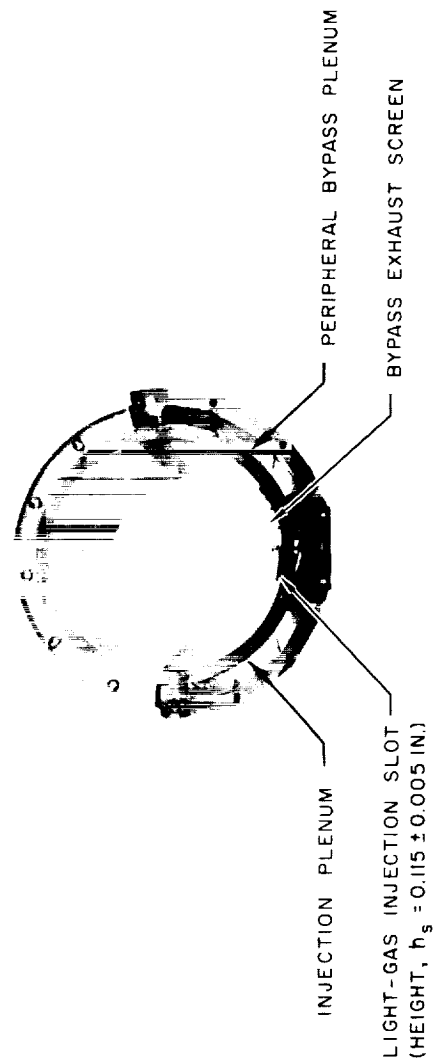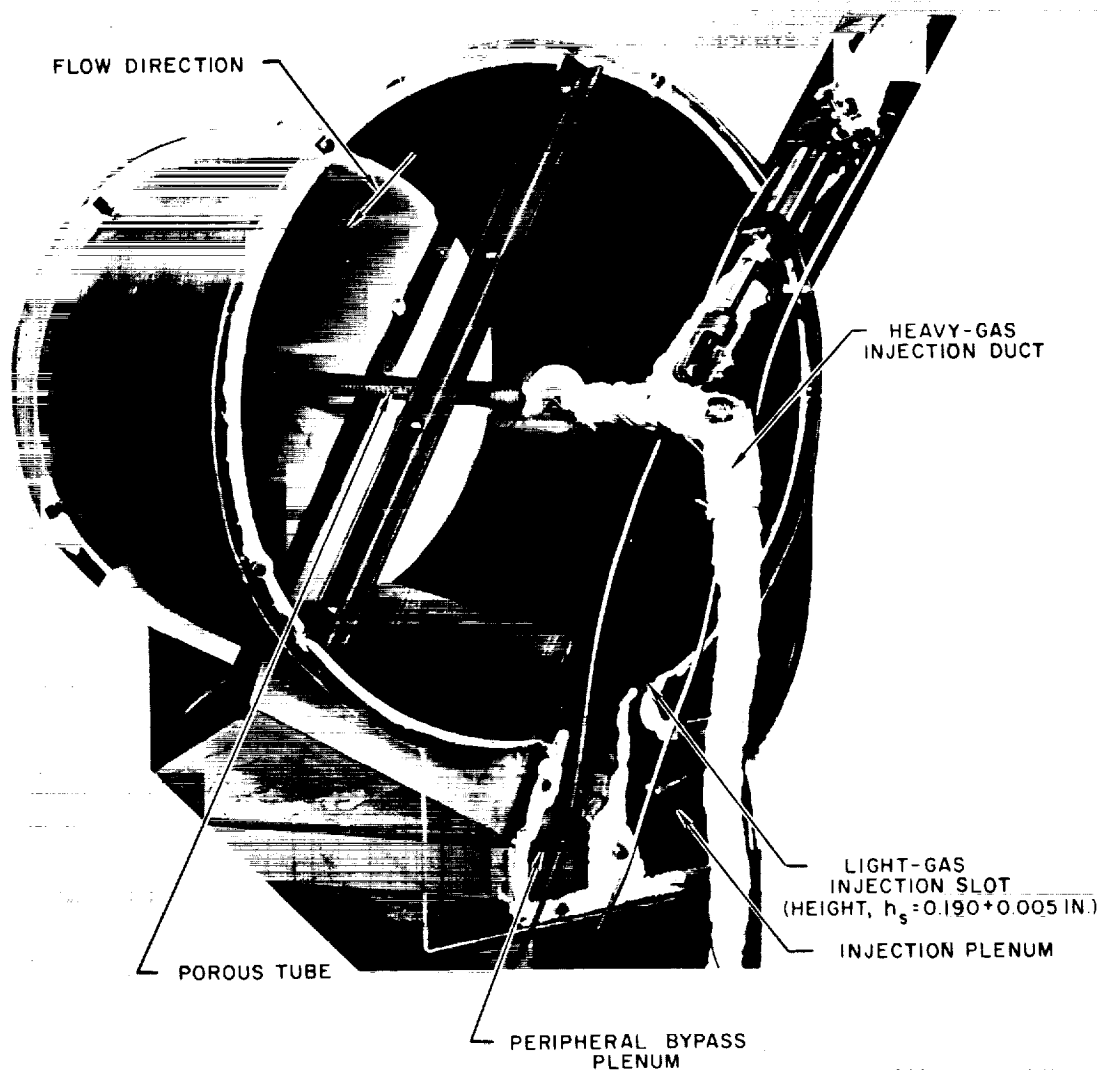
BYPASS EXHAUST DUCT
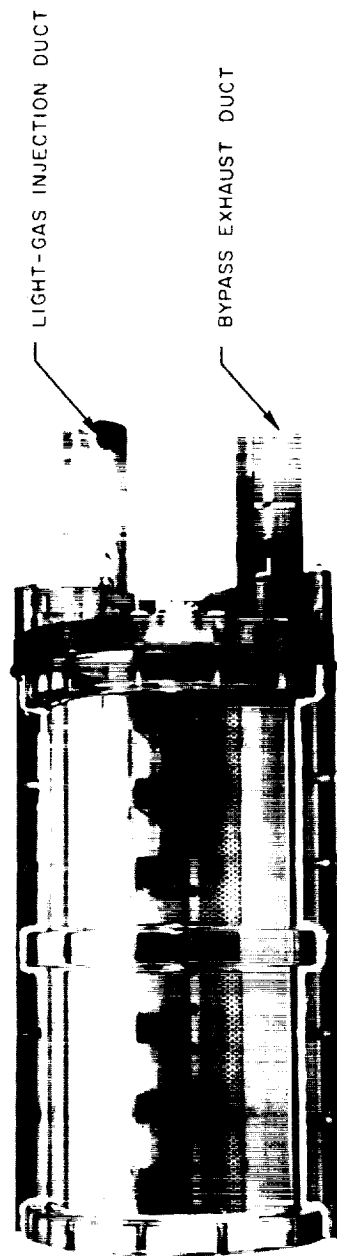
END VIEW WITH END WALLS REMOVED

PERIPHERAL BYPASS PLENUM

BYPASS EXHAUST SCREEN

INJECTION PLENUM

LIGHT-GAS INJECTION SLOT
(HEIGHT, h_s = 0.115 ± 0.005 IN.)

FIG. 41

FIG. 43

PHOTOGRAPH OF 30-IN.-DIA SINGLE-SLOT VORTEX TUBE

VORTEX TUBE LENGTH = 30 IN.

FLOW DIRECTION

HEAVY-GAS
INJECTION DUCT

LIGHT-GAS
INJECTION SLOT
(HEIGHT, $h_s = 0.190 + 0.005$ IN.)

INJECTION PLENUM

POROUS TUBE

PERIPHERAL BYPASS
PLENUM

84

FIG. 42

COMPARISON OF DATA OBTAINED WITH VORTEX TUBE
IN HORIZONTAL POSITION WITH DATA OBTAINED WITH VORTEX TUBE
IN VERTICAL POSITION

SEE FIG. 41 FOR GEOMETRY OF VORTEX TUBE
RADIAL OUTFLOW AND NO SUPERIMPOSED AXIAL FLOW
HEAVY-GAS INJECTION THROUGH CENTERLINE POROUS TUBE

SYMBOL	$Re_{z,w}$	$Re_{t,j}$	$\tau_{F_{I MIN}}$
O	9,500	100,000	0.00120
□	13,300	140,000	0.00086
△	19,000	190,000	0.00060

OPEN SYMBOLS - VORTEX TUBE HORIZONTAL
SOLID SYMBOLS - VORTEX TUBE VERTICAL
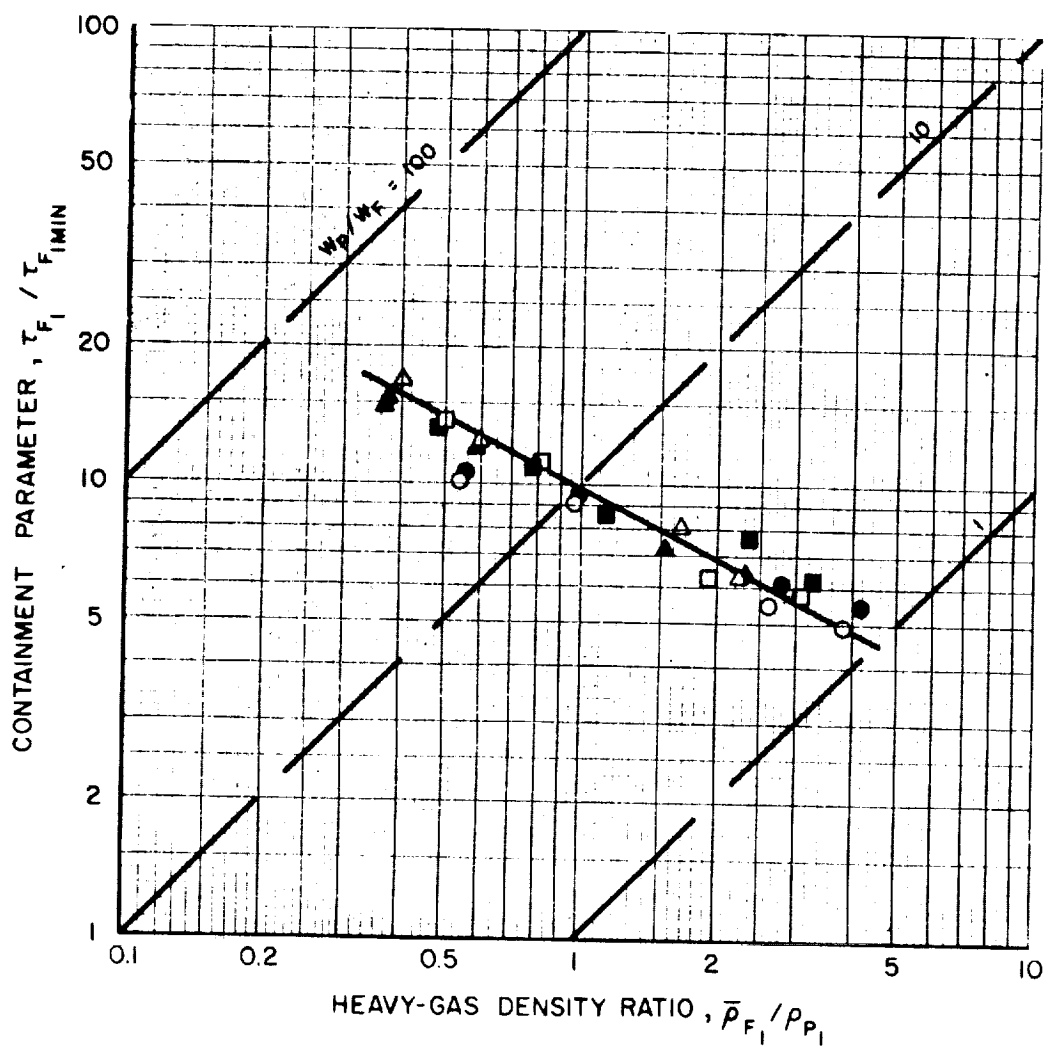
FIG. 44

VARIATION OF CONTAINMENT PARAMETER WITH HEAVY-GAS DENSITY RATIO FOR A RADIAL-OUTFLOW VORTEX IN THE 30-IN.-DIA VORTEX TUBE

SEE FIG. 43 FOR GEOMETRY OF VORTEX TUBE
NO SUPERIMPOSED AXIAL FLOW
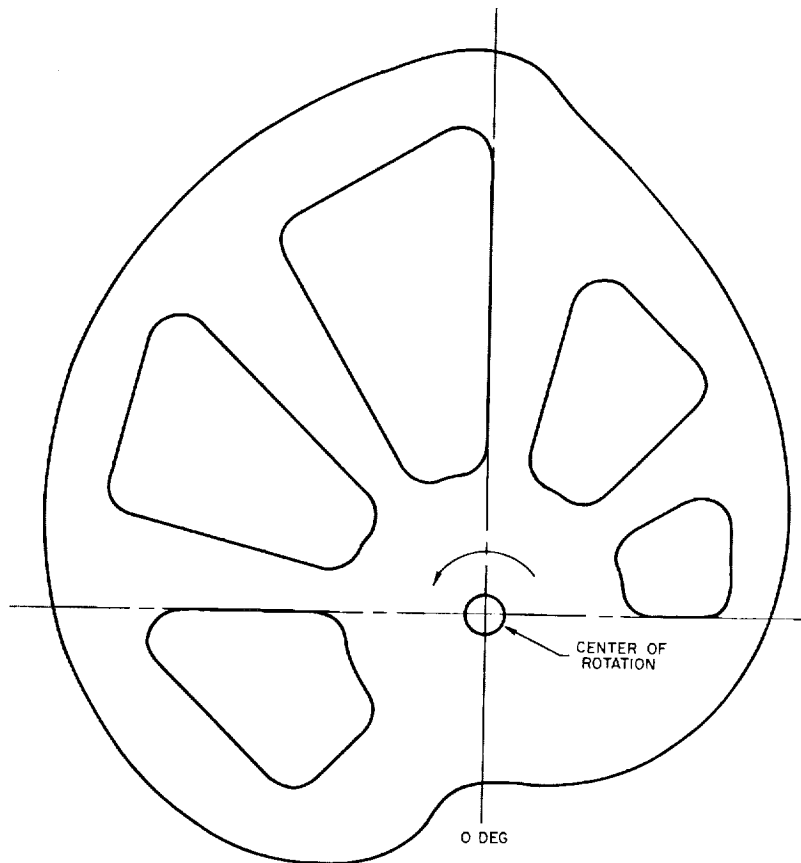$Re_{t,j} = 530,000$, $Re_{z,w} = 8700$

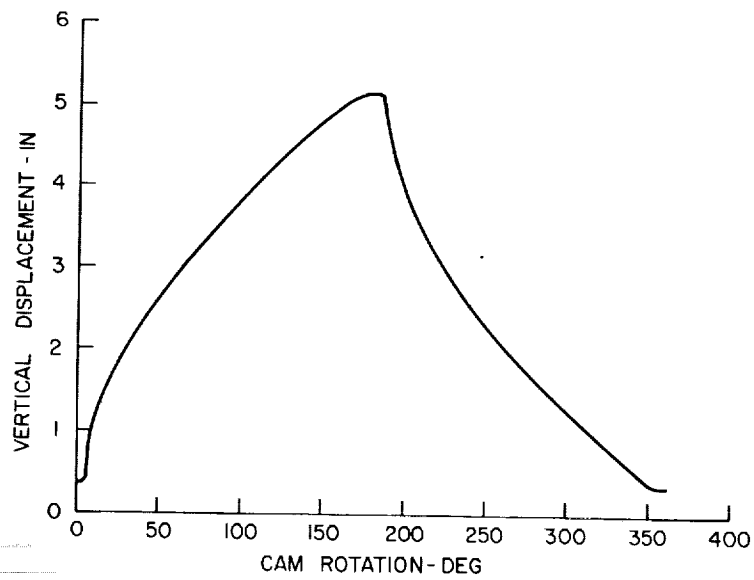| SYMBOL	HEAVY-GAS COMPOSITION
O	NITROGEN AND IODINE
□	SULPHUR HEXAFLOURIDE AND IODINE
△	FC-75 AND IODINE

85
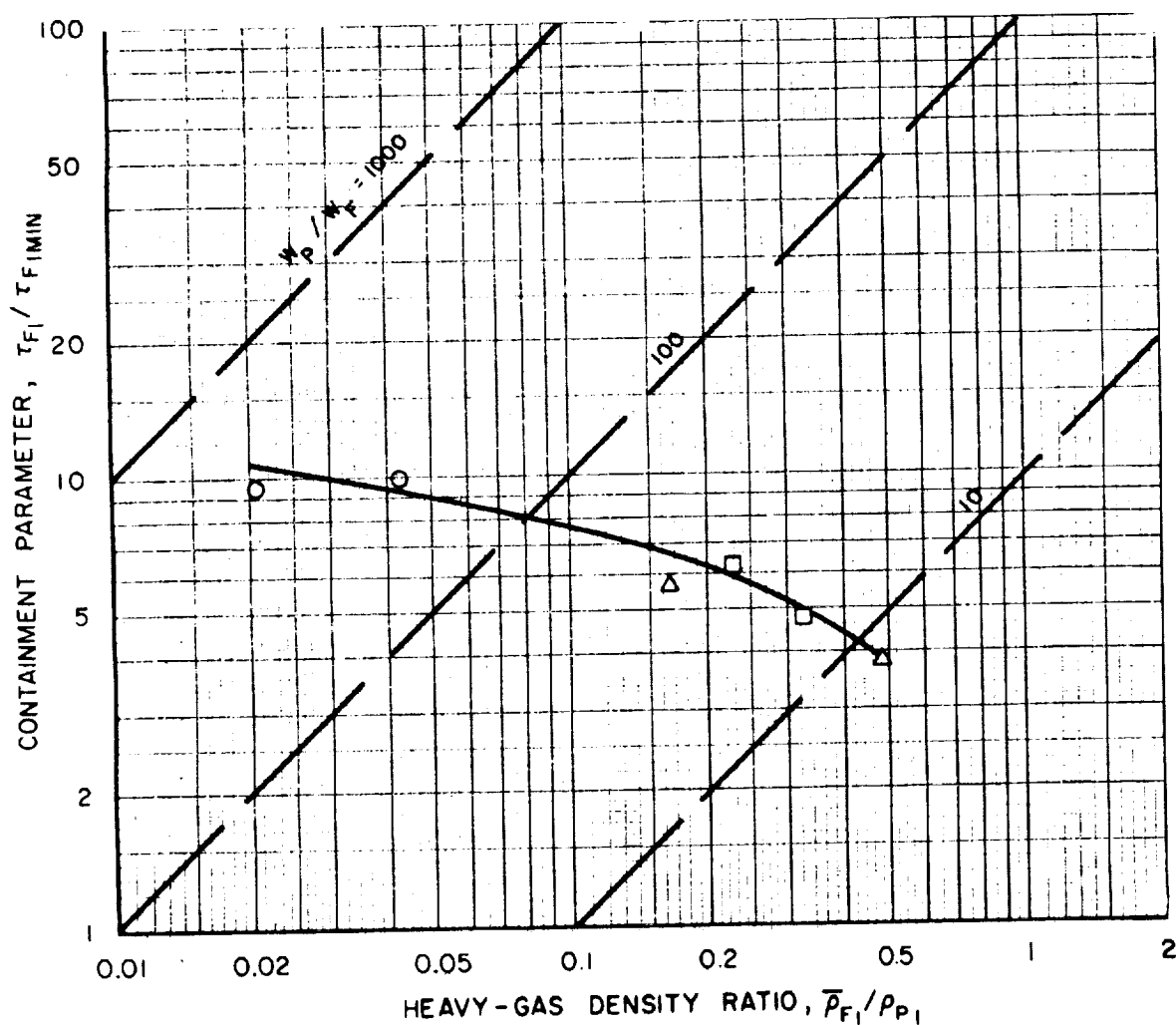
CAM USED IN OPTICAL SCANNER

FIG. 45

a) CAM LAYOUT — 1/2 FULL SIZE

b) VERTICAL DISPLACEMENT OF CAM FOLLOWER

FIG. 46

TYPICAL VARIATIONS OF AXIAL LIGHT BEAM INTENSITY FOR RADIAL TRAVERSES
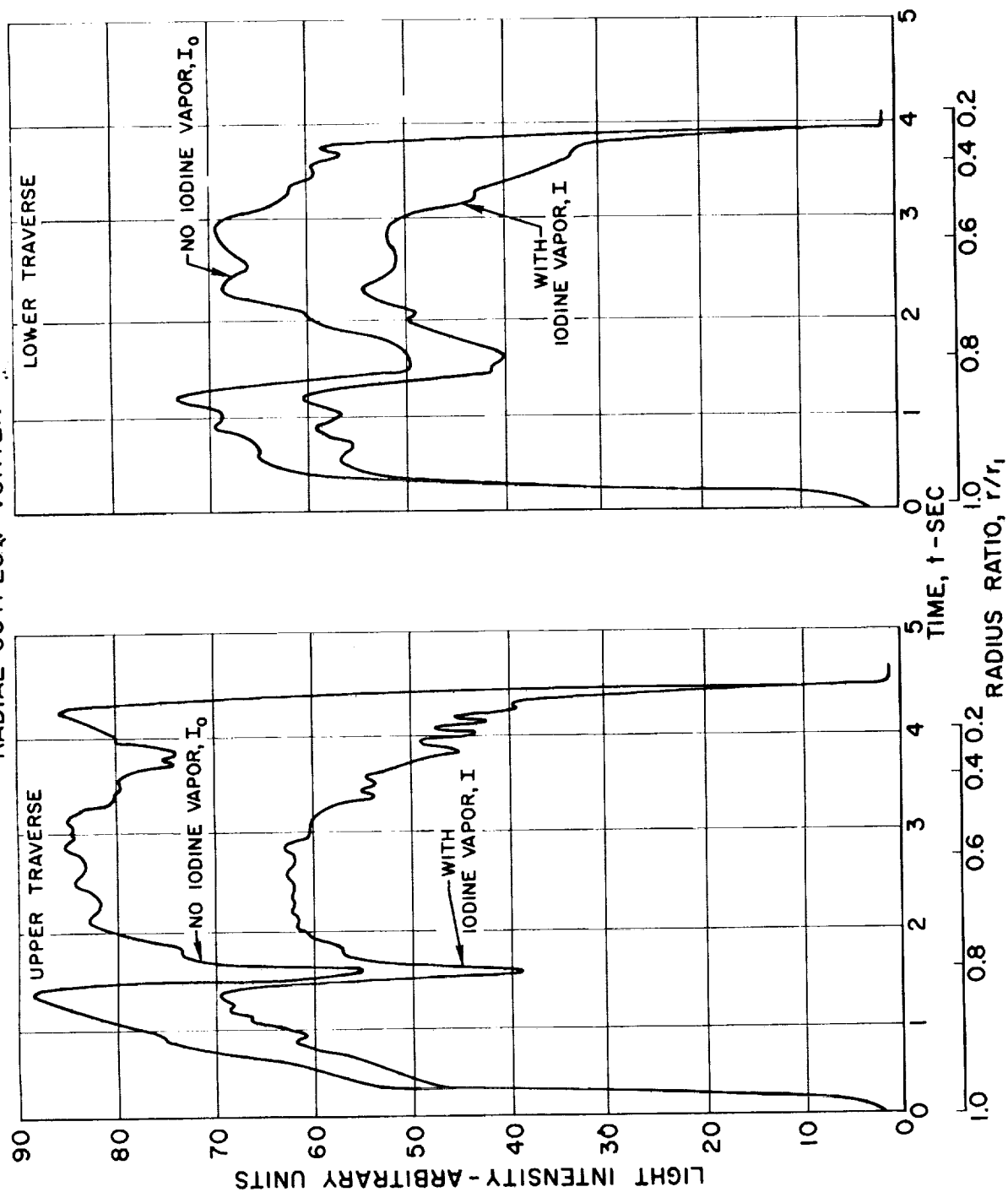## RADIAL OUTFLOW VORTEX